

Dissipative Bose Einstein Condensates

Diploma Thesis
by
Max Lewandowski

Supervisor: Priv.-Doz. Dr. Axel Pelster

Submitted to the
Institut für Physik und Astronomie
Universität Potsdam



July 2012

Selbstständigkeitserklärung

Hiermit versichere ich, die vorliegende Arbeit ohne unzulässige Hilfe Dritter und ohne Benutzung anderer als der angegebenen Hilfsmittel angefertigt zu haben. Die aus fremden Quellen direkt oder indirekt übernommenen Gedanken sind als solche kenntlich gemacht. Die Arbeit wurde bisher weder im In- noch im Ausland in gleicher oder ähnlicher Form einer anderen Prüfungsbehörde vorgelegt.

Potsdam, 16.07.2012

Max Lewandowski

Erstgutachter: Prof. Dr. Martin Wilkens

Zweitgutachter: Priv.-Doz. Dr. Axel Pelster

Kurzzusammenfassung

Seit der theoretischen Vorhersage 1924 war die erste Realisierung eines Bose-Einstein-Kondensats (BEC) 1995 der Beginn vieler und umfassender Experimente mit derartigen Systemen. Ein Bereich solcher Forschungen an BECs sind zum Beispiel dissipative Effekte, die beispielsweise durch die Wechselwirkung eines solchen Kondensats mit einem Elektronenstrahl verursacht werden. In dieser Diplomarbeit untersuchen wir ein theoretisches Modell, das Vorhersagen über die Dynamik und das Verhalten im Allgemeinen eines BECs in einer harmonischen Falle treffen soll, das mit einem Elektronenstrahl wechselwirkt. Für diesen setzen wir eine Gaußsche Form an und modellieren ihn durch ein imaginäres Potenzial, wohingegen die Falle durch ein reelles Potenzial beschrieben wird. Dieser Ansatz führt für ein nichtwechselwirkendes Bose-Gas zu einem nicht-Hermiteschen Hamilton-Operator, dessen Bedeutung in einem kleinen Einschub über nicht-Hermitesche Dynamik beschrieben wird. Beispielsweise sind die Energieeigenwerte komplex, wodurch die Eigenzustände nicht stationär sind. Dieser nichtverschwindende Imaginärteil der Energie führt dazu, dass die Kondensatdichte mit der Zeit gedämpft oder erhöht wird.

Um diese Eigenzustände und Eigenwerte zu berechnen, nehmen wir zunächst starke Vereinfachungen vor. Wir betrachten lediglich ein eindimensionales Potenzial, vernachlässigen jegliche Wechselwirkung der Bosonen des BECs untereinander und nähern das komplexe Potenzial durch zwei ineinander geschachtelte Kastenpotenziale an. Für dieses System lösen wir die Schrödinger-Gleichung für verschiedene Stärken der Dissipation, sowie Strahlbreiten und geben Ausdrücke für die Wellenfunktionen und Bestimmungsgleichungen für die Energien an, die wir anschließend numerisch lösen. Die dadurch erhaltenen Energien weisen einen nicht positiven Imaginärteil auf, so dass der imaginäre Potenzialtopf tatsächlich einen Dämpfungseffekt zur Folge hat. Bei den Eigenzuständen werden wir auf zwei verschiedene Arten von Zuständen geführt, wobei eine von beiden die Dissipation minimiert, während die andere diese maximiert. Da der Imaginärteil der Energie die Stärke der Dämpfung beschreibt, stellt dieser auch den Indikator dar, welcher Zustand gerade vorliegt. In den Dichten äußert sich dies ebenfalls und zwar dadurch, dass die Dichte solcher Zustände, die die Dissipation minimieren, nach außen strebt und im Inneren, wo das imaginäre Potenzial wirkt, für starke Dissipation auf Null abfällt. Im Gegensatz dazu streben Dissipation maximierende Zustände nach innen und ihre Dichte fällt außen auf Null ab für starke Dissipation. Da nur in der Mitte Dämpfung stattfindet, werden mit der Zeit nur solche Zustände übrig bleiben, die nach außen streben, so dass im Endeffekt ein Loch im BEC entsteht, was auch der Anschauung entspricht.

Weiterhin werden Grenzfälle für starke und verschwindende Dissipation, sowie große und kleine Strahlradien durchgeführt. Anschließend diskutieren wir alle Ergebnisse und vergleichen sie mit denen von ähnlichen reellwertigen Systemen. Im folgenden Kapitel verbessern wir unser Modell, indem wir statt eines ineinander geschachtelten Potenzialtopfes zwei harmonische Potenzialtöpfe für den Real- und Imaginärteil des Potentials ansetzen. Obwohl hier eine derart ausführliche Auswertung wie für das einfachere Modell nicht ohne weiteres möglich ist, können wir doch bestätigen, dass die Ergebnisse qualitativ unverändert bleiben.

Am Ende führen wir noch einige Möglichkeiten an, um dieses Modell zu verbessern und auszubauen. Allem voran wird die mögliche Implementierung von Wechselwirkung der Bosonen untereinander diskutiert, sowie die Probleme erörtert, die ein System mit komplexem Potenzial dafür mit sich bringt.

Abstract

Since 1924 theoretically predicted, the first realization of a Bose-Einstein-Condensate (BEC) in 1995 was the begin of many experiments and investigations of such systems. Some of them consider dissipative effects of a BEC, which are caused for example by the interaction of a condensate with an electron beam. This diploma thesis considers a theoretical model which should make predictions about the dynamics and the general behaviour of a harmonic trapped BEC that interacts with such an electron beam. This beam is supposed to be Gaussian and we model it via an imaginary potential, while the harmonic trap is described via a real potential. This ansatz leads under the assumption of a noninteracting Bose gas to a non-Hermitian Hamilton operator, whose influence is concisely discussed in a short section about non-Hermitian dynamics. For example we have to deal with complex energy eigenvalues, which are consequently caused by non-stationary eigenstates. Thus the non-vanishing imaginary part of the energies leads to a damped or increased density.

In order to calculate these eigenvalues and eigenstates, we first consider a crudely simplified system, that is we just take a one-dimensional potential, neglect any interaction of the bosons contained in the BEC and approximate the whole complex potential by two nested square well potentials. For this system we solve the Schrödinger equation for several dissipation strengths as well as beam waists and evaluate expressions for the wave functions and equations for the energies that we solve numerically afterwards. The calculated energies always yield a non-positive imaginary part, so the complex potential well indeed exhibits a damping effect. Furthermore, we obtain two different kinds of eigenstates, where one of them minimizes dissipation, while the other one maximizes it. Since the imaginary part of the energy describes the strength of the damping, this represents an indicator of which kind of state we deal with in particular. This distinction has also to be performed for the densities since the spatial density of states minimizing dissipation tends to the borders and reduces for large dissipation to zero in the center, where the imaginary potential is present. In contrast to this the other kind of states maximizing dissipation tends to the center, where the imaginary potential acts at, and reduces to zero at the borders for large dissipation. Since damping happens only in the center, the time evolution yields that gradually only these states tending to the borders will remain so that in the end a hole in the BEC develops which looks quite plausible recalling the picture of an electron beam interacting with a BEC.

Furthermore we consider the limits for strong and vanishing dissipation as well as small and large beam waists. Afterwards all results for the complex square well potential are discussed and compared to those of similar real valued systems. In the following chapter we improve our model by considering two nested harmonic potential wells for the real and the imaginary part of the potential. Although a discussion to such an extent as for the nested square well potentials is not possible without further ado, we can confirm that all results stay qualitatively unchanged for the harmonic potentials.

Finally we give some possibilities for a further improvement of this model. Especially the implementation of interaction between the bosons of the BEC is discussed as well as difficulties which are caused by a system with a complex valued potential.

Contents

1	Introduction	1
1.1	Bose-Einstein Condensation	1
1.2	Modelling of dissipation in Bose Einstein-Condensates	2
1.3	This Thesis	3
2	Non-Hermitian dynamics	5
3	Complex square well potential	7
3.1	Static solutions of Schrödinger equation	7
3.2	Energies	11
3.2.1	Regime of vanishing areas	14
3.2.2	Three areas regime	16
3.2.3	Critical waists	22
3.3	Densities	22
3.4	Related Systems	26
3.4.1	Asymmetric complex square well potential	26
3.4.2	Related real potential systems	29
4	Complex harmonic potential	35
4.1	Static solutions of Schrödinger equation	36
4.1.1	Symmetric states	40
4.1.2	Antisymmetric states	47
4.2	Energies	54
4.3	Densities	57
5	Outlook	61
	Bibliography	63

1 Introduction

In this chapter we will recall some fundamental issues this diploma thesis is based on, that is Bose-Einstein condensation in general, the particular experiment involving dissipation in a BEC we are considering and which we aim at modelling, and finally some aspects about non-Hermitian dynamics, which is a crucial point of our model. The last section of this chapter provides an overview of this particular diploma thesis.

1.1 Bose-Einstein Condensation

Already in 1924 Satyendranath Bose wrote a paper where he used a novel way for counting states of identical photons to derive Planck's quantum radiation law. In this way he found out that the Maxwell-Boltzmann distribution is not true for microscopic particles and has to be replaced by another distribution [1]. In the same year this idea was extended to massive particles by Albert Einstein [2], therefore this new distribution is called today *Bose-Einstein distribution*. It predicts a macroscopic occupation of the ground state by a dense collection of particles with integer spin, called bosons, for very low temperatures near to absolute zero. This phenomenon is called *Bose-Einstein condensation*. The first experimental realization of a pure Bose-Einstein condensate (BEC) was accomplished in 1995 by Eric Cornell and Carl Wieman at JILA [3] and Wolfgang Ketterle at MIT [4]. The creation of a BEC requires temperatures very near absolute zero to reach the critical temperature for the phase transition. The new techniques of laser cooling [5–7] and magnetic evaporative cooling [8] made it possible for E. Cornell and C. Wiedman to cool down a gas of rubidium-87 atoms confined in a magnetic time-averaged, orbital potential (TOP) trap to 170 nK which undermatches the critical temperature of ^{87}Rb . In the same year W. Ketterle produced at MIT a much larger BEC of sodium-23, which allowed him to observe even first coherence effects like the quantum mechanical interference between two different BECs [9].

So far BECs have been created with many other kinds of atoms like ^1H , ^7Li , ^{23}Na , ^{39}K , ^{41}K , ^{52}Cr , ^{85}Rb , ^{87}Rb , ^{133}Cs , ^{164}Dy , ^{168}Er , ^{170}Yb , ^{174}Yb and ^4He in an excited state. Moreover, experiments with BEC as well as its theory became one of the most interesting physical research topics in the last years like the realization of a BEC in optical lattices which are standing laser fields that yield via the AC Stark effect periodic potential wells for atoms [10]. This leads to a strongly correlated BEC which is well controlled by the respective laser parameters and yields for increasing laser intensities a quantum phase transition from the superfluid to a Mott phase. As the latter is characterized by a fixed number of bosons in each well, a Bose gas in an optical lattice is a promising candidate for quantum simulations like entanglement of atoms or quantum teleportation [11]. Also disordered Bose gases can be realized via laser speckles or incommensurable optical lattices, to create random potentials [12]. Another interesting research field are fermionic condensates. Two weakly correlated fermions called *Cooper pairs* yield a "particle" with integer spin, which therefore also obeys Bose-Einstein statistics despite the fermionic constituents. By

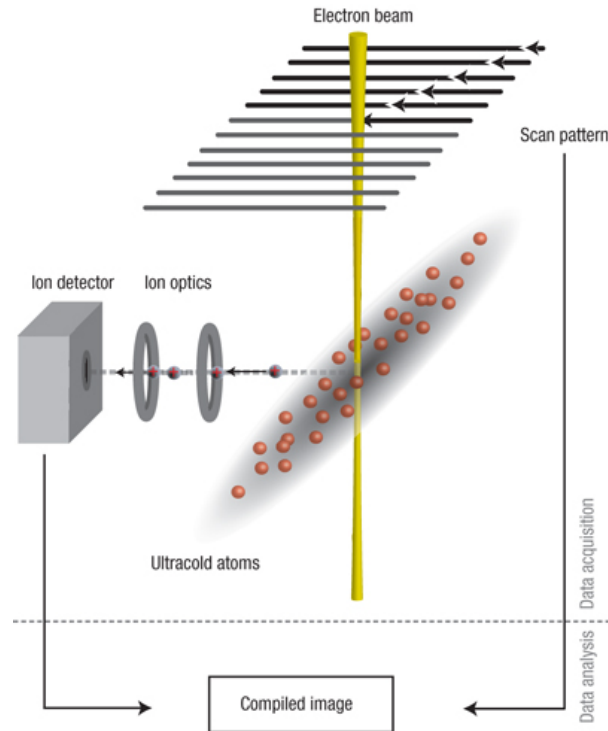


Figure 1.1: The atomic ensemble is prepared in an optical dipole trap. An electron beam with variable beam current and diameter is scanned across the cloud. Electron impact ionization produces ions, which are guided with an ion optical system towards a channeltron detector. The ion signal together with the scan pattern is used to compile the image [17].

increasing the correlation for example by a magnetic trap there is a crossover from this BCS phase of weakly coupled fermions [13] to bound boson molecules condensing to a BEC, which is called BCS-BEC-crossover [14].

1.2 Modelling of dissipation in Bose Einstein-Condensates

Complex potentials are used in a BEC as a heuristic tool to model dissipation processes which occur once a BEC is brought in contact, for instance, with an ion [15]. This diploma thesis is related to an experiment performed by the group of Herwig Ott [16,17] at the Technical University of Kaiserslautern, where a ^{87}Rb -BEC interacts with an electron beam, which is one technique to achieve single-site addressability [18–22].

The BEC is confined by an anisotropic harmonic trap with the frequencies $\Omega_{\perp} = 2\pi \cdot 13$ Hz and $\Omega_{\parallel} = 2\pi \cdot 170$ Hz and contains about 100 000 atoms. The experiment was realized at about 80 nK, the critical temperature of ^{87}Rb is 300 nK.

In contrast to the other applications of complex potentials the experimental setup of Herwig Ott makes it possible to control all experimental parameters to a high degree. Therefore, this electron beam technique seems to be the most promising candidate to compare the respective experimental results with theoretical calculations in a quantitative way. We are now interested in the interaction of the BEC with the beam. The main idea is to model this interaction by an imaginary potential with a width given by the Gaussian profile of the beam [23]. The whole BEC is confined in a

harmonic trap which is modelled by a real potential.

Now we aim at getting a fundamental view on the theory of the properties and effects of a BEC in a complex potential $V(\mathbf{r}) = V_R(\mathbf{r}) + iV_I(\mathbf{r})$ at absolute zero which is described by the Gross-Pitaevskii equation

$$i\hbar \frac{\partial}{\partial t} \Psi(\mathbf{r}, t) = \left[-\frac{\hbar^2}{2M} \Delta + V_R(\mathbf{r}) + g |\Psi(\mathbf{r}, t)|^2 - \frac{i\hbar}{2} \gamma(\mathbf{r}) \right] \Psi(\mathbf{r}, t). \quad (1.1)$$

Here Ψ represents the wave function of the condensate, g describes the strength of the two-particle interaction and $V_R(\mathbf{r}) = \frac{1}{2}M [\Omega_{\perp}^2(x^2 + y^2) + \Omega_{\parallel}^2 z^2]$ stands for the harmonic trap. The imaginary term $\frac{1}{2}\hbar\gamma(\mathbf{r})$ represents the imaginary potential V_I , where $\gamma(\mathbf{r})$ has a Gaussian shape

$$\gamma(\mathbf{r}) = \frac{\sigma_{\text{tot}}}{e} \frac{I}{2\pi w^2} \exp \left[-\frac{(x - x_0)^2 + (y - y_0)^2}{2w^2} \right], \quad (1.2)$$

and models the losses of the BEC caused by the electron beam. In this expression $\sigma_{\text{tot}} = 1.7 \cdot 10^{-20} \text{ m}^2$ denotes the total cross section between electrons and ^{87}Rb -atoms, $I = 20 \text{ nA}$ is the electron current and the waist of the beam is given by $w = 100 \text{ nm}$ [23]. So we have to consider two nested potential wells where the outer one V_R is harmonic and the inner one is a Gaussian imaginary potential:

$$V_I(\mathbf{r}) = -C \exp \left[-\frac{(x - x_0)^2 + (y - y_0)^2}{2w^2} \right], \quad (1.3)$$

whose strength amounts to

$$C = \frac{\hbar\sigma_{\text{tot}}}{e} \frac{I}{4\pi w^2} \approx 1,8 \cdot 10^{-30} \text{ J}. \quad (1.4)$$

1.3 This Thesis

Eq. (1.1) represents a 3-dimensional nonlinear partial differential equation for Ψ . As we aim here at getting a fundamental look at a BEC in a complex potential, we start with simplifying this problem. In this whole thesis we consider a model in only one spatial dimension perpendicular to z -direction so the imaginary potential well (1.4) is considered as a one-dimensional centered Gaussian

$$V_I(x) = -C \exp \left[-\frac{x^2}{2w^2} \right] \quad (1.5)$$

and the extension of the BEC can be estimated by only one quantity which is the perpendicular Thomas-Fermi radius [24]

$$R_{\perp} = \sqrt{\frac{2\mu}{M\Omega_{\perp}^2}}. \quad (1.6)$$

1 Introduction

The chemical potential reads [24]

$$\mu = \left[\frac{15\Omega_{\perp}^2 \Omega_{\parallel} N g}{8\pi} \left(\frac{M}{2} \right)^{\frac{3}{2}} \right]^{\frac{2}{5}} \quad (1.7)$$

with $g = \frac{4\pi\hbar^2}{M} a_s$, where the s-wave scattering length of ^{87}Rb is $a_s = 100 a_0$ with the Bohr radius a_0 and the mass of the Rb-atoms amounts to $M = 1,44 \cdot 10^{-27}$ kg. Inserting (1.7) into (1.6) thus yields about

$$R_{\perp} = 640 \mu\text{m}, \quad (1.8)$$

which is at least three orders in magnitude larger than the electron beam waist w . Nevertheless we will not restrict ourselves to these calculated orders of magnitude of w , R_{\perp} and C but perform a more fundamental evaluation of the energies and densities for various values of C and w .

In this thesis we start with a short trip to non-Hermitian dynamics, that is time evolution of a system caused by a non-Hermitian Hamilton operator, which just arises for our system including a non-vanishing imaginary part of the potential.

In Chapter 3 we consider a particular model which is supposed to represent the regarded system in a quite simplified way. Therefore, we neglect any interaction of the ^{87}Rb -atoms of the BEC, that is we set $g = 0$ in (1.1), which can be experimentally performed by using magnetic traps and taking advantage of hyperfine structures. In this way it is possible to influence scattering parameters like the cross section and the scattering length via magnetic Feshbach resonances [25], which are induced by the additional magnetic field. It is thus possible to manage a vanishing scattering length and cross section, that is a vanishing interaction. Considering this, each particle of the BEC can be separately described by a linear one-dimensional Gross-Pitaevskii equation which is just a Schrödinger equation with a complex potential. To get a first impression of the effects of a complex potential we simplify it here by taking a kind of zeroth order approximation modelling V_I to be a square well potential within the width $2w$ and with a strength given by C . Also the real potential is considered to be a square well potential which is supposed to vanish within a finite length L and to be equal to infinity outside. With these simplifications we solve the time-independent Schrödinger equation and discuss the resulting energies and densities as functions of the width and the depth of V_I . Afterwards we will have a quite detailed discussion of the results even this crudely simplified system provides and compare them to these of some familiar similar potentials in order to underline new aspects of our model.

Chapter 4 then considers a more accurate approximation so we take a better approximation of V_I which is then supposed to be harmonic and the exact formula for the harmonic real potential, that is $V_R = \frac{1}{2}M\Omega^2 x^2$, $\Omega = \Omega_{\perp}$. Furthermore the two-particle interaction is still neglected and thus we are able to describe the system by a Schrödinger equation considering two nested harmonic potentials. We will solve it, discuss the resulting energies and densities and compare it to the results of Chapter 2.

Finally in Chapter 5 we will give an outlook on possible improvements especially concerning the implementation of interaction, that is $g \neq 0$. To this end we will discuss one particular approach in order to obtain results for an interacting BEC involving our results of a non-interacting BEC.

2 Non-Hermitian dynamics

Before considering concrete expressions for the imaginary potential we first provide a concise overview of the results a complex potential yields on the dynamics of a BEC. Generally it involves a non-Hermitian Hamilton operator $H \neq H^\dagger$ since $V \neq V^*$. To this end we consider the one-dimensional time-dependent Schrödinger equation

$$i\hbar \frac{\partial}{\partial t} \Psi(x, t) = H \Psi(x, t), \quad (2.1)$$

where H denotes the one-dimensional, one-particle Hamilton operator in spatial representation

$$H = -\frac{\hbar^2}{2M} \frac{\partial^2}{\partial x^2} + V(x) \quad (2.2)$$

with a complex potential $V(x) := V_R(x) + iV_I(x)$. From the Schrödinger equation (2.1) one can derive the time evolution of the density $\rho(x, t) = \Psi^*(x, t)\Psi(x, t)$:

$$\begin{aligned} \frac{\partial}{\partial t} \rho &= \Psi \frac{\partial}{\partial t} \Psi^* + \Psi^* \frac{\partial}{\partial t} \Psi \\ &\stackrel{(2.1)}{=} -\frac{1}{i\hbar} \Psi H^\dagger \Psi^* + \frac{1}{i\hbar} \Psi^* H \Psi \\ &= \frac{\hbar}{2Mi} \left[\Psi \frac{\partial^2}{\partial x^2} \Psi^* - \Psi^* \frac{\partial^2}{\partial x^2} \Psi \right] + \frac{1}{i\hbar} [V(x) - V^*(x)] \Psi^* \Psi, \end{aligned} \quad (2.3)$$

where $\Psi = \Psi(x, t)$ and $*$ means complex conjugation. This yields the continuity equation

$$\frac{\partial}{\partial t} \rho(x, t) + \frac{\partial}{\partial x} j(x, t) = \frac{2}{\hbar} V_I(x) \rho(x, t), \quad (2.4)$$

with

$$j(x, t) = \frac{\hbar}{2Mi} \left[\Psi^*(x, t) \frac{\partial}{\partial x} \Psi(x, t) - \Psi(x, t) \frac{\partial}{\partial x} \Psi^*(x, t) \right] \quad (2.5)$$

representing the probability current density. It catches the eye that the non-real potential provides an additional term on the right-hand side of (2.4), which can stand for a source ($V_I(x) > 0$) or a drain ($V_I(x) < 0$) of probability.

Now let us come to the time evolution of the wave function. Since the spectrum of an operator is only real iff it is Hermitian, the energy eigenvalues of H have to be complex $E = E_R + iE_I$.

2 Non-Hermitian dynamics

The Hamilton operator does not depend on time so we can directly integrate (2.1) and obtain the separation

$$\Psi(x, t) = \exp\left(-\frac{i}{\hbar}tH\right)\psi(x). \quad (2.6)$$

Let $\psi(x)$ be an eigenstate of H to the eigenvalue E so we can write

$$\Psi(x, t) = \exp\left(-\frac{i}{\hbar}Et\right)\psi(x). \quad (2.7)$$

Now we can derive the time evolution of the density $\rho(x, t)$:

$$\rho(x, t) = \exp\left[\frac{2}{\hbar}E_I(t - t_0)\right]\rho(x, t_0), \quad (2.8)$$

where $\rho(x, t_0) = \psi^*(x)\psi(x)$ is the density at a fixed time $t = t_0$. One can see immediately that this non-stationarity is a direct consequence of the complexity of the potential since H is not Hermitian, which is followed by complex energy eigenvalues $E = E_R + iE_I$ and so the time evolution operator $\exp\left(-\frac{i}{\hbar}tH\right)$ is not unitary any more.

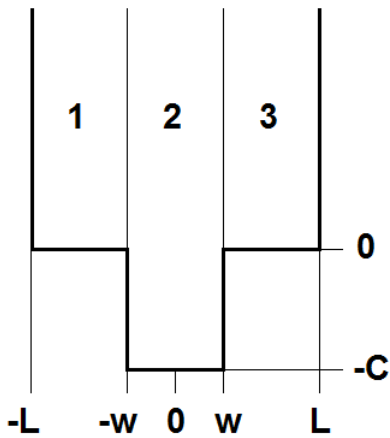
Inserting the separation (2.7) into (2.1) provides that ψ has to fulfill the time independent Schrödinger

$$H(x)\psi(x) = E\psi(x), \quad (2.9)$$

which we will solve in the next two chapters for two different approximations of $V(x)$.

3 Complex square well potential

We start with a crude approximation of $V(x)$ via two nested square well potentials according to Fig. 3.1, where the inner one is imaginary with a width equal to the diameter of the beam $2w$ and vanishes outside. The depth is given by the zeroth-order Taylor approximation of V_I in x at the minimum $x = 0$ which is just the constant $-C$. The real potential vanishes within a width equal to the spatial extension of the BEC perpendicular to the electron beam R_{\perp} , that we call L , and is equal to infinity outside.



$$V_R(x) = \begin{cases} 0 & , |x| < L \\ \infty & , \text{otherwise} \end{cases} \quad (3.1)$$

$$V_I(x) = \begin{cases} -C = \text{const.} & , |x| < w < L \\ 0 & , \text{otherwise} \end{cases} \quad (3.2)$$

Figure 3.1: Schematic sketch of the complex potential well where we call the interval $-L \leq x < -w$ "area 1" and $-w \leq x \leq +w$ "area 2" which is followed by "area 3" $w < x \leq L$.

3.1 Static solutions of Schrödinger equation

Now we derive solutions E and ψ of (2.9) for this considered potential. In the outer region of the well, i.e. $|x| > L$, the wave function vanishes because the probability of the particle to be out of the box is supposed to be equal to zero. In the inner region we have formally to distinguish between the three areas. Therefore, the resulting total wave function should have the following form:

$$\psi(x) = \begin{cases} \psi_1(x), & -L \leq x \leq -w \\ \psi_2(x), & -w \leq x < w \\ \psi_3(x), & w \leq x < L \\ 0, & |x| > L \end{cases} \quad (3.3)$$

As the Hamiltonian (2.2) is symmetric for the complex potential (3.1) and (3.2), its eigenfunctions ψ should have a definite parity with respect to the center of the well, which is $x = 0$. This means we assume ψ to be completely symmetric or antisymmetric with respect to $x = 0$, that is

3 Complex square well potential

$$\psi_1^s(-x) = \psi_3^s(x) \quad \text{and} \quad \psi_2^s(x) = \psi_2^s(-x), \quad (3.4)$$

or

$$\psi_1^a(-x) = -\psi_3^a(x) \quad \text{and} \quad \psi_2^a(-x) = -\psi_2^a(x). \quad (3.5)$$

Therefore it is sufficient to solve (2.9) only in area 1 and 2, since then ψ_3 is determined via symmetry according to (3.4) and (3.5). The Schrödinger equation (2.9) and the Hamilton operator (2.2) with the considered potential yields that this solution ψ has to be continuous at $x = \pm L$ and differentiable at $x = \pm w$. Making the ansatz

$$\psi_{1,2} = A_{1,2} e^{-ik_{1,2}x} + B_{1,2}^{s,a} e^{ik_{1,2}x} \quad (3.6)$$

and demanding continuity provides

$$\psi^s(x) = 2iA^s e^{ik_1^s L} \begin{cases} -\sin[k_1^s(x+L)] \\ \frac{\sin[k_1^s(w-L)]}{\cos(k_2^s w)} \cos(k_2^s x) \\ \sin[k_1^s(x-L)] \end{cases}, \quad \psi^a(x) = -2iA^a e^{ik_1^a L} \begin{cases} \sin[k_1^a(x+L)] \\ \frac{\sin[k_1^a(w-L)]}{\sin(k_2^a w)} \sin(k_2^a x) \\ \sin[k_1^a(x-L)] \end{cases} \quad (3.7)$$

with $A = A_1$ and the complex wavenumbers k_1 and k_2

$$k_1^2 = \frac{2M}{\hbar^2} (E_R + iE_I), \quad k_2^2 = \frac{2M}{\hbar^2} [E_R + i(E_I + C)], \quad (3.8)$$

where the indices R and I denote the real and imaginary part of the quantities, respectively. Normalizing these solutions, that is demanding

$$\int_{-\infty}^{\infty} |\psi(x)| dx = 2 \int_0^w |\psi_2(x)| dx + 2 \int_w^L |\psi_1(x)| dx = 1, \quad (3.9)$$

yields for the absolute value of the constants A^s and A^a

$$|A^s| = \left\{ 2e^{-2k_{I,1}^s L} \left[\frac{\sin 2k_{R,1}^s(w-L)}{k_{R,1}^s} - \frac{\sinh 2k_{I,1}^s(w-L)}{k_{I,1}^s} \right. \right. \\ \left. \left. + \frac{\cosh 2k_{I,1}^s(w-L) - \cos 2k_{R,1}^s(w-L)}{\cosh 2k_{I,2}^s w + \cos 2k_{R,2}^s w} \left(\frac{\sinh 2k_{I,2}^s w}{k_{I,2}^s} + \frac{\sin 2k_{R,2}^s w}{k_{R,2}^s} \right) \right] \right\}^{-\frac{1}{2}} \quad (3.10)$$

and

$$|A^a| = \left\{ 2e^{-2k_{I,1}^a L} \left[\frac{\sin 2k_{R,1}^a(w-L)}{k_{R,2}^a} - \frac{\sinh 2k_{I,1}^a(w-L)}{k_{I,2}^a} + \frac{\cos 2k_{R,1}^a(w-L) - \cosh 2k_{I,1}^a(w-L)}{\cos 2k_{R,2}^a w - \cosh 2k_{I,2}^a w} \left(\frac{\sinh 2k_{I,2}^a w}{k_{I,2}^a} - \frac{\sin 2k_{R,2}^a w}{k_{R,2}^a} \right) \right] \right\}^{-\frac{1}{2}}. \quad (3.11)$$

Thus we can fix them only up to a phase factor $e^{i\varphi}$, $\varphi \in [0, 2\pi)$. Knowing the particular wave function it is possible to calculate the density $\rho = |\psi(x)|^2$ and the current $j(x)$ from (2.5) at some fixed time. The symmetric and antisymmetric wave functions (3.7) are continuous at $x = \pm w$ and $\pm L$. Since (2.9) yields that the second derivative of the wave function ψ'' only has a finite jump discontinuity at $x = \pm w$ and an infinite one at $\pm L$, its first derivative ψ' has to be continuous at $\pm w$, too, but not at $\pm L$. Thus we obtain a relation between k_1 and k_2 and thus via (3.8) an additional condition the energy E has to fulfill, which is our quantization condition

$$\sqrt{E^s} \cot \left[(w-L) \sqrt{\frac{2M}{\hbar^2} E^s} \right] + \sqrt{E^s + iC} \tan \left[w \sqrt{\frac{2M}{\hbar^2} (E^s + iC)} \right] = 0 \quad (3.12)$$

in the symmetric case and in the antisymmetric case

$$\sqrt{E^a} \cot \left[(w-L) \sqrt{\frac{2M}{\hbar^2} E^a} \right] - \sqrt{E^a + iC} \cot \left[w \sqrt{\frac{2M}{\hbar^2} (E^a + iC)} \right] = 0. \quad (3.13)$$

The solutions of these two transcendental equation allow to determine all important physical quantities E, ρ, j etc. of the problem.

For consistency one can evaluate the real limit by setting $C = 0$, which directly yields

$$\cos \left(\sqrt{\frac{2M}{\hbar^2} E^s L} \right) = 0 \quad \text{and} \quad \sin \left(\sqrt{\frac{2M}{\hbar^2} E^s L} \right) = 0. \quad (3.14)$$

This can only be fulfilled by real arguments, since $\cosh(x)$ has no real root and $\cos(x)$ and $\sin(x)$ no mutual one:

$$\cos(x + iy) = \cos(x) \cosh(y) - \sin(x) \sinh(y) = 0 \quad \Rightarrow \quad x = \left(n + \frac{1}{2} \right) \pi, \quad y = 0 \quad (3.15)$$

$$\sin(x + iy) = \sin(x) \cosh(y) + \cos(x) \sinh(y) = 0 \quad \Rightarrow \quad x = n\pi, \quad y = 0. \quad (3.16)$$

Therefore E has to be real and is given by

$$E^s = \frac{\hbar^2 \pi^2}{2ML^2} \left(n + \frac{1}{2} \right)^2 \quad \text{and} \quad E^a = \frac{\hbar^2 \pi^2}{2ML^2} n^2. \quad (3.17)$$

This is followed by $k_1^s = k_2^s =: k_n^s = \frac{\pi}{L} \left(n + \frac{1}{2} \right)$ and $k_1^a = k_2^a =: k_n^a = \frac{\pi}{L} n$ and the identities

3 Complex square well potential

$$e^{\pm ik_n^s L} = \pm i \xi_n, \quad \sin k_n^s(x \pm L) = \pm \xi_n \cos k_n^s x, \quad \cos k_n^s(x \pm L) = \mp \xi_n \sin k_n^s x, \quad (3.18)$$

where we have introduced

$$\xi_n := \begin{cases} -1 & , n \text{ is odd} \\ +1 & , n \text{ is even} \end{cases}. \quad (3.19)$$

Thus, we can extract the solutions of the familiar real potential well by choosing $\varphi^s = 0$ and $\varphi^a = \pi/2$ for the so far undetermined phase factors of A^s and A^a :

$$E_{j,0}^s = \frac{\hbar^2 \pi^2}{8ML^2} (2j+1)^2, \quad \psi^s(x) = \frac{1}{\sqrt{L}} \cos k_j^s x, \quad (3.20)$$

$$E_{j,0}^a = \frac{\hbar^2 \pi^2}{2ML^2} j^2, \quad \psi^a(x) = \frac{1}{\sqrt{L}} \sin k_j^a x, \quad (3.21)$$

with $k_j^s = j \frac{\pi}{L}$ and $k_j^a = (j + \frac{1}{2}) \frac{\pi}{L}$ for $j \in \mathbb{N}$ and $|x| < L$. Thus the real limit provides a reasonable choice for the phase factors of the normalization constants. The same results for E and ψ can be obtained by evaluating $w \rightarrow 0$, which is indeed nothing else than the familiar real potential well, since area 2 disappears. In this context we should spend some time on evaluating the other extreme case of $w \rightarrow L$, that is area 1 and 3 are vanishing. The solutions of the quantization conditions (3.12) and (3.13) in this limit are

$$E_{j,\infty}^s = \frac{\hbar^2 \pi^2}{8ML^2} (2j+1)^2 - iC, \quad \psi^s(x) = \frac{1}{\sqrt{L}} \cos k_j^s x, \quad (3.22)$$

$$E_{j,\infty}^a = \frac{\hbar^2 \pi^2}{2ML^2} j^2 - iC, \quad \psi^a(x) = \frac{1}{\sqrt{L}} \sin k_j^a x. \quad (3.23)$$

There is a reason why we added the indices 0 and ∞ on the different limits, which has something to do with the behaviour of the energy eigenvalues for $C \rightarrow \infty$ and will become clear later. Comparing both limits it catches the eye that the wave functions and the real part of the energies coincide. The imaginary part of E vanishes for $w \rightarrow 0$, while it decreases linearly with C for $w \rightarrow L$. This limit is nothing else than a normal potential well with an additional imaginary depth C . The imaginary part of E has nothing to do with the kinetic energy, since it does not depend on the energy level j . Thus the imaginary depth of the well is simply added to the real kinetic part of E . However, the wave function stays the same in both cases but we have to note that we only deal with static solutions. The imaginary part plays an important role in view of the time evolution of ψ as we have already seen in the previous section. From (2.8) we can read off that, since $C > 0$, we can interpret the imaginary part of E as a measure, how strong the corresponding density is damped if the whole potential well is affected by the imaginary potential.

3.2 Energies

We start with defining dimensionless quantities, which we use to formulate dimensionless quantization conditions for the energy. Therefore we renormalize the length scale by the total extension L of the system so that the total extension in the new variables is given by a fixed real number π . Additionally, also the energy scale is renormalized by the ground-state energy of a real potential well with this dimensionless width:

$$\varepsilon := \frac{E}{\frac{\hbar^2}{2M} \left(\frac{\pi}{2L}\right)^2}, \quad c := \frac{C}{\frac{\hbar^2}{2M} \left(\frac{\pi}{2L}\right)^2}, \quad \kappa := \frac{k}{\frac{\pi}{2L}}, \quad \chi := \frac{x}{\frac{2L}{\pi}}, \quad \omega := \frac{w}{\frac{2L}{\pi}}. \quad (3.24)$$

In these new variables the energy of the symmetric states for vanishing dissipation reads $\varepsilon_{R,j}(0) = (2j + 1)^2$, so the symmetric ground state for the real potential well is characterized by $j = 0$ in (3.20). For the antisymmetric states this condition reads $\varepsilon_{R,j}(0) = (2j)^2$ and thus it seems to be comfortable to assign to every energy of a symmetric state the natural number $m := 2j + 1$ and to every antisymmetric state $m := 2j$ for vanishing c . Therefore, all states denoted with an odd m are symmetric, while all states denoted with an even m are antisymmetric for $c = 0$. Thus the symmetric ground state is denoted by ε_1 , the first antisymmetric excited state by ε_2 and so on. We can conclude that every reasonable solution of (3.26) and (3.27) has now to fulfill $\varepsilon_{R,m}(0) = m^2$ and $\varepsilon_{I,m}(0) = 0$ like we found out in the discussion of the real limit. This new assignment will make it easier to do a general evaluation of all involved states.

In terms of dimensionless variables we can calculate the quantities of interest for our experimental setup by inserting (3.24) into (1.4) and (1.8) for $w = 100$ nm:

$$\omega = \frac{\pi}{2L} = 2 \cdot 10^{-4} \quad \text{and} \quad c = \frac{8ML^2}{\hbar^2\pi^2}C = 8 \cdot 10^4. \quad (3.25)$$

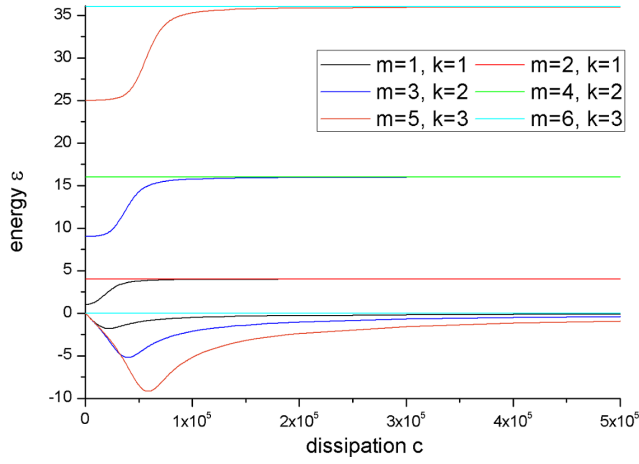
Moreover the quantization conditions (3.12) and (3.13) now read

$$0 = \sqrt{\varepsilon^s} \cot \left[\left(\omega - \frac{\pi}{2} \right) \sqrt{\varepsilon^s} \right] + \sqrt{\varepsilon^s + ic} \tan \left(\omega \sqrt{\varepsilon^s + ic} \right), \quad (3.26)$$

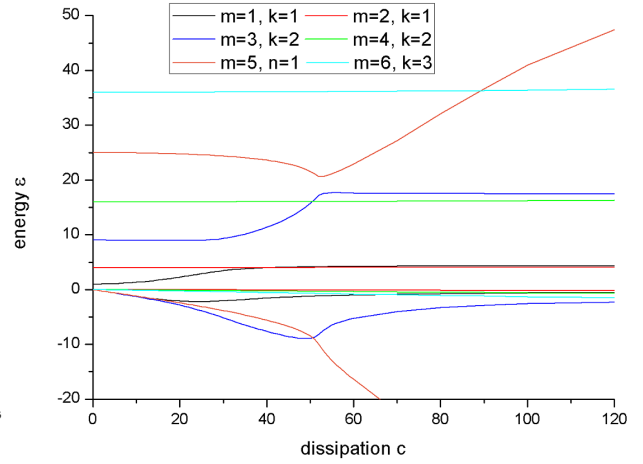
$$0 = \sqrt{\varepsilon^a} \cot \left[\left(\omega - \frac{\pi}{2} \right) \sqrt{\varepsilon^a} \right] - \sqrt{\varepsilon^a + ic} \cot \left(\omega \sqrt{\varepsilon^a + ic} \right). \quad (3.27)$$

It is quite straight forward to find the roots $\varepsilon(c, \omega)$ of the right-hand side of (3.26) and (3.27) for given c and ω numerically. For increasing values of the dimensionless waist ω we find the corresponding results for the first 6 states shown in Figs. 3.2(a) – 3.2(1):

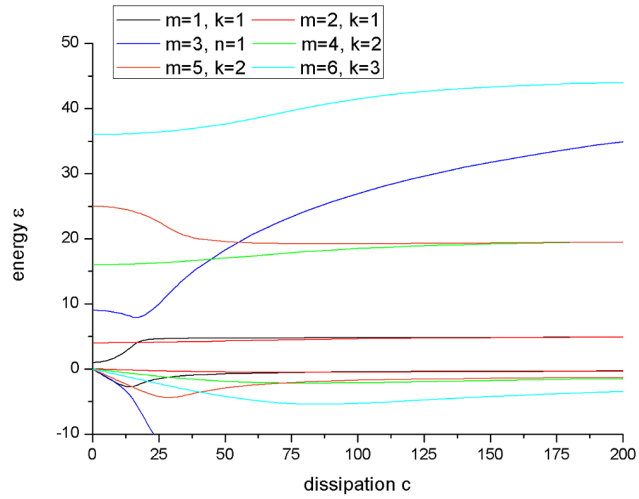
3 Complex square well potential



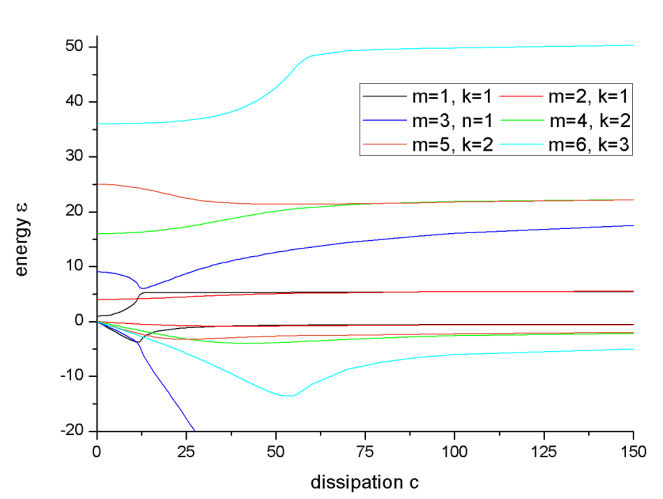
(a) $\omega = 2 \cdot 10^{-4}$



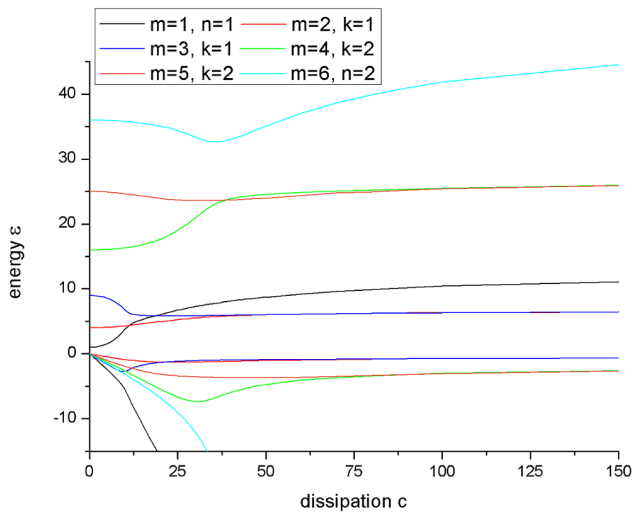
(b) $\omega = 0.1$



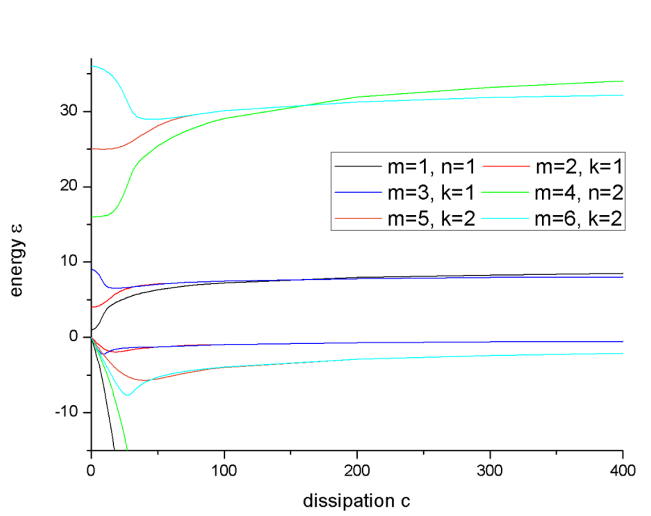
(c) $\omega = 0.2$



(d) $\omega = 0.3$



(e) $\omega = 0.4$



(f) $\omega = 0.5$

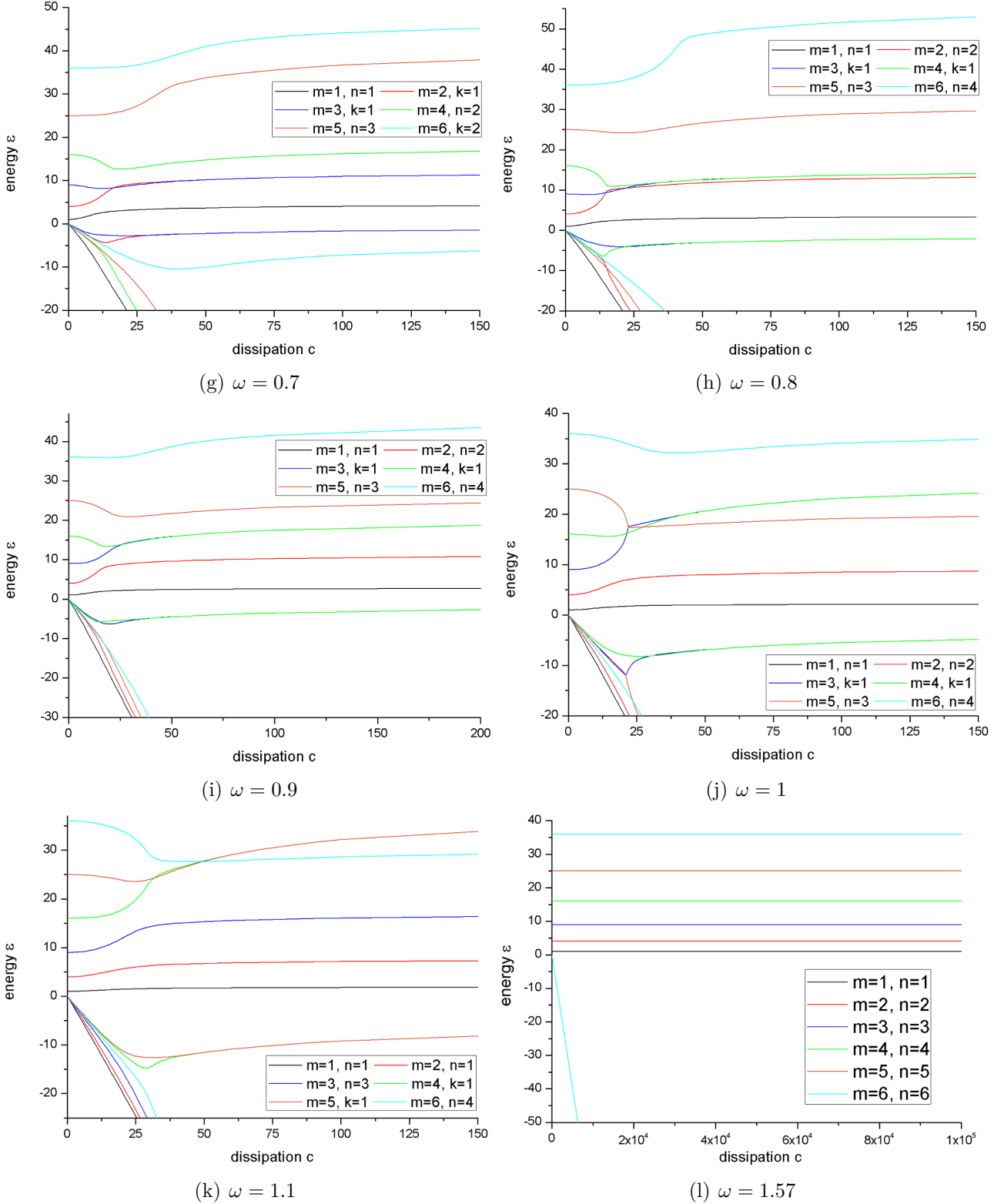


Figure 3.2: Real and imaginary part of the lowest energy eigenvalues as a function of the dimensionless strength c of the imaginary potential. Two curves with the same colour represent the real and imaginary part of the energy of the state, where the real part starts at $\varepsilon_R(c=0) = m^2$ and the imaginary part at $\varepsilon_I(c=0) = 0$. Moreover, ε_∞ -states are counted by integer n while ε_0 -states are counted by integer k . The imaginary parts in Fig. 3.2(l) run quite similarly so only one curve is viewable.

3 Complex square well potential

The most important information these plots give us is the fact that the imaginary part of all states is always negative for $0 < c < \infty$. This consolidates the assumption that the model of an imaginary potential describes dissipation since for the time evolution of the density (2.8) it yields a damping effect.

Furthermore, the results of the real limit $c \rightarrow 0$ are confirmed in Figs. 3.2(a) – 3.2(l) since the real part of the energy starts at some squared natural number $\varepsilon_R(c = 0) = m^2$ and the imaginary part exactly at zero. Thus these solutions include the states of the real square well potential.

It immediately catches the eye that we can generally differ between two kinds of solutions which are characterized by their imaginary part. For the states of the one type it is $\lim_{c \rightarrow \infty} \varepsilon_I = 0$ and for the other type a deeper consideration yields a linear decay $\lim_{c \rightarrow \infty} \varepsilon_I = \lim_{c \rightarrow \infty} (-c) = -\infty$. These limits correspond exactly to the imaginary part of the energies we obtained by evaluating $\omega \rightarrow 0$ and $\omega \rightarrow \frac{\pi}{2}$, which is $\varepsilon_{I,0} = 0$ and $\varepsilon_{I,\infty} = -c$ in dimensionless variables. So while we counted all states for $c = 0$ by m , now for $c \rightarrow \infty$ states with $\lim_{c \rightarrow \infty} \varepsilon_I = 0$ are counted by k so that we call them *k-states* ε_0^k , and states with $\lim_{c \rightarrow \infty} \varepsilon_I = -\infty$ are counted by n so that we call them *n-states* ε_∞^n .

Observing all 12 pictures one can see that for small waists there are only *k-states* among the lowest six states. For some $\omega < 0.1$ the first *n-state* enters these lowest states namely the state starting at $m = 5$. In the course of increasing ω more and more states become *n-states*, so for some big waist $\omega > 1.1$ even the $k = 1$ -state is dropped out. Then we are left with 6 *n-states* among the lowest 6 energy levels so that for $\omega = \frac{\pi}{2}$ we have reached the constellation that we calculated in Section 2 for $w = L$. Thus both limits are connected by a continuous rearrangement of *k-* and *n-states* among the lowest states.

Now let us take a look at the situations where the waist is very close to 0 or $\frac{\pi}{2}$ which yields that area 2 or area 1 and 3 approximately vanish, respectively.

3.2.1 Regime of vanishing areas

We start with comparing Fig. 3.2(a) and Fig. 3.2(l) which represent a very small waist $\omega \gtrsim 0$ and a very large waist $\omega \lesssim \frac{\pi}{2}$, respectively. From our former discussion we expect that approximately the same constellation is represented as we calculated for the limits $\omega = 0$ and $\omega = \frac{\pi}{2}$, that means $\varepsilon_0^k \approx k^2 = m^2$ and $\varepsilon_\infty^n \approx n^2 - ic = m^2 - ic$. This means that in both cases the real part is approximately unaffected of the dissipation c so for every strength of dissipation it should be nearly equal to m^2 . The imaginary part of the *k-states* for $\omega \gtrsim 0$ is nearly equal to zero for all values of c and the imaginary part of the *n-states* for $\omega \lesssim \frac{\pi}{2}$ approximately decreases with $-c$ to $-\infty$, so $\varepsilon_{I,\infty}^n + c$ is nearly equal to zero for all values of c .

Let us compare this with the respective images and start with the *n-states*. Fig. 3.2(l), where $\omega = 1.57 \approx \frac{\pi}{2}$, shows that the real part is nearly constant and equal to $n^2 = m^2$ so the real part is correct. To prove for the imaginary part $\varepsilon_{I,\infty}^n \approx -c$ it seems to be more comfortable to have a look at $\varepsilon_{I,\infty}^n + c$ and to show that it tends to be equal to zero for all c and $\omega \rightarrow \frac{\pi}{2}$:

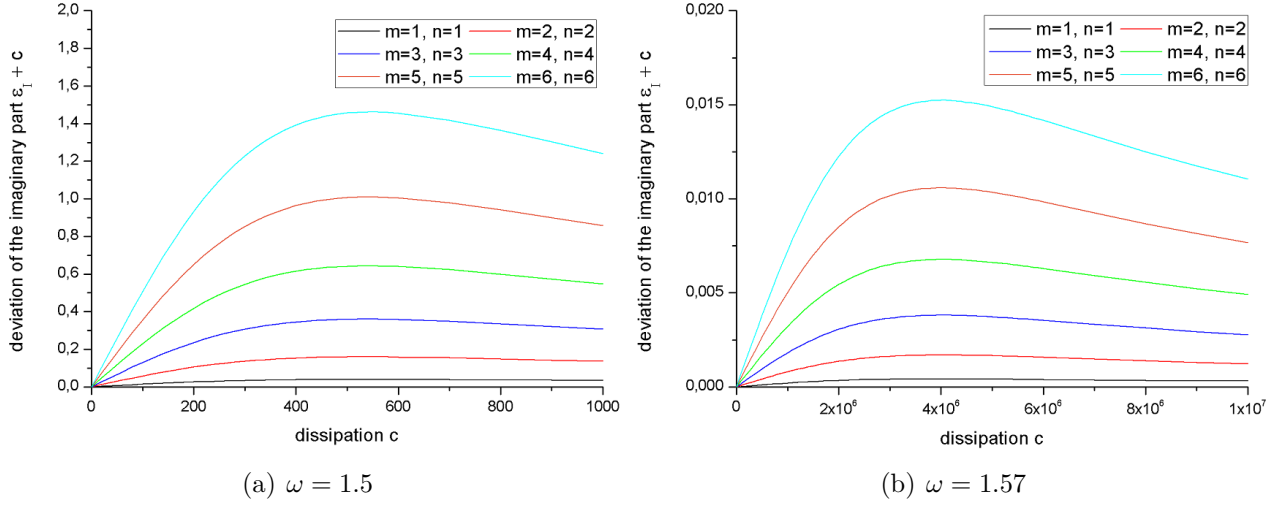


Figure 3.3: The deviation of $\varepsilon_{I,\infty}^n$ from $(-c)$ reveals a maximum at some dissipation and then decreases asymptotically to zero. We see that the height of the maximum decreases with increasing ω .

Figs. 3.3(a) and 3.3(b) imply $\lim_{\omega \rightarrow \frac{\pi}{2}} \varepsilon_{I,\infty}^n = -c$, so for big waists the n -states fulfill the condition $\lim_{\omega \rightarrow \frac{\pi}{2}} \varepsilon_{\infty}^n = n^2 - ic$.

In contrast to this Fig. 3.2(a) unfortunately does not approximately yield the correct results for the limit $\omega \rightarrow 0$ which would be constant $\varepsilon_R = m^2$ and $\varepsilon_I = 0$ for all values of c . This is just true for the antisymmetric states, that means for even m . Here the real part is nearly constant and equal to n^2 and the minimum of the imaginary part decreases with $\omega \rightarrow 0$ and vanishes for $\omega = 0$.

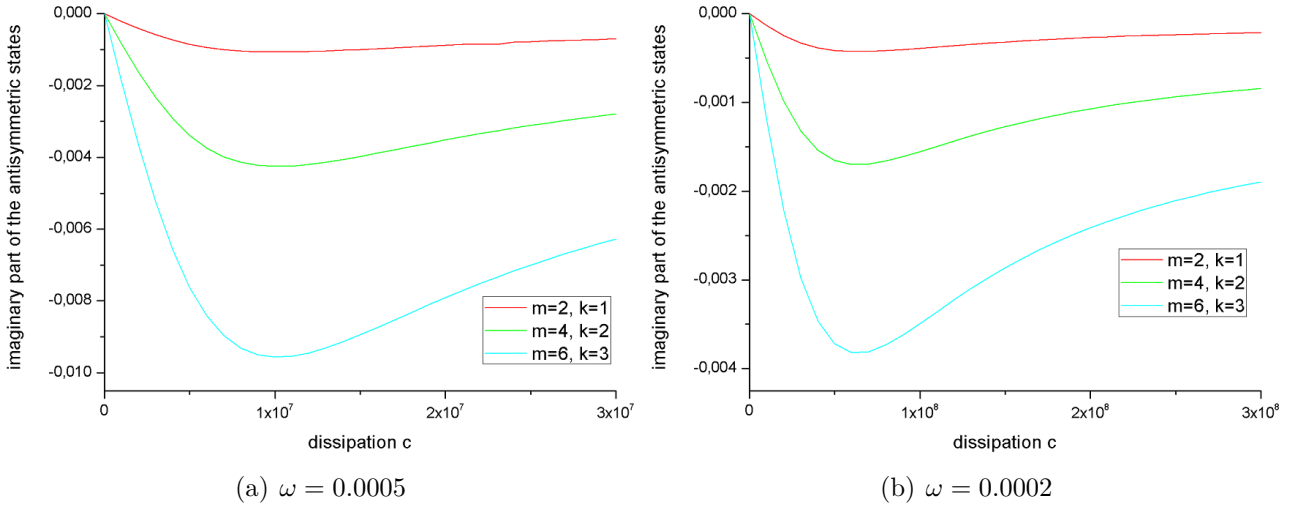


Figure 3.4: The imaginary part $\varepsilon_{I,0}^n$ of the k -states, which are antisymmetric for $c = 0$, reveals a minimum at some dissipation and then decreases asymptotically to zero. We see that the depth of the minimum decreases with decreasing ω .

So the antisymmetric states are fine. In contrast for the symmetric states the real part of the energy $\varepsilon_{R,0}^{k,s}$ indeed starts at the square of some odd m but then raises and ends up at an even one for every $\omega \gtrsim 0$, which means it coincides with an antisymmetric state. Furthermore $\varepsilon_{I,0}^{k,s}$ is not approximately equal to zero for all c . There are minima with a depth that do not decrease with

3 Complex square well potential

$\omega \rightarrow 0$ at all as we can see by comparing with Figs. 3.2(b) – 3.2(k). So from this point of view both real and imaginary part do not show any tendency for $\omega \rightarrow 0$ to coincide with the calculated limit $\lim_{\omega \rightarrow 0} \varepsilon_0^k = k^2 = m^2$ at all. This looks inconsistent but at a later point of this discussion we will give an interpretation that provides an appropriate explanation of this.

First we spend some time on looking at the particular strength of dissipation the maxima and minima of the imaginary part occur at. Let us call it c_{crit} which seems to depend on the particular waist ω and state m we are considering. From Figs. 3.3(a) – 3.4(b) we can read off that c_{crit} obviously increases for $\omega \approx 0$ with decreasing ω and for $\omega \approx \frac{\pi}{2}$ with increasing ω , respectively. Moreover, considering the symmetric states in Fig. 3.2(a) shows that the real part reaches its biggest slope at c_{crit} that means it has an inflection point right there. A closer look on the antisymmetric states in Fig. 3.2(a) and on the n -states in Fig. 3.2(l) as well provides the same insight. So it seems that c_{crit} denotes the dissipation, where the energy has its largest deviation from the limits we just discussed, that is for ε_R being constant and for $\varepsilon_{I,0}^k$ as well as for $\varepsilon_{I,\infty}^n$ being equal to zero.

Many things we have introduced and discussed so far can be generalized to arbitrary waists $0 \leq \omega \leq \frac{\pi}{2}$, so we continue with the regime where all areas yield similar extensions.

3.2.2 Three areas regime

Now let us take a look at the remaining pictures, that is the regime $0.1 \leq \omega \leq 1.1$, where both types of states are coexisting among the lowest six energy levels. First we can generalize the concept of c_{crit} since $\varepsilon_{I,0}^k$ and $\varepsilon_{I,\infty}^n + c$ reveal also in this case minima and maxima.

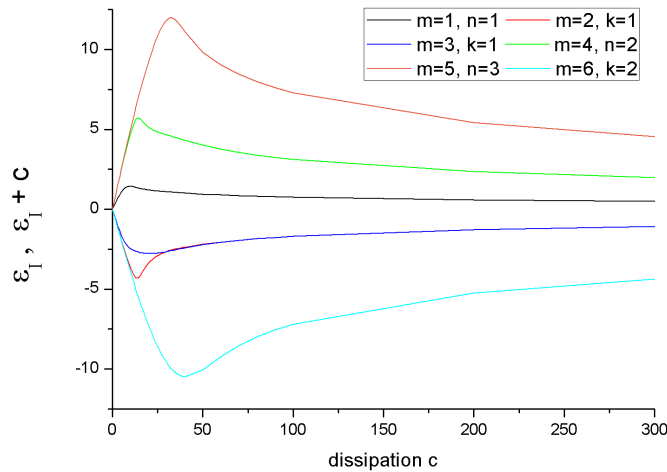


Figure 3.5: $\varepsilon_{I,0}^k \leq 0$ (minima) and $\varepsilon_{I,\infty}^n + c \geq 0$ (maxima) plotted for $\omega = 0.7$.

Considering Figs. 3.2(b) – 3.2(k) yields that for intermediate waists c_{crit} also represents an inflection point of the real part of the energy, so its largest slope. Thus we can conclude that the critical dissipation exhibits the largest deviation from the limits $\omega \gtrsim 0$ and $\omega \lesssim \frac{\pi}{2}$ in the same way as we found out in the end of the previous subsection.

Since there occur only k -states for $\omega \gtrsim 0$ and only n -states for $\omega \lesssim \frac{\pi}{2}$ in the course of continuous rearrangement a kind of continuous transfer of lower k -states with higher n -states for increasing

ω have to take place. Even for $\omega = 0.1$ there are much more k -states than n -states in contrast to $\omega = 1.1$ which is instead dominated by n -states. Let us have a closer look at this process by observing the states for small dissipation $c \ll c_{\text{crit}}$, intermediate dissipation $c \approx c_{\text{crit}}$ and at last for large dissipation $c \gg c_{\text{crit}}$. In this context we will often talk about states, that "start" at some m and "continue" at some k or n . This way of speaking means nothing else than that the state is characterized by m for $c = 0$, so it starts there, and by k or n for $c \rightarrow \infty$. This particular assignment between m on the one hand and k or n on the other hand changes obviously for increasing waists and we are going to describe it this way.

3.2.2.1 Small dissipation

First we will have a more detailed discussion of the energies for $c \ll c_{\text{crit}}$ and start with $c = 0$. Figs. 3.2(a) – 3.2(l) show that the imaginary part of all states starts at $\varepsilon_I(0) = 0$ and the real part at 1, 4, 9, 16, 25 and 36, that is $\varepsilon_R(0) = m^2$ as we claimed. So m is the number characterizing the behaviour of each state for $c = 0$ and represents the connection to the familiar real potential well. This does not change much for small $c > 0$ since for small dissipation the imaginary part is always decreasing with c so it is not possible to decide whether a state is a k -state or an n -state. Thus for $c \ll c_{\text{crit}}$ all states are m -states corresponding to the states of the familiar real potential well for $c = 0$ characterized by the integer number m .

3.2.2.2 Intermediate dissipation

Next we consider $c \approx c_{\text{crit}}$. For small dissipation $c \ll c_{\text{crit}}$ the energy of the states just differ slightly from these of the real potential well. For stronger dissipation this difference generally grows especially for the imaginary part which is continuously decreasing with increasing dissipation for $c < c_{\text{crit}}$. So instead of the exact separation the real parts $\varepsilon_R \approx m^2$ yield for $c \ll c_{\text{crit}}$, now some of them have to get closer together, because some are increasing and others are decreasing for growing $c < c_{\text{crit}}$. Now $c \approx c_{\text{crit}}$ is the particular value of dissipation where the characterization of all states changes from m to k or n , respectively. One can understand this by observing the imaginary part for growing c . For $c < c_{\text{crit}}$ it is decreasing for all states with a slope $-1 < \frac{d\varepsilon_I}{dc} < 0$. For $c = c_{\text{crit}}$ either ε_I exhibits a minimum so that it increases for $c > c_{\text{crit}}$, tends to zero again and thus turns out to be a k -state, or its slope is even decreasing for $c > c_{\text{crit}}$ so that the deviation $\varepsilon_I + c$ exhibits a maximum and the state turns out to be an n -state. Thus for $c = c_{\text{crit}}$ the transfer of the m -states characterized by m to k - and n -states characterized by k and n takes place.

Furthermore, there are various waists for that this assignment of an m -state to a k - or n -state changes, for example for some waist within $\omega = 0.3$ in Fig. 3.2(d), where the $m = 1$ -state continues as the $k = 1$ -state and the $m = 3$ - as the $n = 1$ -state, and $\omega = 0.4$ in Fig. 3.2(e), where this assignment is exactly vice versa. Let us denote waists, where such a transfer occurs at, with $\omega_{\text{crit}}^{k,n}$, where k and n denote the involved k - and n -state. Unfortunately it is not possible to determine a particular value for such critical waists exactly since all solutions for given ω and c have been calculated numerically and then combined to a continuous graph $\varepsilon(\omega, c)$. Thus it is not possible to find an exact value for any $\omega_{\text{crit}}^{k,n}$, because there is no rule to which curve a single numerical solution for fixed c and ω has to assigned if two curves get really close together. So it depends on the particular assignment when the transfer occurs. Since this is performed manually it is not exactly determined:

3 Complex square well potential

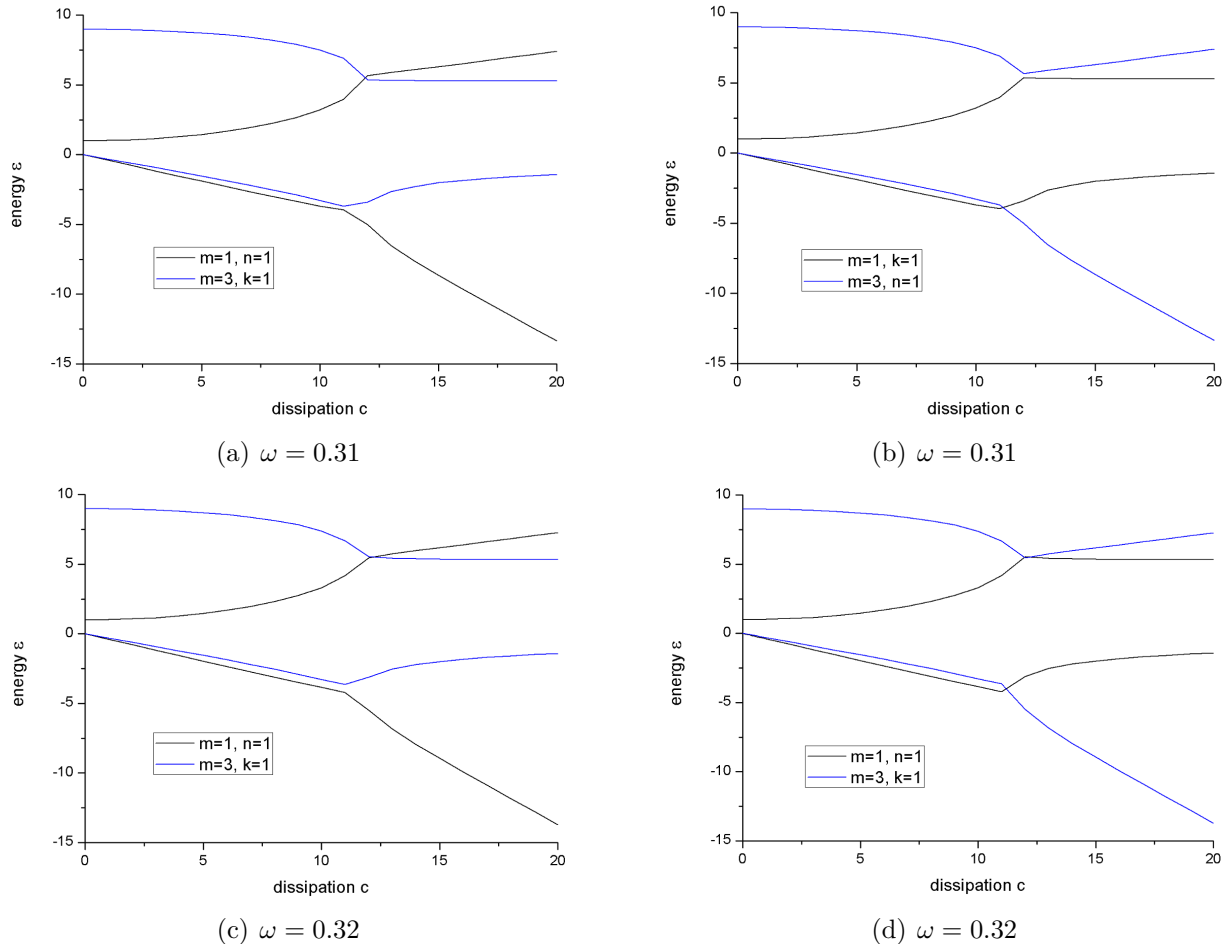


Figure 3.6: Possible assignment of $(k = 1)$ - and $(n = 1)$ -states to $(m = 1)$ - and $(m = 3)$ -states for $\omega = 0.31$ and $\omega = 0.32$. Both assignments seem to be possible, which yields, that until we have no expression for $\varepsilon(c, \omega)$, there is no single value $\omega_{\text{crit}}^{1,1}$ but an interval of waists for which such an exchange occurs.

Nevertheless there are some observable indicators that signalize such a critical waist. First of all it is important to know the circumstances, where such a changeover takes place. It is always a pair of two adjoining m -states with the same parity, so for instance m and $m + 2$, where the lower m -state is a k -state and the upper $(m + 2)$ -state an n -state with the same parity as both m -states for $\omega < \omega_{\text{crit}}^{k,n}$. After the interchange the $(m + 2)$ -state is the k -state and the m -state the n -state. Thus there belongs respectively one $\omega_{\text{crit}}^{k,n}$ to every pair of one k - and n -state with the same parity (both even or both odd).

For all waists such a changeover is imminent, there seems to be a kind of interaction between the involved two states that becomes stronger for $\omega \rightarrow \omega_{\text{crit}}$. Even for very small dissipation their real parts strongly curve towards each other until they get very close. The imaginary parts run nearly equally so that it is not possible to decide clearly which one will continue as a k - and which one as an n -state. Then one of them suddenly reveals a minimum and increases again while the other one also suddenly decreases its slope which then tends to $-c$, so that $\varepsilon_I + c$ reaches a maximum for this state. This is the point where c_{crit} is reached and one k - and one n -state emerge instead of the two m -states as we can see in Fig. 3.6. Since the imaginary parts of both m -states yield quite similar slopes, the particular assignment of the m - and $(m + 2)$ -state to the developing k -

and n -state is not clear. The strong curvature of ε_R effects that this happens even for very small dissipations, so c_{crit} is really small for $\omega \approx \omega_{\text{crit}}$ which is characteristic for such an interchange.

Therefore a strong curvature and a small c_{crit} as well as a deep minimum of $\varepsilon_{I,0}^k$ and a high maximum of $\varepsilon_{I,\infty}^n + c$ are signals for $\omega \approx \omega_{\text{crit}}^{k,n}$. On the other hand if the real parts run very flat, the extrema of $\varepsilon_{I,0}^k$ as well as $\varepsilon_{I,\infty}^n + c$, respectively, are quite flat and c_{crit} is large, this implies that there is no state of the opposite type (k or n) around it with which it can interact with.

With this insight we can give an explanation of the apparent inconsistency that Fig. 3.2(a) does not approximately exhibit the calculated states for the limit $\omega \rightarrow 0$ which would yield a constant real part and an imaginary part equal to zero. Figs. 3.3(a) – 3.4(b) confirm that for an n -state or a k -state, starting at some even m , c_{crit} is very large if there is no state of the opposite type (k or n) around as well as that the maxima of $\varepsilon_{I,\infty}^n + c$ and the minima of $\varepsilon_{I,0}^k$ are very flat. For $\omega \gtrsim 0$ and $\omega \lesssim \frac{\pi}{2}$ this is fulfilled for the lowest energy levels and Figs. 3.3(a) – 3.4(b) yield a very large c_{crit} and very flat maxima and minima for $\varepsilon_I + c$ and ε_I , respectively. We already checked that for $\omega = 0$ and $\omega = \frac{\pi}{2}$ the maxima and minima of the states, we just mentioned, are equal to zero which is equivalent to $\varepsilon_{I,0}^k \equiv 0$ and $\varepsilon_{I,\infty}^n \equiv -c$ for all c . Unfortunately this was not true for the k -states starting at some odd m since we observed that the depth of the minimum does not tend to zero for $\omega \rightarrow 0$. Now we found an additional effect which holds for all states in the limits $\omega \rightarrow 0$ and $\omega \rightarrow \frac{\pi}{2}$. Since c_{crit} becomes very large if no state of the opposite type is around and for $\omega = 0$ and $\omega = \frac{\pi}{2}$ only one type of states is present at all, the deduction $c_{\text{crit}} \rightarrow \infty$ seems to be reasonable. Thus for the symmetric states in Fig. 3.2(a) the particular point, where the minimum of the imaginary part occurs at as well as where the real part suddenly increases and fuses with the upper antisymmetric state, moves over to infinity. Therefore, since the curves look nearly constant and equal to $\varepsilon(c = 0)$ for $c \ll c_{\text{crit}}$, this implies that for $c_{\text{crit}} \rightarrow \infty$ the regime of small dissipation dominates everywhere and these curves are constant and equal to these values so $\varepsilon_R^m \equiv m^2$ and $\varepsilon_I^m \equiv 0$ for all $0 < c < \infty$.

Summing up the discussion of intermediate dissipation it is important that for $c < c_{\text{crit}}$ and $\omega \approx \omega_{\text{crit}}$ there are always two adjoining m -states with the same parity, that is m and $m + 2$, from which one k -state and one n -state arise, respectively. Moreover the n -state succeeds the parity of the corresponding m -states in contrast to the k -state. Thus m -states of the opposite parity, even the $(m + 1)$ -state in between, are completely unaffected of this procedure, since the n -state arising from the m - or $(m + 2)$ -state can never evolve from the $(m + 1)$ -state, because it has the opposite parity.

Now we can understand how both limits, $\omega \gtrsim 0$ dominated by k -states and $\omega \lesssim \frac{\pi}{2}$ dominated by n -states among the 6 lowest energy levels, are connected with each other. Via the described interchange the energy, the curves of the k -states run at, generally increases with ω while the energy of the n -states generally decreases. For some $\omega = \omega_{\text{crit}}^{k,n}$ they have to cross and interchange. Thus the k -states run at increasing energies for increasing ω and for some waist there is no k -state any more among the lowest 6 energy levels.

3.2.2.3 Large dissipation

We already explained that the imaginary part allows us to divide all states generally into two groups, which we already characterized in the general discussion and then called k -states ε_0^k and n -states ε_∞^n . Since m describes the states for small dissipation $c \ll c_{\text{crit}}$ and we just discussed

3 Complex square well potential

that this changes for intermediate waists $c \approx c_{\text{crit}}$ from m to k or n the states for large dissipation $c \gg c_{\text{crit}}$, the states are characterized only by the integer number k or n , which is not clearly ascribable to a particular m as we just stated.

Here always two $\varepsilon_{I,0}^k$ -states are fusing for $c \rightarrow \infty$ so we denoted them with the same k . These pairs consist on a k -state starting at some odd m and one starting at one adjoining even $m \pm 1$ so a symmetric and an antisymmetric state. Moreover we know from Fig. 3.2(a) that it is the state starting at some odd m which approaches to the state started at some even m . The indeterminacy of the assignment $m \leftrightarrow k$ if $\omega \approx \omega_{\text{crit}}^{k,n}$ does not matter since anyhow, if the considered ω is approximately equal to some critical waist, both possible k -states starting at m or $m + 2$ yield the same parity which is opposite to this of the $m + 1$ -state.

It is interesting that all pairs of such fusing k -states have this property that they start at adjoining values of m for all ω . This is related to the fact that the n -states are ordered by the real part of the energy and never intersect each other, that means that the real part of states with higher n run at higher energies than states with smaller n for all c . We already know that the energy, these real parts run at, decreases for increasing ω so that interchanges with the upcoming real parts of the k -states occur but the order of the n -states does not change. So after a k -state starting at some odd m pairing with the k -state starting at $m + 1$, which is even, has interchanged with some symmetric n -state, it then starts at $m + 2$, so the property of pairs m and $m \pm 1$ is still fulfilled. Because of the order of the n -states the next downcoming n -state is an antisymmetric one, which interchanges with the other k -state which starts at $m + 3$ after that and the property is once more fulfilled. This procedure repeats until all k -states populating the potential well for $\omega = 0$ have been redistributed to much more higher energies for $\omega \rightarrow \frac{\pi}{2}$ until exclusively n -states are present when this limit is reached.

Next we still consider the limit $c \rightarrow \infty$. For the imaginary part the limits $\lim_{c \rightarrow \infty} \varepsilon_{I,0}^k = 0$ and $\lim_{c \rightarrow \infty} \varepsilon_{I,\infty}^n = \lim_{c \rightarrow \infty} (-c) = -\infty$ seem to be accurate. For the real parts we assume that they are converging to some finite real number which seems to be plausible since on the one hand it is implied by the numerical evaluation and on the other hand we know that they are converging for $\omega = 0$ and $\omega = \frac{\pi}{2}$ since they are constant in these cases. These should be continuously reached limit cases so the real part should converge for all waists.

So let us make the ansatz $\lim_{c \rightarrow \infty} \varepsilon_{I,0}^k = 0$ and $\lim_{c \rightarrow \infty} \varepsilon_{I,\infty}^n = -c$ and insert this into the quantization conditions (3.26) and (3.27) to derive expressions for symmetric and antisymmetric k - and n -states from these assumptions. Performing this and summing up the results of both (3.26) and (3.27) provides indeed analytical results:

$$\varepsilon_{R,0}^{k,\text{sat}} = \left(k \frac{\pi}{\frac{\pi}{2} - \omega} \right)^2, \quad \varepsilon_{R,\infty}^{n,\text{sat}} = \left(n \frac{\pi}{2\omega} \right)^2. \quad (3.28)$$

The results of these equations coincide perfectly with the numerical solutions for large c . They confirm that for $\omega = 0$ there are only k -states present, since then $\varepsilon_{R,\infty}^n$ diverges, and for $\omega = \frac{\pi}{2}$ the k -states are vanishing since then the energy they run at goes to infinity.

They also include the fact that the symmetric k -states tend to the antisymmetric ones as we can see in Fig 3.2(a), because

$$\lim_{\omega \rightarrow 0} \varepsilon_{R,0}^{k,\text{sat}} = (2k)^2, \quad (3.29)$$

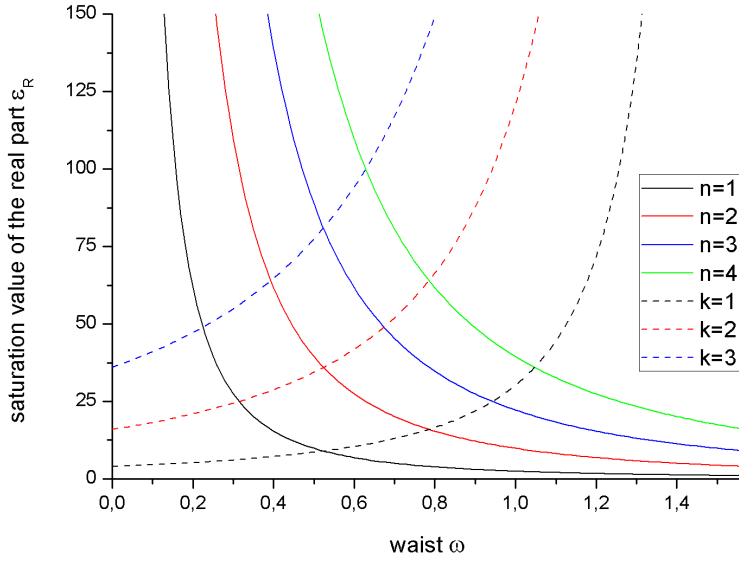


Figure 3.7: Saturation values of the real part of the energy $\varepsilon_R(\omega)$ for the k - and n -states. For $\omega = \frac{\pi}{2}$ the real part of the n -states reach n^2 , while for $\omega = 0$ the k -states reach $(2k)^2$.

which is the energy of the antisymmetric k -states. This shows that the limits of ω and c can not be interchanged since the limit $\omega \rightarrow 0$ yields (3.20) and (3.21) which would be followed by $\varepsilon_{R,0}^{k,\text{sat}} = k^2$. One can explain this by taking both combinations of the limits for the imaginary part of the potential, where the one yields $\lim_{c \rightarrow \infty} \lim_{\omega \rightarrow 0} V_I \equiv 0$ and the other something including the Dirac-delta distribution $\lim_{c \rightarrow \infty} \lim_{\omega \rightarrow 0} V_I \sim \delta(x)$. However we already solved this problem with the assumption $\lim_{\omega \rightarrow 0} c_{\text{crit}} = \infty$.

In contrast to this for the n -states both limits are obviously compatible since

$$\lim_{\omega \rightarrow \frac{\pi}{2}} \varepsilon_{I,\infty}^{n,\text{sat}} = n^2. \quad (3.30)$$

The expressions in (3.28) are integers k^2 and n^2 weighted with the squared ratio of the full extension π of the well and a smaller length 2ω or $\frac{\pi}{2} - \omega$. These are nothing else than the widths of area 2 on the one hand and on the other hand area 1 and 3, respectively. Thus it seems that (3.28) are the energies of two potential wells with the width 2ω and $\frac{\pi}{2} - \omega$, respectively. Reexpressing them in terms of the original quantities makes this interpretation even more apparent:

$$E_{\text{sat},\infty}^n = \frac{\hbar^2 \pi^2}{2M(2w)^2} n^2, \quad E_{\text{sat},0}^k = \frac{\hbar^2 \pi^2}{2M(L-w)^2} k^2. \quad (3.31)$$

These are nothing else than the energies of a potential well with the width $2w$ and $L - w$, respectively. We will have a discussion of this in the next section since the additional evaluation of the densities makes this even clearer. Nevertheless there is one point we can have a look at now. Eq. (3.31) yields one potential well with the width of area 2 and one with the width of the *half* of the complement of it. We argued so far that n -states belong to area 2 and k -states to its complement but (3.31) shows that the k -states have to be identified with the states of a well with only half the width. So if we take this formula, then the limit (3.29) yields the right energy:

$$\lim_{\omega \rightarrow 0} E_{sat,0}^k = \frac{\hbar^2 \pi^2}{2ML^2} k^2. \quad (3.32)$$

These are all energies of a half-width potential well with the width L instead of $2L$. So it seems that we have to decide between area 2 as well as area 1 and 3, respectively. In the next chapter we will have a closer look on this but for the moment the fusion of respective two k -states may have to do something with the symmetry of the well which means that area 1 and 3 are equivalent and thus indistinguishable so that their states are quite similar.

3.2.3 Critical waists

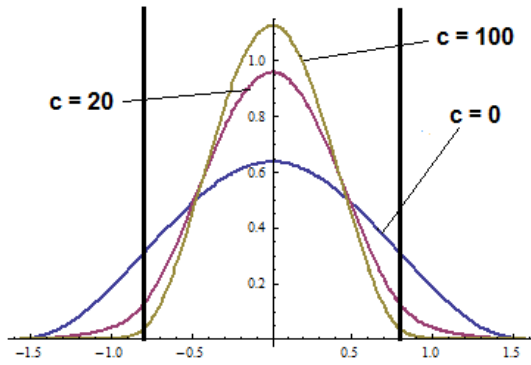
Finally let us have a closer look at the critical waists and Fig. 3.7. Unfortunately the intersections between the curves are not the critical waists we are looking for, because it only reveals when a pair of one k - and one n -state have the same saturation value but provides no insight about as which kind of state an m -state continues for $c > c_{crit}$. Therefore we denote them differently with $\omega_{int}^{k,n}$, where k and n stand for the involved k - and n -state. We can see from Fig. 3.2(b) – 3.2(k) that this does not give much information at which particular waist the interchange occurs, that is $\omega_{crit}^{k,n}$. Having a closer look one additional issue catches the eye. In Figs. 3.2(d) and 3.2(e) the $(n = 1)$ -state interchanges with the $(k = 1)$ -state. Here the interchange occurs for smaller waists than the intersection in Fig. 3.7 between these two states. This means that after the interchange at $\omega_{crit}^{1,1} < 0.4$, when the $(n = 1)$ -state already came down and continues the $(m = 1)$ -state, the saturation value is still higher than this of the corresponding $(k = 1)$ -state until $\omega_{int}^{1,1} = \frac{\pi}{6} > 0.4$. On the other hand Fig. 3.2(j) yields the opposite situation. Here for $\omega = 1$ the interchange is not performed yet but the saturation value of the involved $(n = 3)$ -state is obviously even smaller than this of the corresponding $(k = 2)$ -state as one can also see by comparing with Fig. 3.7 where the intersection occurs at $\omega_{int}^{1,3} = \frac{3}{14}\pi < 1.1$. A third case seems to be revealed by Fig. 3.2(h) where the interchange has just occurred and the curve of the n -state runs only slightly and nearly parallel under the curve of the corresponding k -state. Furthermore, Fig. 3.7 yields with $\omega = \frac{\pi}{4}$ a point of intersection, which would be a quite reasonable choice for $\omega_{crit}^{1,2}$. Exactly the same situation occurs for every pairs of k - and n -state that cross each other in Fig. 3.7 at $\omega = \frac{\pi}{4}$, which are all pairs with $n = 2k$. Thus we assume

$$\omega_{crit}^{k,2k} = \omega_{int}^{k,2k} = \frac{\pi}{4}. \quad (3.33)$$

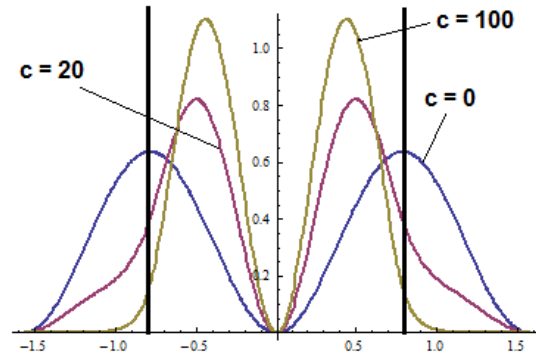
Thus for $\omega = \frac{\pi}{4}$ all k -states interchange with an even n -state, namely $n = 2k$. Fig. 3.2(h) confirms especially for $n = 1$ and $n = 3$ that odd n -states are not interchanging with any k -state for $\omega \approx \frac{\pi}{4}$. A deeper observation of all states exhibits that for all pairs with $\omega_{crit}^{k,n} < \frac{\pi}{4}$ it is $\omega_{crit} < \omega_{int}$ while for $\omega_{crit}^{k,n} > \frac{\pi}{4}$ it is $\omega_{crit} > \omega_{int}$. This might have to do something with the fact, that $\omega = \frac{\pi}{4}$ yields $w = \frac{L}{2}$. This fact should be taken into account for deriving a reasonable definition of ω_{crit} .

3.3 Densities

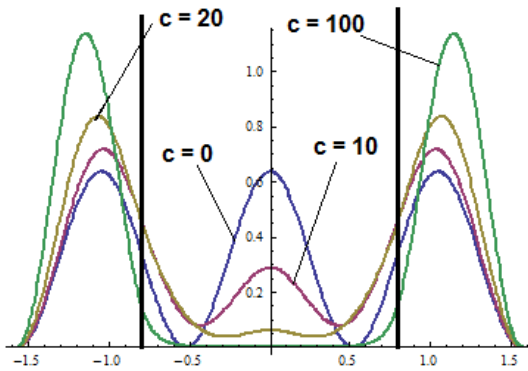
With (3.26) and (3.27) we can directly calculate from $\varepsilon(\omega, c)$ numerical solutions for the dimensionless wavenumbers $\kappa_1(\omega, c)$ and $\kappa_2(\omega, c)$ via (3.8) and (3.24) and thus obtain $\psi(\chi)$ and $\rho(\chi)$.



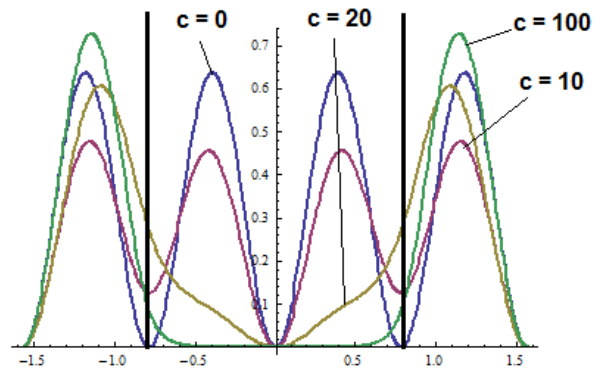
(a) $m = 1, n = 1$



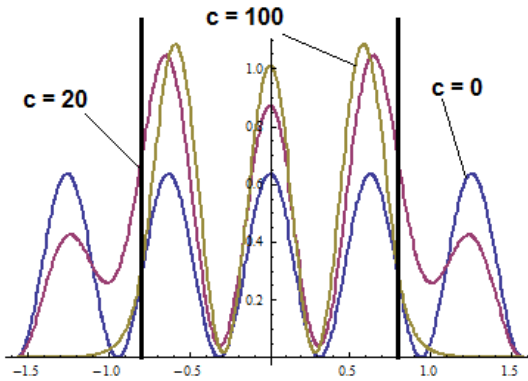
(b) $m = 2, n = 2$



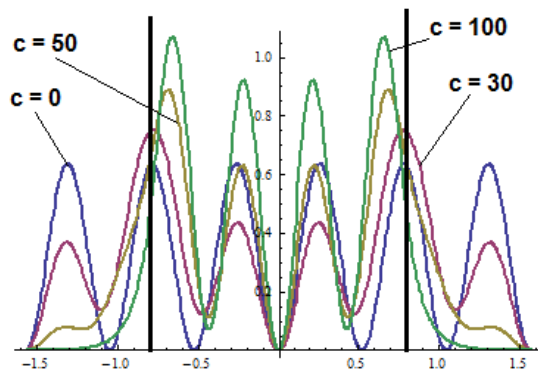
(c) $m = 3, k = 1$



(d) $m = 4, k = 1$



(e) $m = 5, n = 3$



(f) $m = 6, n = 4$

Figure 3.8: Densities of the lowest six states for $\omega = 0.8$ for some values of c . They obviously include the densities of the real limit for $c = 0$ and for large c it catches the eye that k -states tend to the outside, where $V_I = 0$ so they minimize dissipation, while the n -states tend to the center, where $V_I = -C$, so they maximize dissipation. The fusion of two respective k -states, which we already observed in Figs. 3.2(a) – 3.2(l), is confirmed here, too. Furthermore, it shows that two states with the same k indeed end up exactly in the same state.

3 Complex square well potential

We took only an example for one particular waist $\omega = 0.8$, since the general qualitative behaviour of k - and n -states is the same for all waists. Fig. 3.8 shows how the densities develop and change their shape from the familiar form for $c = 0$, which corresponds to the ordinary symmetric and antisymmetric states of the real square well potential with m maxima, to large c . It directly becomes clear how the behaviour of k - and n -states differs for increasing dissipation. While densities of k -states tend to the borders, that is area 1 and 3, these of n -states tend to the center, that is area 2, for increasing c . We remember, that for $\omega \rightarrow \frac{\pi}{2}$, which yields an imaginary potential well affecting the whole system, only n -states occur, while the k -states dominate the system for $\omega = 0$. This is related to the fact that for $c \rightarrow \infty$ two independent potential wells are formed, which means that the states of the respective wells have densities equal to zero in the respective other well.

Thus an appropriate interpretation of the saturation values (3.31) becomes obvious. The observation that two independent potential wells emerge, matches perfectly to the fact that the real part of the energies of the n -states, which then are confined to the inner well with the width $2w$, become these of an ordinary potential well with exactly this width. In contrast a k -state is confined to the borders, that is area 1 and 3. Since this is a non-connected region only antisymmetric states fit since a maximum of the density in the center is not possible. From (3.31) we saw that we can interpret the whole situation also as 3 independent potential wells with the width of each area so that every well is a connected region and thus both symmetric and antisymmetric states emerge. Both interpretations are possible since the corresponding energies are the same:

$$E_k = \frac{\hbar^2 \pi^2}{2M[2(L-w)]^2} (2k)^2 = \frac{\hbar^2 \pi^2}{2M(L-w)^2} k^2. \quad (3.34)$$

The more appropriate interpretation will become apparent while evaluating more general systems where this equality between states living in area 1 and 3, respectively, is not valid any more.

Let us also have a look at the time evolution of these densities. Since we only aim at having a general impression of this, we restrict ourselves only to two cases, that is two waists, where we show the effect of the imaginary potential on the time evolution exemplarily. Therefore we take on the one hand the data of the particular experiment, that is (3.25), and on the other hand $\omega = 0.8$ and $c = 100$ for which we already plotted the densities. First it seems to be reasonable to renormalize also the time t and to deal with the corresponding dimensionless quantity:

$$\tau := \frac{\hbar \pi^2}{8ML^2} t. \quad (3.35)$$

Inserting \hbar , M and L especially for our system provides $t = \tau \cdot 4.5$ s. Thus (2.8) reads

$$\rho(\chi, \tau) = \exp[2\varepsilon_I(\tau - \tau_0)] \rho(\chi, \tau_0). \quad (3.36)$$

Now we consider for both data a superposition of the ($m = 1$)- and the ($m = 4$)-state, that is $\frac{1}{\sqrt{2}}(|1\rangle + |4\rangle)$. Let us start with (3.25). Although we did not plot the corresponding densities in this case, the considered waist is so small that the antisymmetric state does not change much for increasing c , so it is nearly equal to the ($m = 4$)-state for $c = 0$. In contrast to this the

$(m = 1)$ -state changes with increasing c but as we can see from Fig. 3.2(a) it is nearly equal to the antisymmetric $(m = 2)$ -state for $c = 0$. So for $c = 8 \cdot 10^4$ we approximately deal with two antisymmetric states, which are both k -states. Nevertheless the $(m = 1)$ -state yields a much larger absolute value of ε_I while it is approximately equal to zero for the $(m = 4)$ -state. This has a viewable effect on the time evolution:

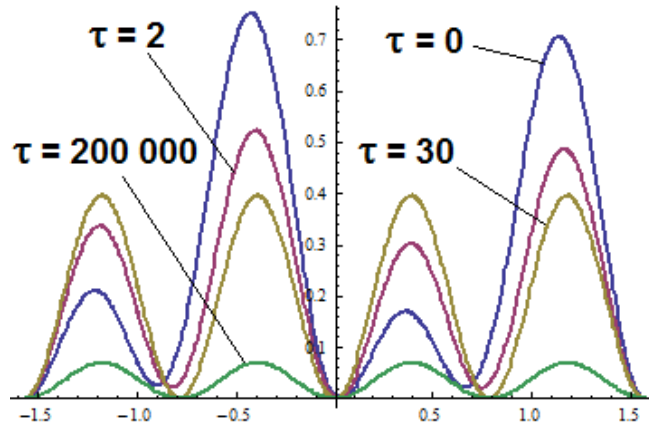


Figure 3.9: The density of the $(m = 1)$ -state is damped much stronger than the $(m = 4)$ -state since even for $\tau = 30$ it has already vanished, while the $(m = 4)$ -state is still present for very large τ .

Here the $(m = 1)$ -state is damped much stronger than the $(m = 4)$ -state which is a consequence of its negligibly small imaginary part of the energy, while for the $(m = 1)$ -state it yields a broad minimum. Let us therefore have a look at the time evolution of both states for $\omega = 0.8$ and $c = 100$. Here we consider not only a symmetric and an antisymmetric one for $c = 0$ but also a k - and an n -state. Thus we expect that the n -state would be damped much stronger since we already argued that this kind of states maximize dissipation:

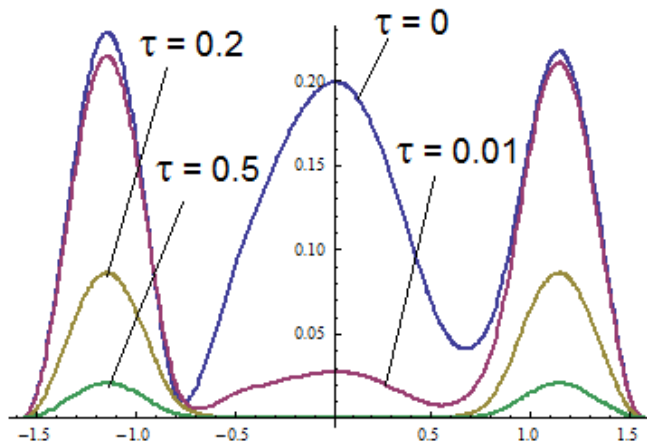


Figure 3.10: This example confirms that n -states are damped much stronger than k -states so n -states maximize dissipation while k -states minimize it.

Here the n -state is damped stronger than the k -state but also both are damped much stronger than for $\omega = 2 \cdot 10^{-4}$. Even for quite small $\tau \approx 1$ even the density of the k -state is almost damped

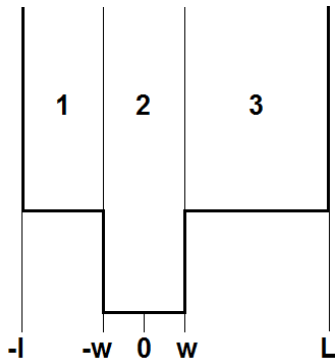
away but we can see again that even for $\tau = 0.2$ only this k -state remains while the n -state has already nearly vanished.

3.4 Related Systems

The last section of this chapter is dedicated to some related systems. On the one hand we consider the asymmetric potential where area 1 and 3 do not yield the same extension and which thus represents a generalization of our so far regarded system. From this we will get an impression in what extent the particular symmetry influences our system and we will be able to evaluate an appropriate interpretation of (3.34). On the other hand we compare the results of our model with these two quite similar real valued systems in order to underline new properties the potential well exhibits only in the complex case.

3.4.1 Asymmetric complex square well potential

So let us first consider the asymmetric complex potential well as depicted in Fig. 3.11, that means area 1 and 3 do not yield the same width but l for area 1 and $L \neq l$ for area 3.



$$V_R(x) = \begin{cases} 0 & , -l < x < L \\ \infty & , \text{otherwise} \end{cases} \quad (3.37)$$

$$V_I(x) = \begin{cases} -C = \text{const.} & , |x| < w \leq \min\{l, L\} \\ 0 & , \text{otherwise} \end{cases} \quad (3.38)$$

Figure 3.11: Schematic sketch of the asymmetric complex potential well where the interval $-l \leq x < -w$ represents area 1, $-w \leq x \leq +w$ area 2 and $w < x \leq L$ area 3.

The Hamiltonian of this system is thus not symmetric with respect to $x = 0$ so its eigenfunctions do not have a defined parity any more. Therefore we only have to deal with one quantization condition for all states instead of separating between symmetric and antisymmetric states:

$$0 = (\varepsilon + ic) \sin \left[\sqrt{\varepsilon}(\omega - \lambda) \right] \sin \left[\sqrt{\varepsilon}(\omega - \Lambda) \right] \quad (3.39)$$

$$- \left\{ \sqrt{\varepsilon + ic} \sin \left[\sqrt{\varepsilon}(\omega - \Lambda) \right] \cos \left(2\omega\sqrt{\varepsilon + ic} \right) - \sqrt{\varepsilon} \cos \left[\sqrt{\varepsilon}(\omega - \Lambda) \right] \sin \left(2\omega\sqrt{\varepsilon + ic} \right) \right\}$$

$$\times \left\{ \sqrt{\varepsilon + ic} \sin \left[\sqrt{\varepsilon}(\omega - \lambda) \right] \cos \left(2\omega\sqrt{\varepsilon + ic} \right) - \sqrt{\varepsilon} \cos \left[\sqrt{\varepsilon}(\omega - \lambda) \right] \sin \left(2\omega\sqrt{\varepsilon + ic} \right) \right\}.$$

Here we introduced dimensionless variables similar to (3.24), but replaced $2L$ by the width of the asymmetric well, that is $L + l$ so that $\Lambda + \lambda = \pi$. The symmetric limit is thus reached for $\Lambda = \frac{\pi}{2} = \lambda$, which we are familiar with. Consequently if we insert this into (3.39) we will obtain both the quantization conditions for the symmetric (3.26) as well as the antisymmetric states (3.27). Solving (3.39) numerically yields for the energy:

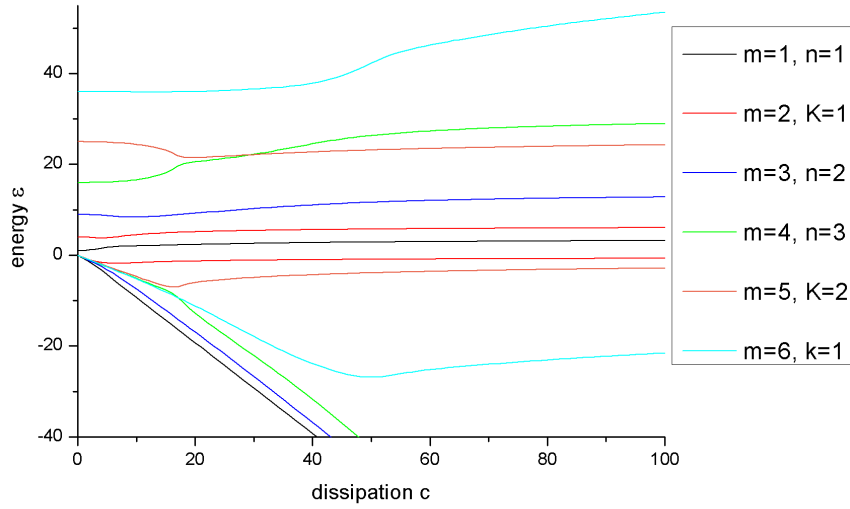


Figure 3.12: Energies of the asymmetric potential well for $\omega = 0.8$ and $\Lambda = 2$. Since we have to deal with two kinds of k -states, as will become clear in Figs. 3.13(a) – 3.13(f), we denote them differently with k and K .

Therefore we have to deal with k - and n -states as well but not with a fusion between adjoining k -states. The real part of every state ends up at one own saturation energy for $c \rightarrow \infty$. Furthermore these k -states have to be separated into those belonging to area 1, denoted by k , and those belonging to area 3, denoted by K . Let us therefore have a look at the corresponding densities:

3 Complex square well potential

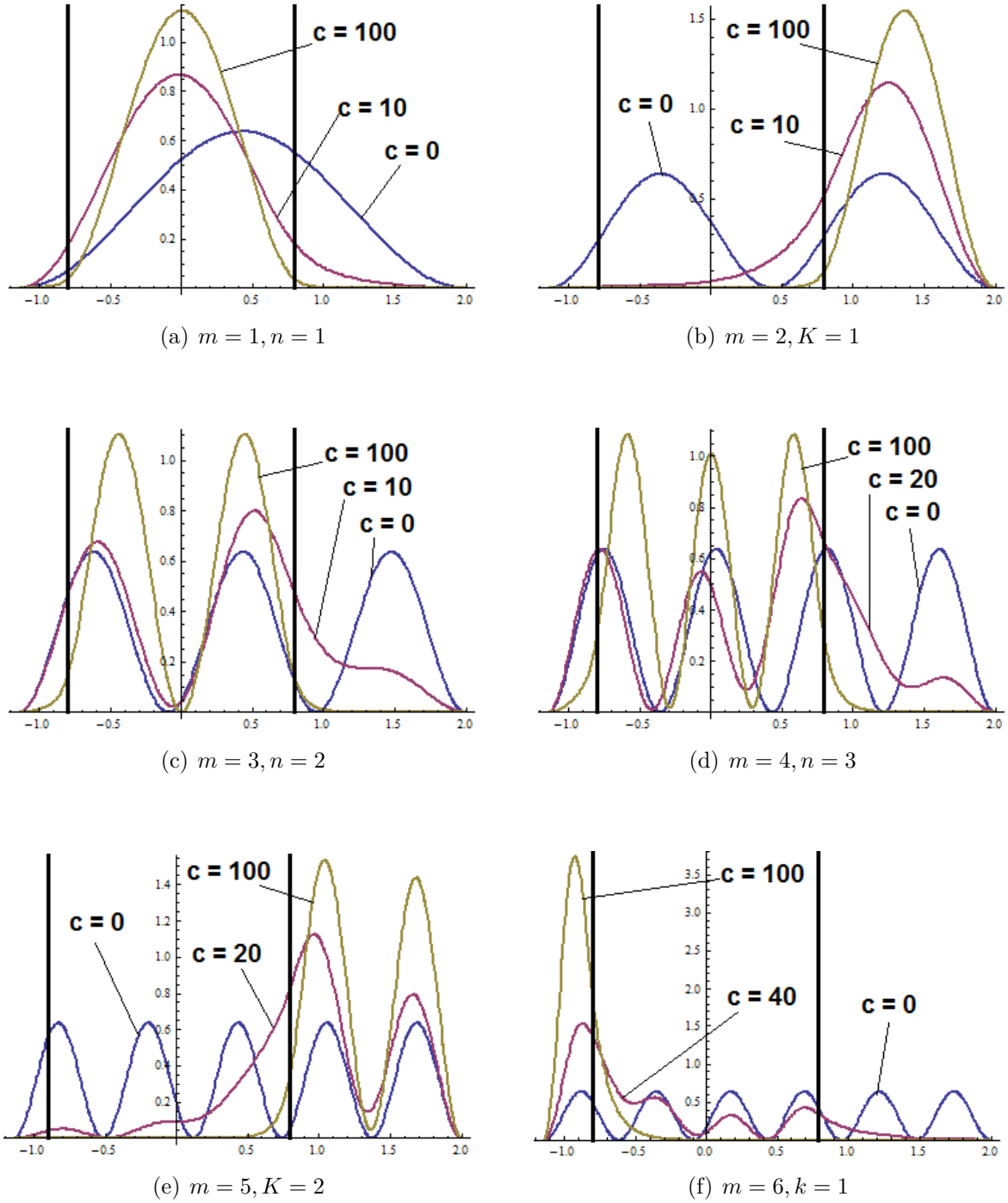


Figure 3.13: One can see the same qualitative behaviour as for the symmetric complex potential well for n - and k -states, but additionally we now have to separate between two kinds of k -states, which we denote with k and K .

Figs. 3.13(a) – 3.13(f) confirm that we really have to separate between three different kinds of states. The k - and K -states differ from each other in the area they are tending to, so even the k -states have maxima in only one area for an asymmetric potential. Thus the fact that the density of k -states yield maxima in area 1 and 3 in the symmetric case is a direct consequence of this symmetry, that is the indistinguishability of area 1 and 3, since physically, for large dissipation, the particle can only be either at one or the other border.

Let us discuss shortly the symmetric limit, that is $\lambda \rightarrow \Lambda$. Observing the energies for $\Lambda \approx \lambda$ shows that, if the difference between λ and Λ becomes very small, then the maxima of the k -states are growing quite equally and only for very large c the maxima in the one area (1 or 3) are dominating. So for $\Lambda = \lambda$ the maxima in area 1 and 3 are growing similarly for all c and thus the parity of the wave functions is ensured due to the symmetry of the system.

Furthermore, we can again calculate the saturation value of the real part of the energy by considering $\lim_{c \rightarrow \infty} \varepsilon_{I,\infty}^n = -c$ as well as $\lim_{c \rightarrow \infty} \varepsilon_{I,\infty}^k = 0$ and obtain results which are not very surprising:

$$\lim_{c \rightarrow \infty} \varepsilon_{R,0}^n = \left(n \frac{\pi}{2\omega} \right)^2, \quad \lim_{c \rightarrow \infty} \varepsilon_{R,0}^k = \left(k \frac{\pi}{\omega - \lambda} \right)^2, \quad \lim_{c \rightarrow \infty} \varepsilon_{R,0}^K = \left(K \frac{\pi}{\omega - \Lambda} \right)^2. \quad (3.40)$$

Indeed we obtain three independent potential wells with three different widths, that is 2ω , $\lambda - \omega$ and $\Lambda - \omega$, and again the symmetric limit becomes obvious for $\Lambda = \frac{\pi}{2}$. This is directly followed by $\lambda = \frac{\pi}{2}$ and yields $\varepsilon^k = \varepsilon^K$ which causes a fusion of the corresponding k - and K -states in Fig. 3.12. We can also extract something mysteriously from the quantization condition (3.39) involving the limit $\lim_{c \rightarrow \infty} \varepsilon_{\infty}^n$. In fact inserting $\left(\frac{n\pi}{2\omega} \right)^2 - ic$ into (3.39) shows that it represents a solution even for all c , not only for $c \rightarrow \infty$. Thus we have energies with a constant real part equal to the saturation value so that c only affects the imaginary part in an exactly linear way. However, it does not fulfill the real limit $\varepsilon_{\infty}^n(0) = n^2$ and is therefore quite unphysical so we neglect them in the further discussion.

So finally this short side-trip into a complex potential well with less symmetry provided some useful insights for a further understanding of our symmetric system. We have seen that in this case for very large dissipation c the whole system consists of three independent potential wells, which was not observable that clearly for the symmetric case. Physically this means the following. For $c \rightarrow \infty$ the particle has to be in area 1 or 3 and can not switch since the imaginary potential in area 2 has the same effect as an infinitely high potential barrier. So the particle, indeed, is in area 1 or 3 but since we can not distinguish between them in the symmetric case, both areas are equal. For the asymmetric potential we have seen that we can differ 3 kinds of states corresponding to the particle being in respectively one of the three distinct areas for $c \rightarrow \infty$. Therefore the interpretation considering three independent potential wells seems to be more appropriate in (3.34) since we account the symmetric potential well a special case of the general potential well yielding an imaginary potential in the center.

3.4.2 Related real potential systems

Next we will compare the results of the complex potential with some familiar real valued systems. Especially the energy limits (3.28) show that our complex square well potential yields quite similar

3 Complex square well potential

results as the familiar real double well potential. Therefore we now consider the following real potential in dimensionless variables:

$$v(\chi) = \begin{cases} \infty & , \quad |\chi| > \frac{\pi}{2} \\ 0 & , \quad \omega \leq |\chi| \leq \frac{\pi}{2} \\ c & , \quad |\chi| < \omega \end{cases} \quad (3.41)$$

but allow for c being also negative, which yields on the one hand the double well potential for $c > 0$ and on the other hand a nested real potential well for $c < 0$.

In any case, due to its symmetry, the real potential (3.41) yields the following quantization conditions for symmetric and antisymmetric states

$$0 = \sqrt{\varepsilon^s} \cot \left[\left(\omega - \frac{\pi}{2} \right) \sqrt{\varepsilon^s} \right] + \sqrt{\varepsilon^s - c} \tan \left(\omega \sqrt{\varepsilon^s - c} \right) \quad , \quad (3.42)$$

$$0 = \sqrt{\varepsilon^a} \cot \left[\left(\omega - \frac{\pi}{2} \right) \sqrt{\varepsilon^a} \right] - \sqrt{\varepsilon^a - c} \cot \left(\omega \sqrt{\varepsilon^a - c} \right) \quad . \quad (3.43)$$

Of course both conditions are looking quite similar to (3.26) and (3.27) and also the solutions will turn out to be not that unfamiliar. We discuss them separately for $c > 0$ and $c < 0$ in the next two subsections.

3.4.2.1 Real double well potential

The so called real double well potential is realized for $c > 0$ in (3.41). We know that for very large c and fixed ω the density reduces to zero in area 2 and is thus displaced to the borders which is area 1 and 3. Since exactly this occurs for the k -states of our complex potential it seems to be reasonable to compare it with the results of this real system. Let us therefore have a look at the solutions of (3.42) and (3.43) for $c > 0$:

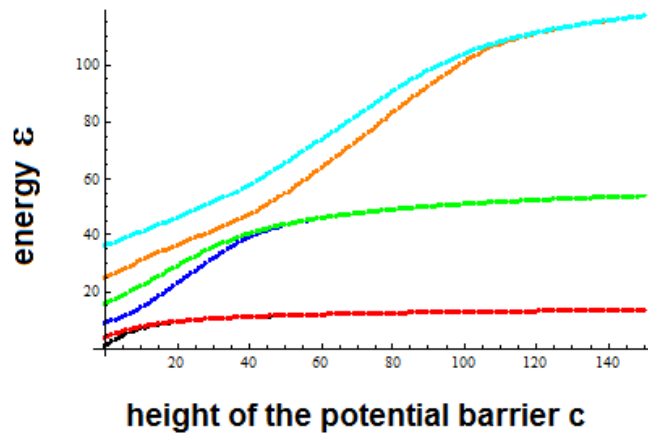


Figure 3.14: Lowest six energies of the real double well for $\omega = 0.8$. Here only k -states are emerging. Similarly to the complex potential well they start at some m^2 for natural m and always two states starting at two adjoining m , so a symmetric and an antisymmetric state, fuse and end up at a mutual finite saturation value for $c \rightarrow \infty$.

As we expected Fig. 3.14 shows that for $c > 0$ there are only k -states present. We can identify them as k -states since always two adjoining states are fusing for increasing c . This is confirmed by considering $c \rightarrow \infty$ in (3.42) and (3.43):

$$\varepsilon_{\text{sat}} = \left(k \frac{\pi}{\omega - \frac{\pi}{2}} \right)^2, \quad k = \left[\frac{m+1}{2} \right] = \begin{cases} \frac{m}{2} & , \quad m \text{ even} \\ \frac{m+1}{2} & , \quad m \text{ odd} \end{cases}, \quad (3.44)$$

which is equal to the saturation value of the k -states in (3.28) and coincides perfectly with the numerical results. Therefore this limit yields nothing else than two equal potential wells separated by an infinitely high real potential barrier. This interpretation is confirmed by the corresponding densities:

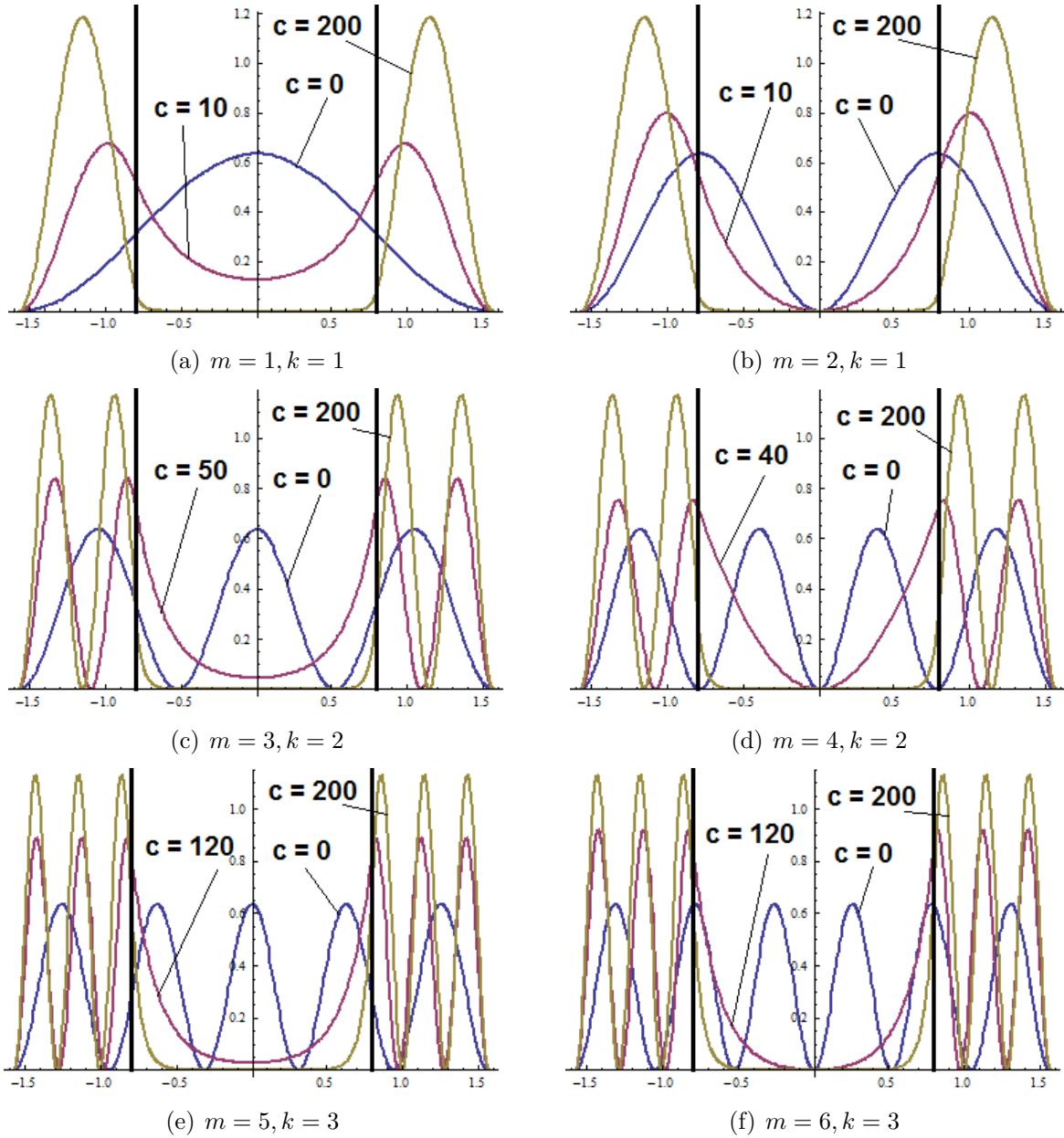


Figure 3.15: Densities of the lowest six states of the real double well potential for $\omega = 0.8$. It yields a real infinite high potential barrier for $c \rightarrow \infty$ so that two equal potential wells develop.

3 Complex square well potential

So finally we can state that the real double well potential yields only one kind of states. Comparing them with the corresponding ones of the complex potential well shows qualitatively the same results for the k -states, that means for $c = 0$ and $c \rightarrow \infty$ they are equal and additionally exhibit this particular fusion for diverging c . Nevertheless there are deviations between the eigenvalues ε of both systems for $0 < c < \infty$.

3.4.2.2 Nested real potential wells

Next we consider the so called nested real potential wells which means nothing else than (3.41) with $(-c) < 0$. Thus we also deal with a well in the center of the system just like we do for the complex potential well. We know that in this case the density tends to the center for $(-c) \rightarrow \infty$ which exactly happens for the n -states of the complex potential well, too. Therefore we should contrast these both systems with each other, too. Solving (3.42) and (3.43) for $c < 0$ provides:

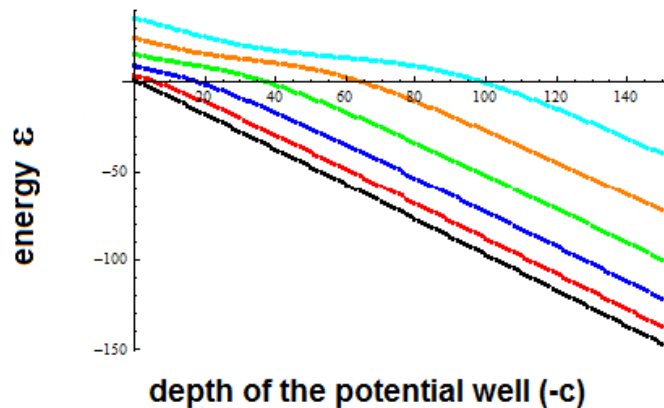


Figure 3.16: Lowest six energies of a system with two nested real potential wells for $\omega = 0.8$. For $c = 0$ all states start at some m^2 for natural m . For decreasing c their energy decreases, especially linearly for large $(-c)$, to $-\infty$.

Recalling the results of the complex potential well yields that in some way the states in Fig. 3.16 show a quite similar behaviour as the n -states although we deal here with real solutions. They start at $\varepsilon(c = 0) = m^2$ for $m = 1, 2, 3, 4, 5, 6, \dots$ like the real part, but then decrease linearly for large c to $-\infty$ like the imaginary part of the energy does in the complex case. We can additionally calculate ε analytically in the limit $c \rightarrow -\infty$ from (3.42) and (3.43), which provides

$$\lim_{c \rightarrow -\infty} \varepsilon = \lim_{c \rightarrow -\infty} \left[\left(n \frac{\pi}{2\omega} \right)^2 - c \right], \quad n = m. \quad (3.45)$$

The plateau occurring in Fig. 3.16, especially for the higher states, is related to the fact that for $c = 0$ all states yield the energy of a potential well with the width π , that is $\varepsilon(0) = m^2$. In contrast the first term in (3.45) exhibits energies of a potential well with the width $2\omega < \pi$ for $c \rightarrow \infty$, so that the energy can not decrease perfectly linearly with c for all c but have to reveal a deviation of this linear decay. Exactly this is reexpressed by this plateau and it becomes more and more viewable for large m since the deviation grows quadratically in m .

Furthermore (3.45) reminds us of the n -states of the complex potential well which yield

$$\lim_{c \rightarrow -\infty} \varepsilon^n = \lim_{c \rightarrow -\infty} \left[\left(\frac{n\pi}{2\omega} \right)^2 - ic \right]. \quad (3.46)$$

The densities confirm this analogy:

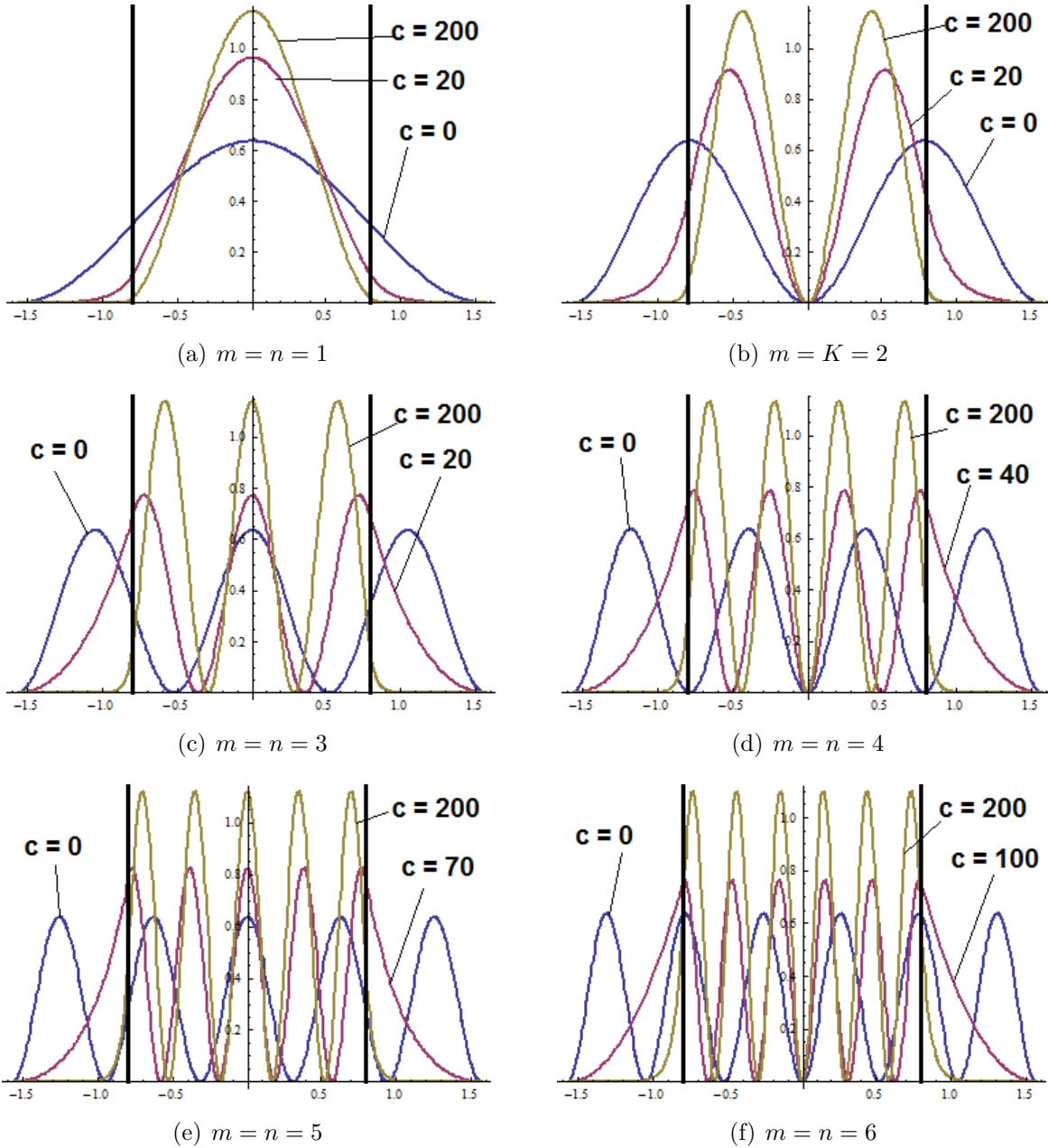


Figure 3.17: Densities of the lowest n states of a system with two nested real potential wells. It yields a decreasing density in area 1 and 3 with increasing c which reduces to zero in the limit $c \rightarrow -\infty$. Thus the states tend to the center just like the n -states of the complex potential well.

3 Complex square well potential

It catches the eye that, just like the n -states of the complex potential well, the states of the two nested real potentials tend to the center and end up as states of a potential well with the width 2ω as (3.45) already implied. This is given by the first summand of (3.45) which exactly coincides with $\varepsilon_{R,\infty}^{n,\text{sat}}$.

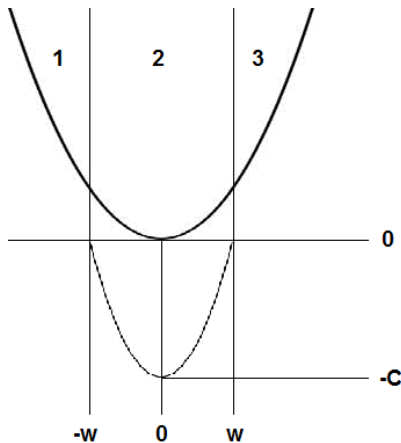
3.4.2.3 Comparison with complex potential well

Let us finally compare the results of both related real valued systems with the corresponding ones of the complex potential well. We have already seen that both systems yield one kind of state, respectively, that is the double well shows k -states and the nested potential well n -states, while for the complex potential well both types of states occur at once. This has several consequences, for example we saw that this coexistence causes a kind of interaction between k - and n -states. We already evaluated similarities between the real part of the energy, the states of the complex potential well yield, and the energies or respective parts of it the real potential systems reveal. We found out that the energies of corresponding states exactly coincide in the limits $c = 0$ and $c \rightarrow \infty$ but this is generally not true for all c . Comparing the energies of corresponding states of the real systems with these of the complex one also for $0 < c < \infty$ exhibit differences which are caused by this kind of interaction we discussed in Section 3.2. This interaction is represented for example by a strong curvature of the graphs that do not occur that strong in Figs. 3.14 and 3.16. If it is weak then energies are in good accordance which confirms the interpretation as a kind of interaction since it only emerges if both kinds of states are present at once. Thus also the interchange of states at some ω_{crit} is an effect only the complex potential well includes since k - and n -states keep their order among each other as we already found out for the complex potential well.

Nevertheless the most important difference consists in the time evolution (2.8). Because all energies of the real valued systems are accordingly real, we deal with stationary solutions in these cases, because $E_I = 0$ is obviously followed by $\rho(x, t) = \rho(x, t_0)$ for all t . Therefore only the complex potential well is able to describe damping and, since the density in area 2 reduces to zero for large t , a hole in the condensate develops and primarily the k -states remain for large dissipation.

4 Complex harmonic potential

After this quite detailed evaluation of that crude square well approximation there are many possibilities to improve our ansatz in order to have a more appropriate description. Some obvious ones are of course to extend the model to three dimensions, including interaction in our theory and finally to have a more accurate approximation of the potential, which we aim at performing in this chapter. Therefore we now take a harmonic complex potential $V(x) = V_R(x) + iV_I(x)$, where $V_R(x) = \frac{M}{2}\Omega^2 x^2$ represents the harmonic trap the BEC is confined in and Ω denotes its frequency. Furthermore, in this chapter we consider the imaginary part of the potential to be harmonic and negative for $|x| \leq w$ and equal to zero otherwise. Moreover it is supposed to be continuous at $x = \pm w$ and again symmetric with respect to $x = 0$, where the beam is focused on. Therefore it can not include any terms linear in x but only constant and quadratic ones so we have to deal with the expression $V_I(x) = C\left(\frac{x^2}{w^2} - 1\right)$ for $|x| \leq w$ which fulfills all demands. Therefore, putting both parts together, we consider the following system:



$$V_R(x) = \frac{M}{2}\Omega^2 x^2 \quad (4.1)$$

$$V_I(x) = \begin{cases} 0 & , |x| > w \\ C\left(\frac{x^2}{w^2} - 1\right) & , |x| \leq w \end{cases} \quad (4.2)$$

Figure 4.1: Schematic sketch of the complex harmonic potential, where again the interval $-L \leq x < -w$ is called area 1, $-w \leq x \leq +w$ area 2 and $w < x \leq L$ area 3.

Just like for the square well potential we have to distinguish between three different areas with a non-vanishing imaginary part V_I only in area 2. So the wave function has also the same piecewise form (3.3).

However, due to various reasons, we will not perform an exactly analogous discussion as in the previous chapter, although many aspects of this complex harmonic potential will be similar to the complex square well potential. Nevertheless one important difference relies in the real part of the potential, which is not piecewise defined, so that the wave function does not vanish for finite x and thus the waist can, in principle, tend to infinity. Beside the quite complicated formulas that will arise from this ansatz, this issue will cause much more numerical effort since for example the limit case $\omega \rightarrow \frac{\pi}{2}$ turns now into $\omega \rightarrow \infty$. Thus we just aim at getting an impression of how the results change due to the new potential and see whether they provide something completely

different or otherwise even this crude approximation of the previous chapter yields qualitatively satisfying results.

4.1 Static solutions of Schrödinger equation

The time-independent Schrödinger equation (2.9) for the considered potential is given by

$$H(x)\psi(x) = \left[-\frac{\hbar^2}{2M} \frac{d^2}{dx^2} + \frac{M}{2} \Omega^2 x^2 + iC \left(\frac{x^2}{w^2} - 1 \right) \right] \psi(x) = E\psi(x). \quad (4.3)$$

Solving this we take an analogues approach as in [29, Ch. 7] and introduce the abbreviations

$$k_1^2 = \frac{2ME}{\hbar^2} \quad \text{and} \quad k_2^2 = \frac{2M}{\hbar^2} (E + iC) \quad (4.4)$$

as well as

$$\lambda_1 = \frac{M\Omega}{\hbar} \quad \text{and} \quad \lambda_2 = \sqrt{\frac{M^2\Omega^2}{\hbar^2} + i\frac{MC}{\hbar^2 w^2}} = \lambda_1 \sqrt{1 + i\frac{C}{M\Omega^2 w^2}}, \quad (4.5)$$

where the index 1 stands for area 1 and 3, i.e. $V_I(x) = 0$, while the index 2 denotes area 2, i.e. $V_I(x) > 0$. Thus (4.3) becomes

$$\frac{d^2}{dx^2} \psi(x) + (k^2 - \lambda^2 x^2) \psi(x) = 0. \quad (4.6)$$

With the substitutions

$$y := \lambda x^2, \quad \psi(y) =: e^{-y/2} \varphi(y) \quad \text{and} \quad \gamma := \frac{k^2}{2\lambda} \quad (4.7)$$

it takes the form of *Kummer's* differential equation

$$y \frac{d^2 \varphi}{dy^2} + \left(\frac{1}{2} - y \right) \frac{d\varphi}{dy} + \left(\frac{\gamma}{2} - \frac{1}{4} \right) \varphi = 0, \quad (4.8)$$

that is generally solved by

$$\varphi(y) = A_1 F_1 \left(a; \frac{1}{2}; y \right) + B \sqrt{y} F_1 \left(a + \frac{1}{2}; \frac{3}{2}; y \right) \quad (4.9)$$

with the confluent hypergeometric functions

$${}_1F_1(p; q; y) = \sum_{\nu=0}^{\infty} \frac{(p)_{\nu} y^{\nu}}{(q)_{\nu} \nu!} \quad (4.10)$$

and the Pochhammer-symbols

$$(a)_\nu = a(a+1)\dots(a+\nu-1), \quad \text{where} \quad a = -\left(\frac{\gamma}{2} - \frac{1}{4}\right) \quad \text{and} \quad (a)_0 := 1. \quad (4.11)$$

Resubstitution to x and ψ provides the general solution

$$\psi(x) = A^s e^{-\frac{1}{2}\lambda x^2} {}_1F_1\left(a; \frac{1}{2}; \lambda x^2\right) + A^a \sqrt{\lambda} x e^{-\frac{1}{2}\lambda x^2} {}_1F_1\left(a + \frac{1}{2}; \frac{3}{2}; \lambda x^2\right), \quad (4.12)$$

with the corresponding series representation

$$\psi(x) = A^s e^{-\frac{1}{2}\lambda x^2} \sum_{\nu=0}^{\infty} \frac{(a)_\nu}{\left(\frac{1}{2}\right)_\nu} \lambda^\nu \frac{x^{2\nu}}{\nu!} + A^a e^{-\frac{1}{2}\lambda x^2} \sum_{\nu=0}^{\infty} \frac{(a)_\nu}{\left(\frac{3}{2}\right)_\nu} \lambda^{\nu+\frac{1}{2}} \frac{x^{2\nu+1}}{\nu!}. \quad (4.13)$$

The first term of this solution is symmetric, while the second term is antisymmetric with respect to $x = 0$, therefore we denoted the respective constants with A^s and A^a . This solution and its first derivative have to be differentiable at $x = \pm w$, since the Schrödinger equation for the whole wave function (4.3) yields that the second derivative of ψ is a continuous function. Moreover one has to demand that, due to normalizability, ψ vanishes for $x \rightarrow \pm\infty$. One can reduce these four conditions to only two by using the symmetry of the Hamiltonian with respect to $x = 0$ on the left hand side of (4.3), which implicates that its eigenfunctions ψ have to be completely symmetric or antisymmetric with respect to $x = 0$, that is

$$\psi_1^s(-x) = \psi_1^s(x) \quad \text{and} \quad \psi_2^s(-x) = \psi_2^s(x) \quad (4.14)$$

for the symmetric wave function ψ^s and

$$\psi_1^a(-x) = -\psi_1^a(x) \quad \text{and} \quad \psi_2^a(-x) = -\psi_2^a(x) \quad (4.15)$$

for the antisymmetric one ψ^a . Especially for the wave function in area 2 this means that ψ_2 is either completely symmetric or antisymmetric so that it takes the following form:

$$\psi_2^s(x) = A_2^s e^{-\frac{1}{2}\lambda_2 x^2} {}_1F_1\left(a_2; \frac{1}{2}; \lambda_2 x^2\right), \quad (4.16)$$

$$\psi_2^a(x) = A_2^a \sqrt{\lambda_2} x e^{-\frac{1}{2}\lambda_2 x^2} {}_1F_1\left(a_2 + \frac{1}{2}; \frac{3}{2}; \lambda_2 x^2\right), \quad (4.17)$$

while we have to express the wave function in area 1 via the general expression

$$\psi_1(x) = A_1^s e^{-\frac{1}{2}\lambda_1 x^2} {}_1F_1\left(a_1; \frac{1}{2}; \lambda_1 x^2\right) + A_1^a \sqrt{\lambda_1} x e^{-\frac{1}{2}\lambda_1 x^2} {}_1F_1\left(a_1 + \frac{1}{2}; \frac{3}{2}; \lambda_1 x^2\right). \quad (4.18)$$

Before taking the symmetry conditions (4.14) and (4.15) into account, we reexpress the wave functions in terms of new dimensionless variables, where the length scale is normalized by the

4 Complex harmonic potential

oscillator length $l = \lambda_1^{-1/2}$ and the energy scale by the ground-state energy $\frac{1}{2}\hbar\Omega$ of a real harmonic potential to make the calculations and the results more clearly:

$$\varepsilon := \frac{E}{\frac{\hbar\Omega}{2}}, \quad c := \frac{C}{\frac{\hbar\Omega}{2}}, \quad \chi := \frac{1}{l}x, \quad \omega := \frac{1}{l}w \quad \text{and} \quad \kappa := lk. \quad (4.19)$$

Furthermore we introduce the following abbreviation:

$$\theta = \theta(c, \omega) = \sqrt{1 + i\frac{c}{\omega^2}}. \quad (4.20)$$

From this we can directly calculate λ and γ and thus finally obtain

$$a_1 = \frac{1}{4}(1 - \varepsilon) \quad \text{and} \quad a_2 = \frac{1}{4}\left(1 - \frac{\varepsilon + ic}{\theta}\right). \quad (4.21)$$

Using these new variables the general solutions now read

$$\psi^s(\chi) = \begin{cases} A_1^s e^{-\frac{1}{2}\chi^2} {}_1F_1\left(a_1; \frac{1}{2}; \chi^2\right) + A_1^a \chi e^{-\frac{1}{2}\chi^2} {}_1F_1\left(a_1 + \frac{1}{2}; \frac{3}{2}; \chi^2\right) & , \chi < -\omega \\ A_2^s e^{-\frac{1}{2}\theta\chi^2} {}_1F_1\left(a_2; \frac{1}{2}; \theta\chi^2\right) & , -\omega < \chi < \omega \\ A_1^s e^{-\frac{1}{2}\chi^2} {}_1F_1\left(a_1; \frac{1}{2}; \chi^2\right) - A_1^a \chi e^{-\frac{1}{2}\chi^2} {}_1F_1\left(a_1 + \frac{1}{2}; \frac{3}{2}; \chi^2\right) & , \omega < \chi \end{cases} \quad (4.22)$$

$$\psi^a(\chi) = \begin{cases} A_1^s e^{-\frac{1}{2}\chi^2} {}_1F_1\left(a_1; \frac{1}{2}; \chi^2\right) + A_1^a \chi e^{-\frac{1}{2}\chi^2} {}_1F_1\left(a_1 + \frac{1}{2}; \frac{3}{2}; \chi^2\right) & , \chi < -\omega \\ A_2^a \theta \chi e^{-\frac{1}{2}\theta\chi^2} {}_1F_1\left(a_2 + \frac{1}{2}; \frac{3}{2}; \theta\chi^2\right) & , -\omega < \chi < \omega \\ -A_1^s e^{-\frac{1}{2}\chi^2} {}_1F_1\left(a_1; \frac{1}{2}; \chi^2\right) + A_1^a \chi e^{-\frac{1}{2}\chi^2} {}_1F_1\left(a_1 + \frac{1}{2}; \frac{3}{2}; \chi^2\right) & , \omega < \chi \end{cases} \quad (4.23)$$

Now we demand continuity of the wave function and its first derivative at $\chi = \pm\omega$. With the symmetry conditions (4.14) it is sufficient to evaluate this at $\chi = -\omega$ and to ensure that $\psi_1(\chi)$ vanishes for $\chi \rightarrow -\infty$, because then the same is automatically fulfilled for ψ_3 at $\chi = +\omega$ and $\chi \rightarrow \infty$. We start with the normalizability:

$$\lim_{\chi \rightarrow -\infty} \psi_1(\chi) = \lim_{\chi \rightarrow -\infty} e^{-\frac{1}{2}\chi^2} \left[A_1^s {}_1F_1\left(a_1; \frac{1}{2}; \chi^2\right) + A_1^a \chi {}_1F_1\left(a_1 + \frac{1}{2}; \frac{3}{2}; \chi^2\right) \right] \stackrel{!}{=} 0. \quad (4.24)$$

If the confluent hypergeometric functions (4.10) reduce to polynomials, this would be automatically fulfilled because of the exponential function. In the real case this allows us immediately to formulate the quantization condition $a_1 = -n$ for some $n \in \mathbb{N}$. Unfortunately this does not work here since a is, in general, a complex number so that the Pochhammer symbol $(a_1)_\nu$ does not vanish even for any $n \in \mathbb{R}$ and ${}_1F_1\left(a_1; \frac{1}{2}; \chi^2\right)$ does not become a polynomial. Therefore we have to demand that the sum of two confluent hypergeometric functions vanishes for $\chi \rightarrow -\infty$:

$$\lim_{\chi \rightarrow -\infty} \left[A_1^s {}_1F_1\left(a_1; \frac{1}{2}; \chi^2\right) + A_1^a \chi {}_1F_1\left(a_1 + \frac{1}{2}; \frac{3}{2}; \chi^2\right) \right] \stackrel{!}{=} 0. \quad (4.25)$$

The occurring confluent hypergeometric functions are continuous and symmetric in χ , since their argument is χ^2 , while χ is obviously antisymmetric with respect to χ , so that we can rewrite this to

$$A_1^a = A_1^s \lim_{\chi \rightarrow \infty} \frac{{}_1F_1\left(a_1; \frac{1}{2}; \chi^2\right)}{\chi {}_1F_1\left(a_1 + \frac{1}{2}; \frac{3}{2}; \chi^2\right)} \quad (4.26)$$

and use the asymptotic behaviour of the confluent hypergeometric functions for $x \rightarrow \infty$ from [29, (34.21)]:

$${}_1F_1(a; c; x) \longrightarrow \frac{\Gamma(c)}{\Gamma(c-a)} e^{-ia\pi} x^{-a} + \frac{\Gamma(c)}{\Gamma(a)} e^x x^{a-c}. \quad (4.27)$$

Applying this to (4.26) provides

$$A_1^a = A_1^s \lim_{\chi \rightarrow \infty} \frac{\frac{\Gamma(1/2)}{\Gamma(1/2-a_1)} e^{-ia_1\pi} \chi^{-2a_1} + \frac{\Gamma(1/2)}{\Gamma(a_1)} e\chi^2 \chi^{2a_1-1}}{\chi \left[\frac{\Gamma(3/2)}{\Gamma(1-a_1)} e^{-i(a_1+1/2)\pi} \chi^{-2a_1-1} + \frac{\Gamma(3/2)}{\Gamma(a_1+1/2)} e\chi^2 \chi^{2a_1-2} \right]} \quad (4.28)$$

$$= A_1^s \lim_{\chi \rightarrow \infty} \frac{\Gamma\left(\frac{1}{2}\right) \left[\Gamma\left(\frac{1}{2} - a_1\right)^{-1} e^{-ia_1\pi} \chi^{-2a_1} + \Gamma(a_1)^{-1} e\chi^2 \chi^{2a_1-1} \right]}{\Gamma\left(\frac{3}{2}\right) \left[-i\Gamma(1-a_1)^{-1} e^{-i(a_1+1/2)\pi} \chi^{-2a_1-1} + \Gamma\left(a_1 + \frac{1}{2}\right)^{-1} e\chi^2 \chi^{2a_1-1} \right]} \quad (4.29)$$

$$= 2A_1^s \lim_{\chi \rightarrow \infty} \frac{\Gamma\left(\frac{1}{2} - a_1\right)^{-1} + \Gamma(a_1)^{-1} e\chi^2 \chi^{4a_1-1}}{-i\Gamma(1-a_1)^{-1} + \Gamma\left(a_1 + \frac{1}{2}\right)^{-1} e\chi^2 \chi^{4a_1-1}}, \quad (4.30)$$

where we used the recurrence formula of the Γ -function $\Gamma(x+1) = x\Gamma(x)$. Now we neglect the terms not including $e\chi^2$ so that the χ -dependency cancels and we are directly left with

$$A_1^a = 2A_1^s \frac{\Gamma\left(a_1 + \frac{1}{2}\right)}{\Gamma(a_1)}. \quad (4.31)$$

From this expression one can read off $A_1^a = 0$ if a_1 is equal to some integer number $a_1 = -n \leq 0$ and, for normalizability, $A_1^s = 0$ if $a_1 = -n - \frac{1}{2} < 0$. This yields, that then ψ_1 is also symmetric or antisymmetric with respect to $\chi = 0$, respectively. Now we can express ψ_1 via only one normalization constant:

$$\psi_1(\chi) = A_1^s e^{-\frac{1}{2}\chi^2} \left[{}_1F_1\left(a_1; \frac{1}{2}; \chi^2\right) + 2\chi \frac{\Gamma\left(a_1 + \frac{1}{2}\right)}{\Gamma(a_1)} {}_1F_1\left(a_1 + \frac{1}{2}; \frac{3}{2}; \chi^2\right) \right]. \quad (4.32)$$

In the following we discuss symmetric and antisymmetric states separately.

4.1.1 Symmetric states

With (4.22) the continuity condition $\psi_1^s(-w) = \psi_2^s(-w)$ provides

$$A_1^s e^{-\frac{1}{2}\omega^2} \left[{}_1F_1 \left(a_1; \frac{1}{2}; \omega^2 \right) - 2\omega \frac{\Gamma(a_1 + \frac{1}{2})}{\Gamma(a_1)} {}_1F_1 \left(a_1 + \frac{1}{2}; \frac{3}{2}; \omega^2 \right) \right] = A_2^s e^{-\frac{1}{2}\theta\omega^2} {}_1F_1 \left(a_2; \frac{1}{2}; \theta\omega^2 \right). \quad (4.33)$$

With this we reexpress A_2^s in terms of A_1^s , which then exhibits the normalization constant of the whole symmetric wave function, so that we call it from now on $\mathcal{N}^s := A_1^s$. Then the continuity condition reads

$$A_2^s = \mathcal{N}^s e^{\frac{1}{2}(\theta-1)\omega^2} \frac{{}_1F_1 \left(a_1; \frac{1}{2}; \omega^2 \right) - 2\omega \frac{\Gamma(a_1 + \frac{1}{2})}{\Gamma(a_1)} {}_1F_1 \left(a_1 + \frac{1}{2}; \frac{3}{2}; \omega^2 \right)}{{}_1F_1 \left(a_2; \frac{1}{2}; \theta\omega^2 \right)} =: \mathcal{N}^s R^s, \quad (4.34)$$

where $R^s = R^s(\omega, \varepsilon, c)$ represents an abbreviation. We can now write down the wave functions in all 3 areas obeying (4.14), which yields the symmetric wave function ψ^s :

$$\psi^s(\chi) = \mathcal{N}^s \begin{cases} e^{-\frac{1}{2}\chi^2} \left[{}_1F_1 \left(a_1; \frac{1}{2}; \chi^2 \right) + 2\chi \frac{\Gamma(a_1 + \frac{1}{2})}{\Gamma(a_1)} {}_1F_1 \left(a_1 + \frac{1}{2}; \frac{3}{2}; \chi^2 \right) \right] & , \chi < -\omega \\ R^s e^{-\frac{1}{2}\theta\chi^2} {}_1F_1 \left(a_2; \frac{1}{2}; \theta\chi^2 \right) & , -\omega \leq \chi \leq \omega \\ e^{-\frac{1}{2}\chi^2} \left[{}_1F_1 \left(a_1; \frac{1}{2}; \chi^2 \right) - 2\chi \frac{\Gamma(a_1 + \frac{1}{2})}{\Gamma(a_1)} {}_1F_1 \left(a_1 + \frac{1}{2}; \frac{3}{2}; \chi^2 \right) \right] & , \chi > \omega \end{cases} . \quad (4.35)$$

4.1.1.1 Quantization condition

Now we have to ensure the continuity of the first derivative of ψ^s at $\chi = -\omega$

$$\left. \frac{d}{d\chi} \psi_1^s(\chi) \right|_{\chi=-\omega} = \left. \frac{d}{d\chi} \psi_2^s(\chi) \right|_{\chi=-\omega}, \quad (4.36)$$

which yields with (4.35)

$$\begin{aligned} & \omega {}_1F_1 \left(a_1; \frac{1}{2}; \omega^2 \right) - 4a_1\omega {}_1F_1 \left(a_1 + 1; \frac{3}{2}; \omega^2 \right) + \\ & 2 \frac{\Gamma(a_1 + \frac{1}{2})}{\Gamma(a_1)} \left[(1 - \omega^2) {}_1F_1 \left(a_1 + \frac{1}{2}; \frac{3}{2}; \omega^2 \right) + \frac{4}{3} \left(a_1 + \frac{1}{2} \right) \omega^2 {}_1F_1 \left(a_1 + \frac{3}{2}; \frac{5}{2}; \omega^2 \right) \right] \\ & = \frac{{}_1F_1 \left(a_1; \frac{1}{2}; \omega^2 \right) - 2\omega \frac{\Gamma(a_1 + \frac{1}{2})}{\Gamma(a_1)} {}_1F_1 \left(a_1 + \frac{1}{2}; \frac{3}{2}; \omega^2 \right)}{{}_1F_1 \left(a_2; \frac{1}{2}; \theta\omega^2 \right)} \left[\theta\omega {}_1F_1 \left(a_2; \frac{1}{2}; \theta\omega^2 \right) - 4a_2\theta\omega {}_1F_1 \left(a_2 + 1; \frac{3}{2}; \theta\omega^2 \right) \right]. \end{aligned} \quad (4.37)$$

Here we used the derivative of the confluent hypergeometric functions with respect to the last argument

$$\begin{aligned}
 \frac{d}{d\chi} {}_1F_1(a; c; \beta\chi^2) &= \sum_{\nu=1}^{\infty} \frac{(a)_{\nu}}{(c)_{\nu}} \beta^{\nu} \frac{2\nu\chi^{2\nu-1}}{\nu!} \\
 &= 2\chi\beta \frac{a}{c} \sum_{\nu=1}^{\infty} \frac{(a+1)_{\nu-1}}{(c+1)_{\nu-1}} \beta^{\nu-1} \frac{\chi^{2(\nu-1)}}{(\nu-1)!} \\
 &= 2\chi\beta \frac{a}{c} {}_1F_1(a+1; b+1; \beta\chi^2). \tag{4.38}
 \end{aligned}$$

Eq. (4.37) represents the quantization condition for the symmetric states. Its solutions are the energy eigenvalues ε^s of the eigenstates ψ^s . Since θ and a are functions of c and ω via (4.20) and (4.21) these energies just depend on the waist ω and the strength of dissipation c . The quantization condition for the energy is a transcendental equation in ε so that we have to solve it numerically, which we do in the next section.

4.1.1.2 Normalization constant

Finally we derive an expression for the normalization constant \mathcal{N}^s . For this purpose we have to calculate the following integral by using the symmetry of ψ :

$$1 = \int_{-\infty}^{\infty} |\psi(\chi)| d\chi = 2 \int_0^{\omega} |\psi_2(\chi)|^2 d\chi + 2 \int_{\omega}^{\infty} |\psi_3(\chi)|^2 d\chi. \tag{4.39}$$

One can generally write for the following integral including ${}_1F_1$:

$$\int_r^{\infty} x^p \left| e^{-\frac{1}{2}\beta x^2} {}_1F_1(a; c; \beta x^2) \right|^2 dx = \sum_{\mu, \nu=0}^{\infty} \frac{(a)_{\nu} (a^*)_{\mu}}{(c)_{\nu} (c^*)_{\mu} \nu! \mu!} \beta^{\nu} (\beta^*)^{\mu} \int_r^{\infty} e^{-\operatorname{Re}(\beta)x^2} x^{2(\mu+\nu)+p} dx, \tag{4.40}$$

where $\operatorname{Re}(\beta)$ represents the real part of β . With the substitution $z := \operatorname{Re}(\beta)x^2$ one obtains

$$\begin{aligned}
 &\sum_{\mu, \nu=0}^{\infty} \frac{(a)_{\nu} (a^*)_{\mu}}{(c)_{\nu} (c^*)_{\mu} \nu! \mu!} \beta^{\nu} (\beta^*)^{\mu} \int_{\operatorname{Re}(\beta)r^2}^{\infty} e^{-z} z^{\mu+\nu+\frac{p}{2}} \frac{dz}{2\sqrt{\operatorname{Re}(\beta)z}} \\
 &= \frac{1}{2} \sum_{\mu, \nu=0}^{\infty} \frac{(a)_{\nu} (a^*)_{\mu}}{(c)_{\nu} (c^*)_{\mu} \nu! \mu!} \frac{\beta^{\nu} (\beta^*)^{\mu}}{\sqrt{\operatorname{Re}(\beta)}} \int_{\operatorname{Re}(\beta)r^2}^{\infty} e^{-z} z^{\mu+\nu+\frac{p+1}{2}-1} dz \\
 &= \frac{1}{2} \sum_{\mu, \nu=0}^{\infty} \frac{(a)_{\nu} (a^*)_{\mu}}{(c)_{\nu} (c^*)_{\mu} \nu! \mu!} \frac{\beta^{\nu} (\beta^*)^{\mu}}{\sqrt{\operatorname{Re}(\beta)}} \Gamma\left(\mu + \nu + \frac{p+1}{2}, \operatorname{Re}(\beta)r^2\right), \tag{4.41}
 \end{aligned}$$

where

$$\Gamma(x, r) := \int_r^{\infty} e^{-t} t^{x-1} dt \tag{4.42}$$

denotes the *Plica-function*, which is a generalization of the familiar Γ -function, namely $\Gamma(x, 0) = \Gamma(x)$. So for the first integral in (4.39) follows

$$\begin{aligned}
 & 2 \int_0^\omega |\psi_2^s(\chi)|^2 d\chi = 2 |\mathcal{N}^s R^s|^2 \int_0^\omega \left| e^{-\frac{1}{2}\theta\chi^2} {}_1F_1\left(a_2; \frac{1}{2}; \theta\chi^2\right) \right|^2 d\chi \\
 & = 2 |\mathcal{N}^s R^s|^2 \left[\int_0^\infty \left| e^{-\frac{1}{2}\theta\chi^2} {}_1F_1\left(a_2; \frac{1}{2}; \theta\chi^2\right) \right|^2 d\chi - \int_\omega^\infty \left| e^{-\frac{1}{2}\theta\chi^2} {}_1F_1\left(a_2; \frac{1}{2}; \theta\chi^2\right) \right|^2 d\chi \right] \\
 & = |\mathcal{N}^s R^s|^2 \sum_{\mu, \nu=0}^{\infty} \frac{(a_2)_\nu (a_2^*)_\mu}{\left(\frac{1}{2}\right)_\nu \left(\frac{1}{2}\right)_\mu} \frac{\theta^\nu (\theta^*)^\mu}{\nu! \mu! \sqrt{\operatorname{Re}(\theta)}} \left[\Gamma\left(\mu + \nu + \frac{1}{2}\right) - \Gamma\left(\mu + \nu + \frac{1}{2}, \operatorname{Re}(\theta)\omega^2\right) \right]. \quad (4.43)
 \end{aligned}$$

The second integral in (4.39) reads

$$\begin{aligned}
 & 2 \int_\omega^\infty |\psi_3^s(\chi)|^2 d\chi = 2 |\mathcal{N}^s|^2 \int_\omega^\infty e^{-\chi} \left| {}_1F_1\left(a_1; \frac{1}{2}; \chi^2\right) - 2\chi \frac{\Gamma\left(a_1 + \frac{1}{2}\right)}{\Gamma a_1} {}_1F_1\left(a_1 + \frac{1}{2}; \frac{3}{2}; \chi^2\right) \right|^2 d\chi \\
 & = 2 |\mathcal{N}^s|^2 \left\{ \int_\omega^\infty e^{-\chi} \left| {}_1F_1\left(a_1; \frac{1}{2}; \chi^2\right) \right|^2 d\chi + 4 \left| \frac{\Gamma\left(a_1 + \frac{1}{2}\right)}{\Gamma(a_1)} \right|^2 \int_\omega^\infty e^{-\chi} \chi^2 \left| {}_1F_1\left(a_1 + \frac{1}{2}; \frac{3}{2}; \chi^2\right) \right|^2 d\chi \right. \\
 & \quad \left. - 4 \operatorname{Re} \left[\frac{\Gamma\left(a_1 + \frac{1}{2}\right)}{\Gamma(a_1)} \int_\omega^\infty \chi e^{-\chi^2} {}_1F_1\left(a_1^*; \frac{1}{2}; \chi^2\right) {}_1F_1\left(a_1 + \frac{1}{2}; \frac{3}{2}; \chi^2\right) d\chi \right] \right\} \\
 & = |\mathcal{N}^s|^2 \left\{ \sum_{\mu, \nu=0}^{\infty} \frac{1}{\nu! \mu!} \left[\frac{(a_1)_\nu (a_1^*)_\mu}{\left(\frac{1}{2}\right)_\nu \left(\frac{1}{2}\right)_\mu} \Gamma\left(\mu + \nu + \frac{1}{2}, \omega^2\right) + 4 \left| \frac{\Gamma\left(a_1 + \frac{1}{2}\right)}{\Gamma(a_1)} \right|^2 \frac{(a_1 + \frac{1}{2})_\nu (a_1^* + \frac{1}{2})_\mu}{\left(\frac{3}{2}\right)_\nu \left(\frac{1}{2}\right)_\mu} \Gamma\left(\mu + \nu + \frac{3}{2}, \omega^2\right) \right. \right. \\
 & \quad \left. \left. - 4 \operatorname{Re} \left\{ \frac{\Gamma\left(a_1 + \frac{1}{2}\right)}{\Gamma(a_1)} \frac{(a_1^*)_\nu (a_1 + \frac{1}{2})_\mu}{\left(\frac{1}{2}\right)_\nu \left(\frac{3}{2}\right)_\mu} \Gamma\left(\mu + \nu + 1, \omega^2\right) \right\} \right] \right\}, \quad (4.44)
 \end{aligned}$$

where we used (4.41). Thus for the absolute value of the normalization constant of the whole symmetric wave function follows

$$\begin{aligned}
 |\mathcal{N}^s| & = \left[\sum_{\mu, \nu=0}^{\infty} \frac{1}{\mu! \nu!} \left(|R^s|^2 \frac{(a_2)_\nu (a_2^*)_\mu}{\left(\frac{1}{2}\right)_\nu \left(\frac{1}{2}\right)_\mu} \frac{\theta^\nu (\theta^*)^\mu}{\sqrt{\operatorname{Re}(\theta)}} \left[\Gamma\left(\mu + \nu + \frac{1}{2}\right) - \Gamma\left(\mu + \nu + \frac{1}{2}, \operatorname{Re}(\theta)\omega^2\right) \right] \right. \right. \\
 & \quad \left. \left. + \frac{(a_1)_\nu (a_1^*)_\mu}{\left(\frac{1}{2}\right)_\nu \left(\frac{1}{2}\right)_\mu} \Gamma\left(\mu + \nu + \frac{1}{2}, \omega^2\right) + 4 \left| \frac{\Gamma\left(a_1 + \frac{1}{2}\right)}{\Gamma(a_1)} \right|^2 \frac{(a_1 + \frac{1}{2})_\nu (a_1^* + \frac{1}{2})_\mu}{\left(\frac{3}{2}\right)_\nu \left(\frac{1}{2}\right)_\mu} \Gamma\left(\mu + \nu + \frac{3}{2}, \omega^2\right) \right. \right. \\
 & \quad \left. \left. - 4 \operatorname{Re} \left\{ \frac{\Gamma\left(a_1 + \frac{1}{2}\right)}{\Gamma(a_1)} \frac{(a_1^*)_\nu (a_1 + \frac{1}{2})_\mu}{\left(\frac{1}{2}\right)_\nu \left(\frac{3}{2}\right)_\mu} \Gamma\left(\mu + \nu + 1, \omega^2\right) \right\} \right] \right]^{-1/2}. \quad (4.45)
 \end{aligned}$$

We have to note that this is only the absolute value of the normalization constant so that a general expression for \mathcal{N}^s would include an additional phase factor:

$$\mathcal{N}^s = |\mathcal{N}^s| e^{i\varphi^s}. \quad (4.46)$$

4.1.1.3 Real limit

Now let us evaluate for consistency reasons our results in the limit $c \rightarrow 0$ in order to see whether the familiar results of the real harmonic potential

$$E_0^s = \hbar\Omega \left(2n + \frac{1}{2}\right), \quad \psi_0^s(x) = \sqrt{\sqrt{\frac{\lambda_1}{\pi}} \frac{1}{2^{2n}(2n)!}} e^{-\frac{1}{2}\lambda_1 x^2} H_{2n}(\sqrt{\lambda_1}x) \quad (4.47)$$

are included. Here $H_{2n}(\chi)$ denotes the Hermite polynomials of even order $2n$, which are special cases of the confluent hypergeometric functions according to the formula [29, (34.23)]

$$H_{2n}(\chi) = (-1)^n \frac{(2n)!}{n!} {}_1F_1\left(-n; \frac{1}{2}; \chi^2\right). \quad (4.48)$$

Let us start with evaluating the quantization condition in this limit. First of all taking a look at (4.11) and (4.20) allows us to calculate directly

$$\lim_{c \rightarrow 0} \theta = 1 \quad \Rightarrow \quad \lim_{c \rightarrow 0} a_2 = a_1 =: a, \quad \lim_{c \rightarrow 0} \lambda_2 = \lambda_1 =: \lambda. \quad (4.49)$$

Thus (4.37) reads

$$\begin{aligned} & \omega {}_1F_1\left(a; \frac{1}{2}; \omega^2\right) - 4a\omega {}_1F_1\left(a+1; \frac{3}{2}; \omega^2\right) \\ & + 2 \frac{\Gamma\left(a + \frac{1}{2}\right)}{\Gamma(a)} \left[(1 - \omega^2) {}_1F_1\left(a + \frac{1}{2}; \frac{3}{2}; \omega^2\right) + \frac{4}{3} \left(a + \frac{1}{2}\right) \omega^2 {}_1F_1\left(a + \frac{3}{2}; \frac{5}{2}; \omega^2\right) \right] \\ & = \left[1 - 2\omega \frac{\Gamma\left(a + \frac{1}{2}\right)}{\Gamma(a)} \frac{{}_1F_1\left(a + \frac{1}{2}; \frac{3}{2}; \omega^2\right)}{{}_1F_1\left(a; \frac{1}{2}; \omega^2\right)} \right] \left[\omega {}_1F_1\left(a; \frac{1}{2}; \omega^2\right) - 4a\omega {}_1F_1\left(a+1; \frac{3}{2}; \omega^2\right) \right], \quad (4.50) \end{aligned}$$

which reduces to

$$\begin{aligned} & \frac{\Gamma\left(a + \frac{1}{2}\right)}{\Gamma(a)} \left[{}_1F_1\left(a + \frac{1}{2}; \frac{3}{2}; \omega^2\right) + \frac{4}{3} \left(a + \frac{1}{2}\right) \omega^2 {}_1F_1\left(a + \frac{3}{2}; \frac{5}{2}; \omega^2\right) \right. \\ & \left. - 4a\omega^2 \frac{{}_1F_1\left(a + \frac{1}{2}; \frac{3}{2}; \omega^2\right)}{{}_1F_1\left(a; \frac{1}{2}; \omega^2\right)} {}_1F_1\left(a+1; \frac{3}{2}; \omega^2\right) \right] = 0. \quad (4.51) \end{aligned}$$

We have to obtain a solution a , which does not depend on the waist ω , since in the real limit this quantity obviously has no influence on the whole system at all. To ensure this the first factor has to vanish so the solutions are $\frac{\Gamma\left(a + \frac{1}{2}\right)}{\Gamma(a)} = 0$, which are all $-n$ for non-negative integers n . Thus we conclude by using (4.21)

$$a = -n \quad \Rightarrow \quad \varepsilon_0^s = 4n + 1 \quad \Rightarrow \quad E_0^s = \hbar\Omega \left(2n + \frac{1}{2}\right), \quad n \in \mathbb{N}, \quad (4.52)$$

4 Complex harmonic potential

which coincides with the energy in (4.47). Next we derive an expression for the normalization constant in the real limit. For this purpose we also set $a_1 = a_2 = -n$ in (4.45) and conclude that all terms containing $\Gamma(a_1)^{-1}$ vanish and thus $R^s = 1$ from (4.34). Furthermore all infinite sums including $(-n)_\nu$ now have n as their upper summation index, since we have $(-n)_\nu = 0$ for all $\nu > n$. Finally there only remains

$$|\mathcal{N}^s| = \left\{ \sum_{\mu, \nu=0}^n \frac{1}{\mu! \nu!} \left[\frac{(-n)_\nu (-n)_\mu}{\left(\frac{1}{2}\right)_\nu \left(\frac{1}{2}\right)_\mu} \left[\Gamma\left(\mu + \nu + \frac{1}{2}\right) - \Gamma\left(\mu + \nu + \frac{1}{2}, \omega^2\right) \right] + \frac{(-n)_\nu (-n)_\mu}{\left(\frac{1}{2}\right)_\nu \left(\frac{1}{2}\right)_\mu} \Gamma\left(\mu + \nu + \frac{1}{2}, \omega^2\right) \right] \right\}^{-1/2}, \quad (4.53)$$

which reduces to

$$|\mathcal{N}^s| = \left\{ \sum_{\mu, \nu=0}^n \frac{1}{\mu! \nu!} \frac{(-n)_\nu (-n)_\mu}{\left(\frac{1}{2}\right)_\nu \left(\frac{1}{2}\right)_\mu} \Gamma\left(\mu + \nu + \frac{1}{2}\right) \right\}^{-1/2}. \quad (4.54)$$

Taking into account (4.41) we obtain

$$|\mathcal{N}^s| = \left\{ \int_{-\infty}^{\infty} e^{-\chi^2} \left| {}_1F_1\left(-n, \frac{1}{2}; \chi^2\right) \right|^2 d\chi \right\}^{-1/2}, \quad (4.55)$$

where we used the symmetry of $e^{-\chi^2} \left| {}_1F_1\left(-n, \frac{1}{2}; \chi^2\right) \right|^2$ with respect to $\chi = 0$ in the last step to expand the integral over the whole real axis. With the definition of the Hermite polynomials (4.48) we can write for this integral

$$|\mathcal{N}^s| = \frac{(2n)!}{n!} \left\{ \int_{-\infty}^{\infty} e^{-\chi^2} |H_{2n}(\chi)|^2 d\chi \right\}^{-1/2} = \frac{(2n)!}{n!} \sqrt{\frac{1}{\sqrt{\pi} 2^{2n} (2n)!}}, \quad (4.56)$$

where we used the calculation of the integral from [29, Chap. 35].

Taking the real limit $a_1 = a_2 = -n$ of (4.35) yields directly one and the same form in all 3 areas

$$\psi_0^s(\chi) = \mathcal{N}^s e^{-\frac{1}{2}\chi^2} {}_1F_1\left(-n; \frac{1}{2}; \chi^2\right). \quad (4.57)$$

Now we insert the absolute value of the normalization constant (4.56) into the general expression (4.46), so that we can write for the wave function

$$\psi_0^s(\chi) = \frac{(2n)!}{n!} \sqrt{\frac{1}{\sqrt{\pi} 2^{2n} (2n)!}} e^{i\varphi} e^{-\frac{1}{2}\chi^2} {}_1F_1\left(-n; \frac{1}{2}; \chi^2\right), \quad (4.58)$$

which reduces with (4.48) to

$$\psi_0^s(\chi) = (-1)^n \sqrt{\frac{1}{\sqrt{\pi} 2^{2n} (2n)!}} e^{i\varphi} e^{-\frac{1}{2}\chi^2} H_{2n}(\chi). \quad (4.59)$$

Thus the phase has to be $\varphi = n\pi$, that is $e^{i\varphi} = (-1)^n$, and we obtain the correct real limit

$$\psi_0^s(\chi) = \sqrt{\frac{1}{\sqrt{\pi}2^{2n}(2n)!}} e^{-\frac{1}{2}\chi^2} H_{2n}(\chi) \quad \Leftrightarrow \quad \psi_0^s(x) = \sqrt{\sqrt{\frac{\lambda}{\pi}} \frac{1}{2^{2n}(2n)!}} e^{-\frac{1}{2}\lambda x^2} H_{2n}(\sqrt{\lambda}x), \quad (4.60)$$

where $\lambda_1 = \lambda_2 =: \lambda$ in the limit $C \rightarrow 0$. The λ in the prefactor arises, because the integration has now to be performed with respect to x instead of $\chi = \sqrt{\lambda}x$.

4.1.1.4 Limit of vanishing waist

Next we evaluate the special case $\omega \rightarrow 0$, that should directly correspond to the real limit just like for the square well potential, since in this particular limit area 2 and thus the region, where $V_I \neq 0$, vanishes. Therefore, only the familiar system of a real harmonic potential remains, which is, indeed, nothing else than the real limit. Thus we have to show that in the limit $\omega \rightarrow 0$ all area-1- and area-3-quantities of our complex system turn into the familiar form of the real system. Area 2 and its variables are not of any interest in this case but nevertheless we must derive a_1 and thus also ε from the quantization condition (4.37). Therefore we have to write down an expression of it in the limit $\omega \rightarrow 0$. To perform this we first need the limits of the following quantities:

$$\lim_{x \rightarrow 0} {}_1F_1(a; c; x) = 1, \quad \lim_{\omega \rightarrow 0} \theta = \lim_{\omega \rightarrow 0} \sqrt{1 + \frac{ic}{\omega^2}} = \infty, \quad \lim_{\omega \rightarrow 0} a_2 = \frac{1}{4}. \quad (4.61)$$

From them we conclude

$$\lim_{\omega \rightarrow 0} \theta\omega = \sqrt{ic}, \quad \lim_{\omega \rightarrow 0} \theta\omega^2 = 0. \quad (4.62)$$

Inserting these results into (4.37) yields the following condition for a_1 :

$$2 \frac{\Gamma(a_1 + \frac{1}{2})}{\Gamma(a_1)} = -2 \lim_{\omega \rightarrow 0} \omega \frac{\Gamma(a_1 + \frac{1}{2})}{\Gamma(a_1)} \left[\sqrt{i\frac{c}{2}} - \sqrt{i\frac{c}{2}} \right] \quad \Leftrightarrow \quad \frac{\Gamma(a_1 + \frac{1}{2})}{\Gamma(a_1)} = 0. \quad (4.63)$$

This is only fulfilled if a_1 is equal to some negative natural number $a_1 = -n$, which indeed yields exactly the same result like in the real limit so that all the following steps can be adopted and we finally obtain for the limit of vanishing waist $\omega \rightarrow 0$ the familiar result:

$$E_0^s = \hbar\Omega \left(2n + \frac{1}{2} \right), \quad \psi_{1,0}^s(x) =: \psi_0^s(x) = \sqrt{\sqrt{\frac{\lambda}{\pi}} \frac{1}{2^{2n}(2n)!}} e^{-\frac{1}{2}\lambda x^2} H_{2n}(\sqrt{\lambda}x). \quad (4.64)$$

4.1.1.5 Limit of big waist

Similar to the limit of vanishing waist, that is $\omega \rightarrow 0$, we also evaluate the limit of big waist $\omega \rightarrow \infty$. To this end we rewrite the quantization condition (4.37) in the limit $\omega \rightarrow \infty$ and extract some information about a_2 and thus ε , since area 1 vanishes and thus a_1 is not important any

more. Taking the limit $\omega \rightarrow \infty$ in (4.37) we have to use the limit of the confluent hypergeometric functions (4.27) and neglect the first term since the exponential function in the second grows much stronger than every polynomial in ω . Furthermore we calculate from (4.20) that $\theta \rightarrow 1$ and multiply the whole expression with the denominator of R^s so that all remaining terms have the denominator $\Gamma(a_1)\Gamma(a_2)$. This may be also reasonable since in the considered limit we have $\psi_2^s = \psi^s$ on the whole axis so that it should be $\lim_{\chi \rightarrow \infty} \psi_2^s(\chi) = 0$. Otherwise the calculation of R^s in (4.34) could include some division by zero. Since the prefactor of the right-hand side, which is then the numerator of R^s , vanishes in the highest order and all terms of the order $2(a_1 + a_2) - 1$ in ω cancel each other, there remains only one term of order $2(a_1 + a_2) - 3$ which has to be equal to zero. Thus the quantization condition for $\omega \rightarrow \infty$ reads

$$\lim_{\omega \rightarrow \infty} \frac{\omega^{2(a_1+a_2)}}{\Gamma(a_1)\Gamma(a_2)} = 0. \quad (4.65)$$

We want to extract a condition for a_2 from that, which is fulfilled (4.65) for all a_1 , since it is not realized any more in this system for $\omega \rightarrow \infty$. Eq. (4.65) is always ensured if a_2 is equal to some negative integer number $a_2 = -n$. This yields nothing else than the "real limit" for area 2 since it is the same result for a_2 like for a_1 in the limit $c \rightarrow 0$ or $\omega \rightarrow 0$ when area 2 disappeared. Nevertheless it is followed by a different energy which is still complex and contains an imaginary part which is linear in the depth c of the well:

$$\lim_{\omega \rightarrow \infty} a_2 = \frac{1}{4}(1 - \varepsilon_\infty - ic) = -n \quad \Leftrightarrow \quad \varepsilon_\infty^s = 4n + 1 - ic \quad (4.66)$$

$$\Leftrightarrow \quad E_\infty^s = \hbar\Omega \left(2n + \frac{1}{2}\right) - iC. \quad (4.67)$$

For the wave function this provides

$$\begin{aligned} \psi_{2,\infty}^s(\chi) &= \psi_\infty^s(\chi) = \mathcal{N}^s e^{-\frac{1}{2}\chi^2} {}_1F_1\left(-n; \frac{1}{2}; \omega^2\right) \\ &= (-1)^n \mathcal{N}^s \frac{n!}{(2n)!} e^{-\frac{1}{2}\chi^2} H_{2n}(\chi). \end{aligned} \quad (4.68)$$

Evaluating the normalization constant (4.45) in the limit $\omega \rightarrow \infty$ yields

$$\begin{aligned} |\mathcal{N}^s| &= \frac{1}{|R^s|} \left[\sum_{\mu,\nu=0}^n \frac{(-n)_\nu (-n)_\mu}{\nu! \mu! \left(\frac{1}{2}\right)_\nu \left(\frac{1}{2}\right)_\mu} \Gamma\left(\mu + \nu + \frac{1}{2}\right) \right]^{-1/2} \\ &\stackrel{(4.41)}{=} \frac{1}{|R^s|} \left[2 \int_0^\infty e^{-\frac{1}{2}\chi^2} \left| {}_1F_1\left(-n; \frac{1}{2}; \chi^2\right) \right|^2 d\chi \right]^{-1/2} \\ &\stackrel{(4.48)}{=} \frac{(2n)!}{n! |R^s|} \left[\int_{-\infty}^\infty e^{-\frac{1}{2}\chi^2} |H_{2n}(\chi)|^2 d\chi \right]^{-1/2} \\ &\stackrel{(4.56)}{=} \frac{(2n)!}{n! |R^s|} \sqrt{\frac{1}{\sqrt{\pi} 2^{2n} (2n)!}}, \end{aligned} \quad (4.69)$$

since $\lim_{\omega \rightarrow \infty} \Gamma(a, \omega^2) = 0$. Before inserting this into the wave function (4.68) in area 2 we have to consider that this is only the absolute value of \mathcal{N}^s and also includes only the absolute value of R^s which are in general complex numbers. Thus we have to add an arbitrary phase factor $\mathcal{N}^s = |\mathcal{N}^s| e^{i\varphi}$, $R^s = |R^s| e^{i\vartheta}$. We already know $\varphi = n\pi$ from the real limit, when area 2 vanishes, and, since R^s only contains real functions for $\omega \rightarrow \infty$, we can state $|R^s| = R^s$. This seems to be right since exactly $\vartheta = 0$ leads us to the correct wave function

$$\begin{aligned} \psi_{2,\infty}^s(\chi) &= \psi_{\infty}^s(\chi) = (-1)^n \frac{(2n)!}{n!} \sqrt{\frac{1}{\sqrt{\pi} 2^{2n} (2n)!}} e^{-\frac{1}{2}\chi^2} {}_1F_1\left(-n; \frac{1}{2}; \chi^2\right) \\ &= \sqrt{\frac{1}{\sqrt{\pi} 2^{2n} (2n)!}} e^{-\frac{1}{2}\chi^2} H_{2n}(\chi). \end{aligned} \quad (4.70)$$

Thus, we have

$$\psi_{\infty}^s(x) = \sqrt{\sqrt{\frac{\lambda}{\pi}} \frac{1}{2^{2n} (2n)!}} e^{-\frac{1}{2}\lambda x^2} H_{2n}(\sqrt{\lambda}x) = \psi_0^s(x). \quad (4.71)$$

So finally we got in some sense the same result as for the complex square well potential since the wave function and the real part of the energy yield nothing else than the real limit and only the imaginary part of the energy provides something new. Thus the imaginary potential does not influence the wave function qualitatively but yields an imaginary part of the energy which is linear in c . The interesting issue is that this seems to be independent of the particular shape of the imaginary potential since in both cases, square well in the limit $\omega \rightarrow \pi/2$ as well as harmonic potential for $\omega \rightarrow \infty$, we get the same result for the imaginary part.

4.1.2 Antisymmetric states

Let us now evaluate along similar lines the antisymmetric wave function (4.23), that means the wave functions $\psi_1^a, \psi_2^a, \psi_3^a$ have to fulfill

$$\psi_1^a(-\chi) = -\psi_3^a(\chi), \quad \psi_2^a(-\chi) = -\psi_2^a(\chi). \quad (4.72)$$

Next we derive conditions for A_2^a and ε by demanding continuity and differentiability of ψ^a at $\chi = -\omega$. But first of all we change slightly the notation for ψ_1 , which seems to be reasonable in the antisymmetric case. Instead of expressing A_1^a via A_1^s we now do it vice versa and get for the constant of the antisymmetric part

$$A_1^s = A_1^a \lim_{\chi \rightarrow \infty} \frac{\chi {}_1F_1\left(a_1 + \frac{1}{2}; \frac{3}{2}; \chi^2\right)}{{}_1F_1\left(a_1; \frac{1}{2}; \chi^2\right)}. \quad (4.73)$$

Performing an analogous discussion as we did for A_1^s provides correspondingly

$$A_1^s = A_1^a \frac{\Gamma(a_1)}{2\Gamma\left(a_1 + \frac{1}{2}\right)}, \quad (4.74)$$

where we have to note $A_1^a = 0$ if a_1 is equal to some negative integer number $a_1 = -n, n \in \mathbb{N}$, similar to the symmetric case. Moreover the wave function is completely antisymmetric for $a_1 = -n - \frac{1}{2}$, because in this case A_1^s vanishes. Thus the antisymmetric wave function in area 1 reads

$$\psi_1(\chi) = A_1^a e^{-\frac{1}{2}\chi^2} \left[\frac{\Gamma(a_1)}{2\Gamma\left(a_1 + \frac{1}{2}\right)} {}_1F_1\left(a_1; \frac{1}{2}; \chi^2\right) + \chi {}_1F_1\left(a_1 + \frac{1}{2}; \frac{3}{2}; \chi^2\right) \right]. \quad (4.75)$$

Now we consider the continuity conditions of ψ^a and its first derivative. We start with the continuity of ψ^a at $\chi = -\omega$:

$$\psi_1^a(-\omega) = \psi_2^a(-\omega), \quad (4.76)$$

which reads in detail

$$A_2^a = \mathcal{N}^a e^{\frac{1}{2}(\theta-1)\omega^2} \frac{\omega {}_1F_1\left(a_1 + \frac{1}{2}; \frac{3}{2}; \omega^2\right) - \frac{\Gamma(a_1)}{2\Gamma\left(a_1 + \frac{1}{2}\right)} {}_1F_1\left(a_1; \frac{1}{2}; \omega^2\right)}{\theta \omega {}_1F_1\left(a_2 + \frac{1}{2}; \frac{3}{2}; \theta\omega^2\right)} =: \mathcal{N}^a R^a, \quad (4.77)$$

where we set $\mathcal{N}^a := A_1^a$ and introduced the abbreviation $R^a = R^a(\omega, \varepsilon, c)$ similar to the symmetric case. Therefore obeying (4.72) the antisymmetric wave function in all 3 areas reads

$$\psi^a(\chi) = \mathcal{N}^a \begin{cases} e^{-\frac{1}{2}\chi^2} \left[\chi {}_1F_1\left(a_1 + \frac{1}{2}; \frac{3}{2}; \chi^2\right) + \frac{\Gamma(a_1)}{2\Gamma\left(a_1 + \frac{1}{2}\right)} {}_1F_1\left(a_1; \frac{1}{2}; \chi^2\right) \right] & , \chi < -\omega \\ R^a \theta \chi e^{-\frac{1}{2}\theta\chi^2} {}_1F_1\left(a_2 + \frac{1}{2}; \frac{3}{2}; \theta\chi^2\right) & , -\omega \leq \chi \leq \omega \\ e^{-\frac{1}{2}\chi^2} \left[\chi {}_1F_1\left(a_1 + \frac{1}{2}; \frac{3}{2}; \chi^2\right) - \frac{\Gamma(a_1)}{2\Gamma\left(a_1 + \frac{1}{2}\right)} {}_1F_1\left(a_1; \frac{1}{2}; \chi^2\right) \right] & , \chi > \omega \end{cases} . \quad (4.78)$$

4.1.2.1 Quantization condition

Next we derive the quantization condition for the antisymmetric states which can be derived similar to the symmetric case by demanding continuity of $\frac{\partial}{\partial\chi}\psi^a$ at $\chi = -\omega$, that is

$$\frac{\partial}{\partial\chi}\psi_1^a(\chi) \Big|_{\chi=-\omega} = \frac{\partial}{\partial\chi}\psi_2^a(\chi) \Big|_{\chi=-\omega}, \quad (4.79)$$

which reads

$$\begin{aligned}
 & \frac{\omega\Gamma(a_1)}{2\Gamma(a_1+\frac{1}{2})} \left[{}_1F_1\left(a_1; \frac{1}{2}; \omega^2\right) - 4a_1 {}_1F_1\left(a_1+1; \frac{3}{2}; \omega^2\right) \right] + (1-\omega^2) {}_1F_1\left(a_1+\frac{1}{2}; \frac{3}{2}; \omega^2\right) \\
 & + \frac{4}{3}\omega^2\left(a_1+\frac{1}{2}\right) {}_1F_1\left(a_1+\frac{3}{2}; \frac{5}{2}; \omega^2\right) = \frac{\omega {}_1F_1\left(a_1+\frac{1}{2}; \frac{3}{2}; \omega^2\right) - \frac{\Gamma(a_1)}{2\Gamma(a_1+\frac{1}{2})} {}_1F_1\left(a_1; \frac{1}{2}; \omega^2\right)}{\omega {}_1F_1\left(a_2+\frac{1}{2}; \frac{3}{2}; \theta\omega^2\right)} \\
 & \times \left[{}_1F_1\left(a_2+\frac{1}{2}; \frac{3}{2}; \theta\omega^2\right) - \theta\omega^2 {}_1F_1\left(a_2+\frac{1}{2}; \frac{3}{2}; \theta\omega^2\right) + \frac{4}{3}\theta\omega^2\left(a_2+\frac{1}{2}\right) {}_1F_1\left(a_2+\frac{3}{2}; \frac{5}{2}; \theta\omega^2\right) \right], \quad (4.80)
 \end{aligned}$$

where we used again (4.38). Since a_1, a_2 and θ are functions of ϵ, ω and c via (4.20) and (4.21) the quantization condition for the antisymmetric states (4.80) does only depend on these three quantities. Similar to the symmetric case this is a transcendental equation in ϵ , so that we have to solve it numerically later on.

4.1.2.2 Normalization constant

The next step should be the normalization of the wave function for which we have to determine \mathcal{N}^a from the condition

$$\int_{-\infty}^{\infty} |\psi^a(\chi)|^2 d\chi = 2 \int_0^{\omega} |\psi_2^a(\chi)|^2 d\chi + 2 \int_{\omega}^{\infty} |\psi_3^a(\chi)|^2 d\chi = 1. \quad (4.81)$$

We calculate the integrals separately and start with the first one. With (4.41) we can write

$$\begin{aligned}
 & 2 \int_0^{\omega} |\psi_2^a(\chi)|^2 d\chi = 2 |\mathcal{N}^a R^a|^2 \theta^2 \int_0^{\omega} \chi^2 \left| e^{-\frac{1}{2}\theta\chi^2} {}_1F_1\left(a_2+\frac{1}{2}; \frac{3}{2}; \theta\chi^2\right) \right|^2 d\chi \\
 & = |\mathcal{N}^a R^a|^2 \sum_{\mu, \nu=0}^{\infty} \frac{(a_1)_{\nu} (a_1^*)_{\mu}}{\left(\frac{1}{2}\right)_{\nu} \left(\frac{1}{2}\right)_{\mu} \nu! \mu!} \frac{\theta^{\nu+1} (\theta^*)^{\mu+1}}{\sqrt{\text{Re}(\theta)}} \left[\Gamma\left(\mu+\nu+\frac{3}{2}\right) - \Gamma\left(\mu+\nu+\frac{3}{2}, \text{Re}(\theta)\omega^2\right) \right]. \quad (4.82)
 \end{aligned}$$

For the second one follows

$$\begin{aligned}
 & 2 \int_{\omega}^{\infty} |\psi_3^a(\chi)|^2 d\chi = 2 |\mathcal{N}^a|^2 \int_{\omega}^{\infty} e^{-\chi^2} \left| \chi {}_1F_1\left(a_1+\frac{1}{2}; \frac{3}{2}; \chi^2\right) - \frac{\Gamma(a_1)}{2\Gamma(a_1+\frac{1}{2})} {}_1F_1\left(a_1; \frac{1}{2}; \chi^2\right) \right|^2 d\chi \\
 & = 2 |\mathcal{N}^a|^2 \left[\int_{\omega}^{\infty} \chi^2 e^{-\chi^2} \left| {}_1F_1\left(a_1+\frac{1}{2}; \frac{3}{2}; \chi^2\right) \right|^2 d\chi + \left| \frac{\Gamma(a_1)}{2\Gamma(a_1+\frac{1}{2})} \right|^2 \int_{\omega}^{\infty} e^{-\chi^2} \left| {}_1F_1\left(a_1; \frac{1}{2}; \chi^2\right) \right|^2 d\chi \right. \\
 & \quad \left. - \text{Re} \left\{ \frac{\Gamma(a_1)}{\Gamma(a_1+\frac{1}{2})} \int_{\omega}^{\infty} \chi e^{-\chi^2} {}_1F_1\left(a_1^*+\frac{1}{2}; \frac{3}{2}; \chi^2\right) {}_1F_1\left(a_1; \frac{1}{2}; \chi^2\right) d\chi \right\} \right] \\
 & = |\mathcal{N}^a|^2 \sum_{\nu, \mu=0}^{\infty} \frac{1}{\mu! \nu!} \left[\frac{(a_1+\frac{1}{2})_{\nu} (a_1^*+\frac{1}{2})_{\mu}}{\left(\frac{3}{2}\right)_{\nu} \left(\frac{3}{2}\right)_{\mu}} \Gamma\left(\mu+\nu+\frac{3}{2}, \omega^2\right) + \left| \frac{\Gamma(a_1)}{2\Gamma(a_1+\frac{1}{2})} \right|^2 \frac{(a_1)_{\nu} (a_1^*)_{\mu}}{\left(\frac{1}{2}\right)_{\nu} \left(\frac{1}{2}\right)_{\mu}} \Gamma\left(\mu+\nu+\frac{1}{2}, \omega^2\right) \right. \\
 & \quad \left. - \text{Re} \left\{ \frac{\Gamma(a_1)}{\Gamma(a_1+\frac{1}{2})} \frac{(a_1)_{\nu} (a_1^*+\frac{1}{2})_{\mu}}{\left(\frac{1}{2}\right)_{\nu} \left(\frac{3}{2}\right)_{\mu}} \Gamma\left(\mu+\nu+1, \omega^2\right) \right\} \right]. \quad (4.83)
 \end{aligned}$$

Thus the normalization constant for the whole antisymmetric wave function reads

4 Complex harmonic potential

$$\begin{aligned}
|\mathcal{N}^a| = & \left[\sum_{\mu, \nu=0}^{\infty} \frac{1}{\mu! \nu!} \left(|R^a|^2 \frac{(a_1 + \frac{1}{2})_{\nu} (a_1^* + \frac{1}{2})_{\mu}}{(\frac{3}{2})_{\nu} (\frac{3}{2})_{\mu}} \frac{\theta^{\nu+1} (\theta^*)^{\mu+1}}{\sqrt{\operatorname{Re}(\theta)}} \left[\Gamma\left(\mu + \nu + \frac{3}{2}\right) - \Gamma\left(\mu + \nu + \frac{3}{2}, \operatorname{Re}(\theta)\omega^2\right) \right] \right. \right. \\
& + \frac{(a_1 + \frac{1}{2})_{\nu} (a_1^* + \frac{1}{2})_{\mu}}{(\frac{3}{2})_{\nu} (\frac{3}{2})_{\mu}} \Gamma\left(\mu + \nu + \frac{3}{2}, \omega^2\right) + \left| \frac{\Gamma(a_1)}{2\Gamma(a_1 + \frac{1}{2})} \right|^2 \frac{(a_1)_{\nu} (a_1^*)_{\mu}}{(\frac{1}{2})_{\nu} (\frac{1}{2})_{\mu}} \Gamma\left(\mu + \nu + \frac{1}{2}, \omega^2\right) \\
& \left. \left. - \operatorname{Re} \left\{ \frac{\Gamma(a_1)}{\Gamma(a_1 + \frac{1}{2})} \frac{(a_1)_{\nu} (a_1^* + \frac{1}{2})_{\mu}}{(\frac{1}{2})_{\nu} (\frac{3}{2})_{\mu}} \Gamma(\mu + \nu + 1, \omega^2) \right\} \right]^{-1/2}, \tag{4.84}
\end{aligned}$$

where we have to note again that this only represents the absolute value so that the complete expression of \mathcal{N}^a also contains an additional phase φ^a :

$$\mathcal{N}^a = |\mathcal{N}^a| e^{i\varphi^a}. \tag{4.85}$$

4.1.2.3 Real limit

Next we evaluate for consistency reasons the real limit, that is $c \rightarrow 0$, and ensure that our results contain the familiar harmonic potential well

$$E^a = \hbar\Omega \left(2n + \frac{3}{2}\right), \quad \psi^a(x) = \sqrt{\frac{\lambda_1}{\pi}} \frac{1}{2^{2n+1} (2n+1)!} e^{-\frac{1}{2}\lambda_1 x^2} H_{2n+1} \left(\sqrt{\lambda_1} x\right) \tag{4.86}$$

as the limit for vanishing imaginary potential. To this end we introduce the Hermite polynomials of odd order $2n + 1$, that are special cases of the confluent hypergeometric functions, via the relation [29, (34.23)]

$$H_{2n+1}(\chi) = (-1)^n \frac{2(2n+1)!}{n!} \chi {}_1F_1\left(-n; \frac{3}{2}; \chi^2\right). \tag{4.87}$$

We start with the quantization condition (4.80). In the limit $c \rightarrow 0$ we can use (4.49) again which leads us to

$$\begin{aligned}
& \frac{\omega\Gamma(a)}{2\Gamma(a + \frac{1}{2})} \left[{}_1F_1\left(a; \frac{1}{2}; \omega^2\right) - 4a {}_1F_1\left(a + 1; \frac{3}{2}; \omega^2\right) \right] - \omega^2 {}_1F_1\left(a + \frac{1}{2}; \frac{3}{2}; \omega^2\right) + {}_1F_1\left(a + \frac{1}{2}; \frac{3}{2}; \omega^2\right) \\
& + \frac{4}{3}\omega^2 \left(a + \frac{1}{2}\right) {}_1F_1\left(a + \frac{3}{2}; \frac{5}{2}; \omega^2\right) = \left[1 - \frac{\Gamma(a)}{2\Gamma(a + \frac{1}{2})} \frac{{}_1F_1\left(a; \frac{1}{2}; \omega^2\right)}{{}_1F_1\left(a + \frac{1}{2}; \frac{3}{2}; \omega^2\right)} \right] \\
& \times \left[{}_1F_1\left(a + \frac{1}{2}; \frac{3}{2}; \omega^2\right) - \omega^2 {}_1F_1\left(a + \frac{1}{2}; \frac{3}{2}; \theta\omega^2\right) + \frac{4}{3}\omega^2 \left(a + \frac{1}{2}\right) {}_1F_1\left(a + \frac{3}{2}; \frac{5}{2}; \omega^2\right) \right]. \tag{4.88}
\end{aligned}$$

This simplifies to

$$\begin{aligned}
& \frac{\Gamma(a)}{\Gamma(a + \frac{1}{2})} \left[{}_1F_1\left(a; \frac{1}{2}; \omega^2\right) - 4a\omega^2 {}_1F_1\left(a + 1; \frac{3}{2}; \omega^2\right) \right. \\
& \left. + \frac{4}{3}\omega^2 \left(a + \frac{1}{2}\right) \frac{{}_1F_1\left(a; \frac{1}{2}; \omega^2\right)}{{}_1F_1\left(a + \frac{1}{2}; \frac{3}{2}; \omega^2\right)} {}_1F_1\left(a + \frac{3}{2}; \frac{5}{2}; \omega^2\right) \right] = 0. \tag{4.89}
\end{aligned}$$

From this we extract a condition for a and thus for the energy, which has to be independent of the waist ω , because in the real limit it has obviously no influence on the system any more. Since the Γ -function has no roots, the only possible choice of a is at a singularity of $\Gamma\left(a + \frac{1}{2}\right)$ which is $a = -n - \frac{1}{2}$ for some arbitrary natural number $n \in \mathbb{N}$. From this we can directly calculate the energy of the antisymmetric states in the real limit via (4.21)

$$a = \frac{1}{4}(1 - \varepsilon_0^a) = -n - \frac{1}{2} \quad \Leftrightarrow \quad \varepsilon_0^a = 4n + 3 \quad \Leftrightarrow \quad E_0^a = \hbar\Omega \left(2n + \frac{3}{2}\right). \quad (4.90)$$

So the quantization condition in the real limit directly provides the correct energy of the antisymmetric states of the real harmonic potential well. Next we evaluate the wave function in the real limit and start with the normalization. Therefore we take the expression for the antisymmetric normalization constant (4.84) in the limit $c = 0$, that means $\theta = 1$ and $a_1 = a_2 = a = -n - \frac{1}{2}$. The last condition yields directly that we can neglect all terms including $\Gamma\left(a + \frac{1}{2}\right)^{-1}$ because of the singularity of Γ at this particular value for a . Furthermore, one can calculate $R^a = 1$ for $c = 0$, so that \mathcal{N}^a finally reads

$$\begin{aligned} |\mathcal{N}^a| &= \left\{ \sum_{\mu, \nu=0}^n \frac{1}{\mu! \nu!} \left[\frac{(-n)_\nu (-n)_\mu}{\left(\frac{3}{2}\right)_\nu \left(\frac{3}{2}\right)_\mu} \left[\Gamma\left(\mu + \nu + \frac{3}{2}\right) - \Gamma\left(\mu + \nu + \frac{3}{2}, \omega^2\right) \right] + \frac{(-n)_\nu (-n)_\mu}{\left(\frac{3}{2}\right)_\nu \left(\frac{3}{2}\right)_\mu} \Gamma\left(\mu + \nu + \frac{3}{2}, \omega^2\right) \right] \right\}^{-1/2} \\ &= \left\{ \sum_{\mu, \nu=0}^n \frac{1}{\mu! \nu!} \frac{(-n)_\nu (-n)_\mu}{\left(\frac{3}{2}\right)_\nu \left(\frac{3}{2}\right)_\mu} \Gamma\left(\mu + \nu + \frac{3}{2}\right) \right\}^{-1/2} \\ &\stackrel{(4.41)}{=} \left\{ \int_{-\infty}^{\infty} \chi^2 e^{-\chi^2} \left| {}_1F_1\left(-n, \frac{3}{2}; \chi^2\right) \right|^2 d\chi \right\}^{-1/2}. \end{aligned} \quad (4.91)$$

In the last step we used the symmetry of the integrand with respect to $\chi = 0$ to extend the integration over the whole real axis. With (4.87) we can write for this

$$|\mathcal{N}^a| = \frac{2(2n+1)!}{n!} \left\{ \int_{-\infty}^{\infty} e^{-\chi} |H_{2n+1}(\chi)|^2 d\chi \right\}^{-1/2} = \frac{2(2n+1)!}{n!} \sqrt{\frac{1}{\sqrt{\pi} 2^{2n+1} (2n+1)!}}, \quad (4.92)$$

where we took the particular evaluation of the integral again from [29, Chap. 35]. We have to note again that this is only the absolute value for \mathcal{N}^a so that we calculated the normalization constant only up to a phase φ^a which we want to determine by demanding consistence in the real limit. Now we are able to derive the correct expression for the antisymmetric wave function in the real limit. Therefore we insert all results we calculated so far for a , θ , R^a and \mathcal{N}^a into (4.78) and see directly that alle three wave functions end up in one and the same expression:

$$\psi^a(\chi) = \frac{2(2n+1)!}{n!} \sqrt{\frac{1}{\sqrt{\pi} 2^{2n+1} (2n+1)!}} e^{i\varphi^a} e^{-\frac{1}{2}\chi^2} \chi {}_1F_1\left(-n; \frac{3}{2}; \chi^2\right) \quad (4.93)$$

$$= (-1)^n e^{i\varphi^a} \sqrt{\frac{1}{\sqrt{\pi} 2^{2n+1} (2n+1)!}} e^{-\frac{1}{2}\chi^2} H_{2n+1}(\chi), \quad (4.94)$$

4 Complex harmonic potential

so that we have to choose $\varphi^a = n\pi$ to get the correct formulation for the antisymmetric wave function of the real harmonic potential

$$\psi^a(\chi) = \sqrt{\frac{1}{\sqrt{\pi}2^{2n+1}(2n+1)!}} e^{-\frac{1}{2}\chi^2} H_{2n+1}(\chi) \quad (4.95)$$

$$\Leftrightarrow \psi^a(x) = \sqrt{\frac{\sqrt{\lambda}}{\pi} \frac{1}{2^{2n+1}(2n+1)!}} e^{-\frac{1}{2}\lambda x^2} H_{2n+1}(\sqrt{\lambda}x), \quad (4.96)$$

where $\lambda := \lambda_1 = \lambda_2$ for $C = 0$. The additional $\sqrt{\lambda}$ enters the equation similarly to the real limit of the symmetric states because of the substitution of the integration variable $\chi = \sqrt{\lambda}x$ in (4.92). Thus we have derived the familiar results for the real harmonic potential for the symmetric and antisymmetric states. Putting both results together allows us to write generally for $C = 0$:

$$E = \hbar\Omega \left(n + \frac{1}{2}\right) \quad \text{and} \quad \psi(x) = \sqrt{\frac{\sqrt{\lambda}}{\pi} \frac{1}{2^n n!}} e^{-\frac{1}{2}\lambda x^2} H_n(\sqrt{\lambda}x). \quad (4.97)$$

4.1.2.4 Limit of vanishing waist

Similar to the symmetric case we next evaluate the equivalent limit $\omega \rightarrow 0$ and show that this provides the same results as $c \rightarrow 0$. In order to perform this we adopt the argumentation in the beginning of Subsection 4.1.1.4 and the limits (4.61) and (4.62). Using them for the limit $\omega \rightarrow 0$ of (4.80) directly provides

$$0 = \frac{\Gamma(a_1)}{\Gamma\left(a_1 + \frac{1}{2}\right)}, \quad (4.98)$$

which is nothing else than the same quantization condition for ε^a as we got for the real limit and which is solved by $a_1 = -n - \frac{1}{2}$. Thus the limit of vanishing waist $\omega \rightarrow 0$ provides the same results as $c \rightarrow 0$ as we exactly wanted to show.

4.1.2.5 Limit of big waist

Next we evaluate again the other special case for ω which is the limit $\omega \rightarrow \infty$. For this purpose, just like we did in the former subsection, we adopt the argumentation Subsection 4.1.1.5 starts with. That means we multiply the whole quantization condition (4.80) with ${}_1F_1\left(a_2 + \frac{1}{2}; \frac{3}{2}; \omega^2\right)$ and use (4.27), where we neglect all terms not including e^{ω^2} . Calculating this it turns out that only one term remains which yields

$$\lim_{\omega \rightarrow \infty} \frac{\omega^{2(a_1+a_2)}}{\Gamma\left(a_1 + \frac{1}{2}\right) \Gamma\left(a_2 + \frac{1}{2}\right)} = 0. \quad (4.99)$$

This looks quite similar to the quantization condition in the limit of big waist for the symmetric states but, in contrast to that, it is always fulfilled by $a_2 = -n - \frac{1}{2}$, since the solution should not

depend on a_1 . The following discussion is just the same, which means that we found again a kind of real limit unless in this case area 1 and 3 are vanishing and area 2 with the imaginary potential is extended over the whole axis. It turns out that the imaginary part of the energy is the same but the real part is equal to the energy in the real limit:

$$a_2 = \frac{1}{4}(1 - \varepsilon - ic) = -n - \frac{1}{2} \quad \Leftrightarrow \quad \varepsilon_\infty^a = 4n + 3 - ic \quad (4.100)$$

$$\Leftrightarrow \quad E_\infty^a = \hbar\Omega \left(2n + \frac{3}{2}\right) - iC. \quad (4.101)$$

In order to evaluate the corresponding wave function, we start with the normalization constant (4.84), where we can use that $\lim_{\omega \rightarrow \infty} \Gamma(a, \omega^2) = 0$ and $\lim_{\omega \rightarrow \infty} \theta = 1$. Thus the normalization constant reads

$$|\mathcal{N}^a| = \frac{1}{|R^a|} \left[\sum_{\mu, \nu=0}^{\infty} \frac{1}{\mu! \nu!} \frac{(-n)_\nu (-n)_\mu}{\left(\frac{3}{2}\right)_\nu \left(\frac{3}{2}\right)_\mu} \Gamma\left(\mu + \nu + \frac{3}{2}\right) \right]^{-1/2}. \quad (4.102)$$

Applying (4.41) this simplifies to

$$|\mathcal{N}^a| = \frac{1}{|R^a|} \left[2 \int_0^\infty \chi^2 e^{-\chi^2} \left| {}_1F_1\left(-n; \frac{3}{2}; \chi^2\right) \right|^2 d\chi \right]^{-1/2}. \quad (4.103)$$

Using the definition of the Hermite polynomials (4.87) provides

$$|\mathcal{N}^a| = \frac{2(2n+1)!}{n! |R^a|} \left[\int_{-\infty}^\infty e^{-\chi^2} |H_{2n+1}(\chi)|^2 d\chi \right]^{-1/2} \quad (4.104)$$

and with (4.92) this finally reduces to

$$|\mathcal{N}^a| = \frac{2(2n+1)!}{n! |R^a|} \sqrt{\frac{1}{\sqrt{\pi} 2^{2n+1} (2n+1)!}}. \quad (4.105)$$

Since R^a contains only real functions for $\omega \rightarrow \infty$, we can conclude that R^a is also real and does not include a non-trivial phase factor. In contrast to this we know that \mathcal{N}^a has to be completed by a phase factor $e^{in\pi} = (-1)^n$, so that the wave function in our considered limit reads

$$\psi_{2,\infty}^a(\chi) = \psi_\infty^a(\chi) = (-1)^n \frac{2(2n+1)!}{n!} \sqrt{\frac{1}{\sqrt{\pi} 2^{2n+1} (2n+1)!}} e^{-\frac{1}{2}\chi^2} \chi {}_1F_1\left(-n; \frac{3}{2}; \chi^2\right). \quad (4.106)$$

With the definition of H_{2n+1} in Eq. (4.87) follows

$$\psi_{2,\infty}^a(\chi) = \sqrt{\frac{1}{\sqrt{\pi} 2^{2n+1} (2n+1)!}} e^{-\frac{1}{2}\chi^2} H_{2n+1}(\chi). \quad (4.107)$$

4 Complex harmonic potential

It catches the eye that, in contrast to the energy, the limit of big waist yields exactly the same wave function as the limit of vanishing waist and thus also the real limit:

$$\psi_{\infty}^a(x) = \sqrt{\sqrt{\frac{\lambda}{\pi}} \frac{1}{2^{2n+1}(2n+1)!}} e^{-\frac{1}{2}\lambda x^2} H_{2n+1}(\sqrt{\lambda}x) = \psi_0^a(x). \quad (4.108)$$

So finally it turns out that we can also express the energy and the wave function in the limit $\omega \rightarrow \infty$ by only one expression. independent from the particular parity:

$$E_{\infty} = \hbar\Omega \left(n + \frac{1}{2} \right) - iC \quad \text{and} \quad \psi_{\infty}(x) = \sqrt{\sqrt{\frac{\lambda}{\pi}} \frac{1}{2^{2n}n!}} e^{-\frac{1}{2}\lambda x^2} H_n(\sqrt{\lambda}x) = \psi_0(x). \quad (4.109)$$

This looks reasonable since, if one takes the limit $\omega \rightarrow \infty$ of the time-independent Schrödinger equation (4.3), the imaginary part reads

$$\lim_{w \rightarrow \infty} V_I(x) = C \lim_{w \rightarrow \infty} \left(\frac{x^2}{w^2} - 1 \right) = -C \quad (4.110)$$

and just represents a constant energy shift. Knowing the eigenvalue in the real case

$$H\psi(x) = \left[-\frac{\hbar^2}{2M} \frac{d^2}{dx^2} + \frac{M}{2} \Omega^2 x^2 \right] \psi(x) = E_0 \psi(x) = \hbar\Omega \left(n + \frac{1}{2} \right) \psi(x), \quad (4.111)$$

one can directly conclude

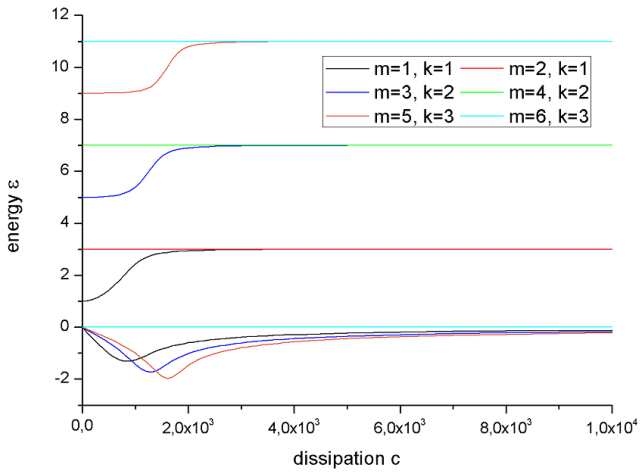
$$\lim_{w \rightarrow \infty} H\psi(x) = \left[-\frac{\hbar^2}{2M} \frac{d^2}{dx^2} + \frac{M}{2} \Omega^2 x^2 - iC \right] \psi(x) = \left[\hbar\Omega \left(n + \frac{1}{2} \right) - iC \right] \psi(x). \quad (4.112)$$

4.2 Energies

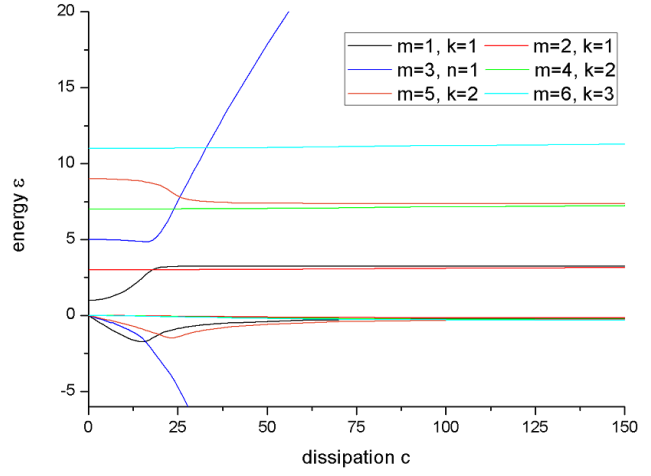
Next we solve the quantization conditions (4.37) and (4.80) numerically. Note that in our dimensionless variables the specific value of c and ω for $w = 100$ nm and $l = 30$ μ m is

$$c = 420 \quad , \quad \omega = 3 \cdot 10^{-3}. \quad (4.113)$$

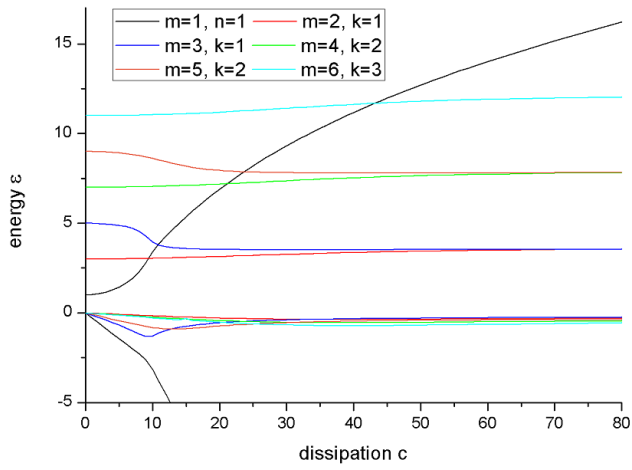
Now let us have a look at the energies of the lowest six states for several waists:



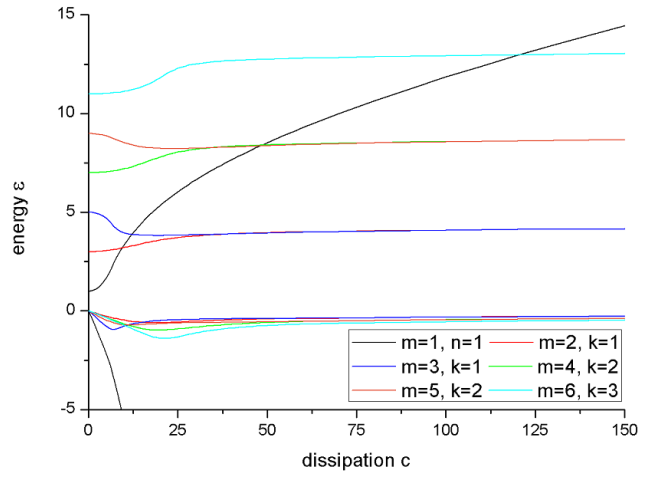
(a) $\omega = 3 \cdot 10^{-3}$



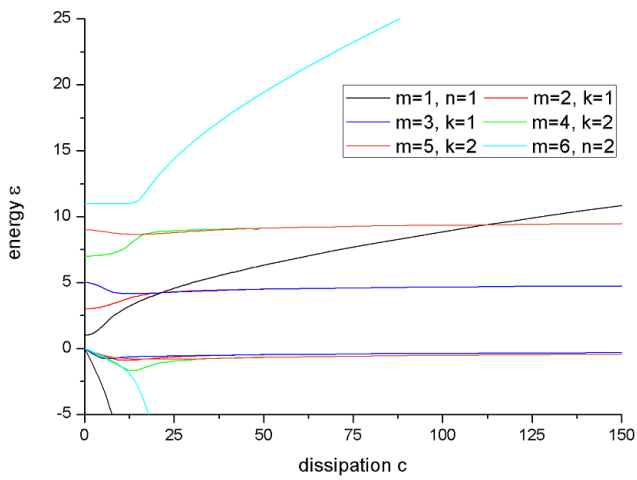
(b) $\omega = 0.2$



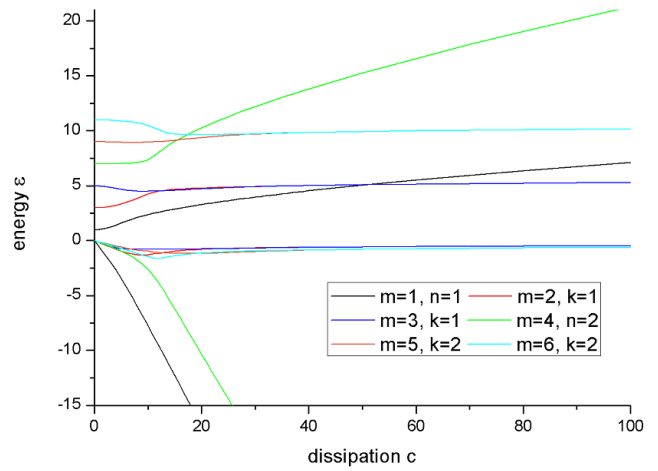
(c) $\omega = 0.4$



(d) $\omega = 0.6$



(e) $\omega = 0.8$



(f) $\omega = 1$

4 Complex harmonic potential

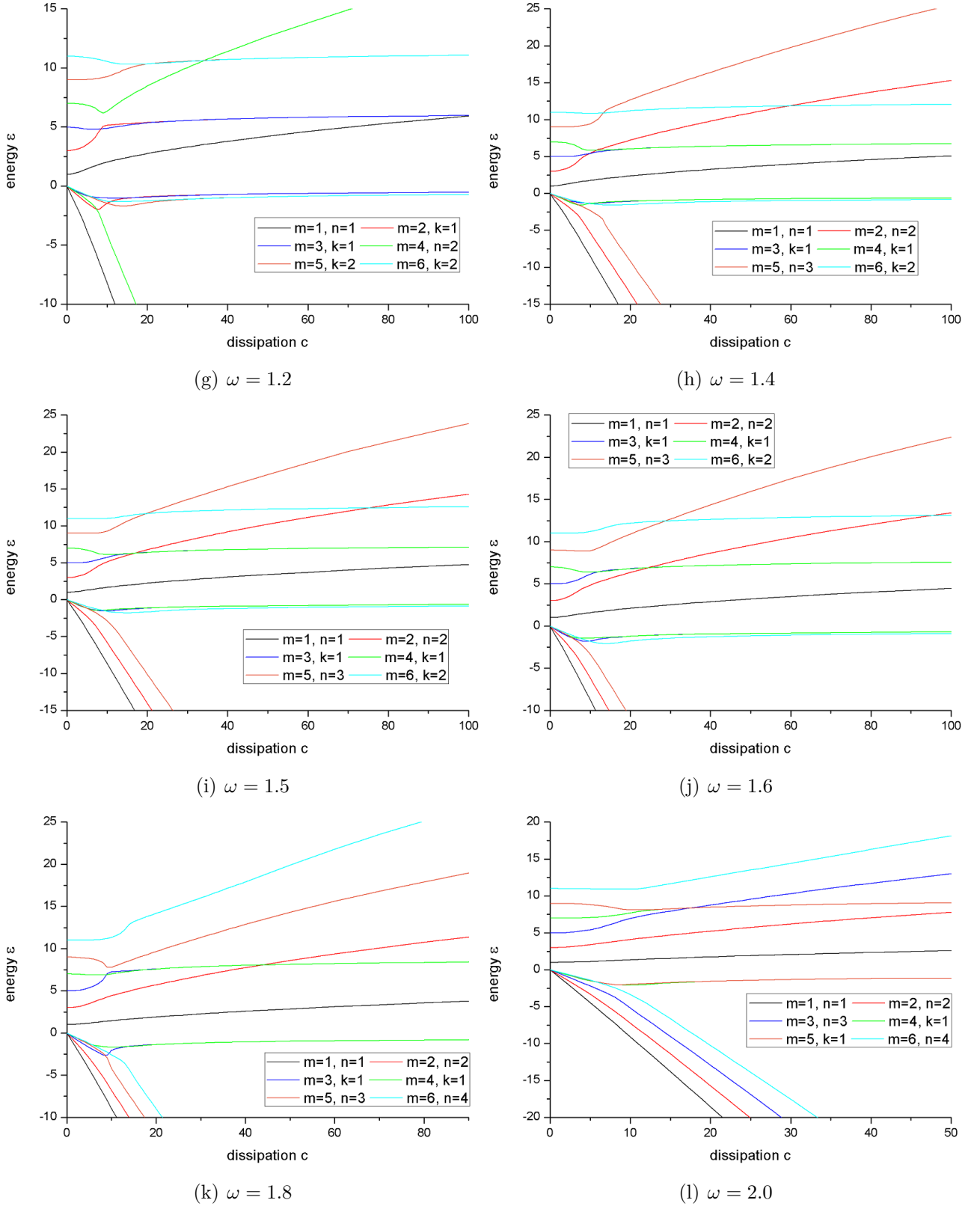


Figure 4.2: Real and imaginary part of the lowest six states as a function of the dissipation strength c of the imaginary potential. Two curves with the same colour represent the real and imaginary part of the energy of the state, where the real part starts at $\varepsilon_R(c = 0) = 2m - 1$ and the imaginary part at $\varepsilon_I(c = 0) = 0$. Moreover, ε_∞ -states are counted by integer n while ε_0 -states are counted by integer k .

Figs. 4.2(a)–4.2(l) show qualitatively an analogous behaviour for the energies of the harmonic potential as for the square well except the fact that here the real part of the energy yields $\varepsilon_R = 2m - 1$ instead of m^2 . The imaginary part of the energy is always non-positive which confirms that our imaginary potential model really describes a damping effect and thus dissipation. Furthermore we can separate all states in two groups of n -states and k -states again, where we resumed the notation of the last chapter which means $\lim_{c \rightarrow \infty} \varepsilon_I^k = 0$ and $\lim_{c \rightarrow \infty} \varepsilon_I^n = -\infty$. Also the well known fusion of always two adjoining k -states is a property of the harmonic potential and an effect of its natural symmetry, as well as the interchange of states being k - or n -state at some waists ω_{crit} . Observing the imaginary parts of the k -states reveals again a minimum so we can see that after it ε_I^k indeed increases to zero. Unfortunately we can not derive the analogon of this for the n -states that is a maximum of $\varepsilon_I^n + c$. This is related to the behaviour of the left hand side of (4.37) and (4.80) which yields an increasing effort of the numerical calculation for large values of c and ω for the n -states. So the numerical evaluation of the n -states for large waists and dissipations can unfortunately not be included in this diploma thesis.

Nevertheless we know from the last chapter that the limit $\omega \rightarrow \infty$ yields finite values for ε_R^n and there is some additional evidence that also $c \rightarrow \infty$ is followed by finite results. We can take for instance the obvious analogy of all results to the square well potential where a finite saturation value exists which we even can calculate. Moreover we found out that the imaginary potential does not directly affect the real part of the energy but yields the same effect as a potential barrier confining the n -states in a square well potential with the width $2w$ for $c \rightarrow \infty$. Thus the ε_R^n become the real energies of states of exactly this potential well and should be therefore finite. The general situation actually did not change since the harmonic potential becomes a square well one for $c \rightarrow \infty$ and $w = \text{const.} < \infty$. So the assumption, that also in the harmonic case a kind of independent potential well containing states with finite energy eigenvalues develops, seems to be reasonable. We will have a deeper look at exactly this issue while discussing the corresponding densities of the energies.

4.3 Densities

Taking (4.35) and (4.78) we can calculate via (4.21) the densities for given c and ω :

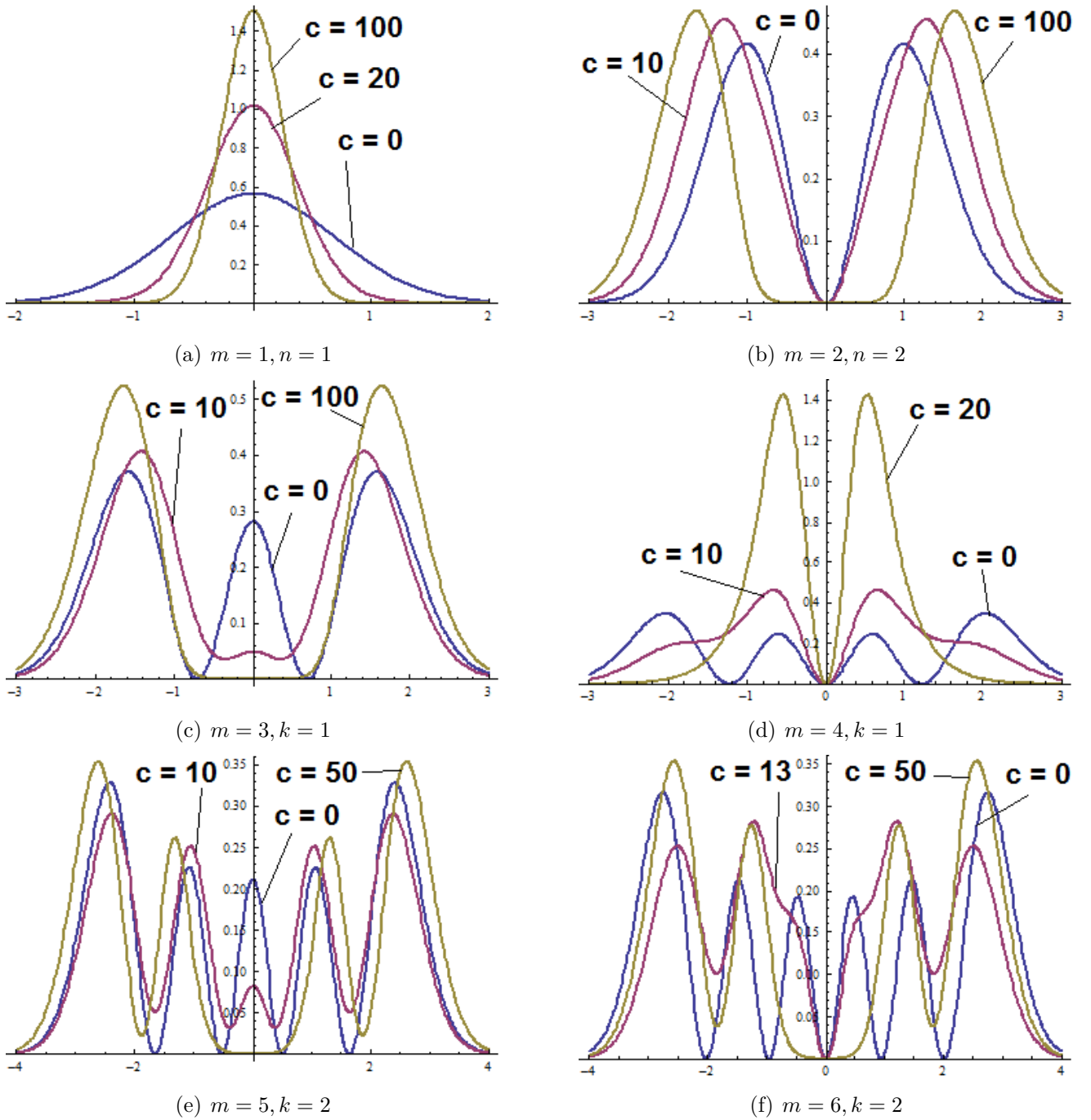
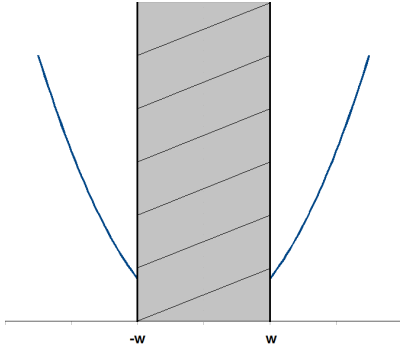


Figure 4.3: Densities of the lowest states for $\omega = 1$ for some values of c , where all states are counted by m for $c < c_{\text{crit}}$ and by k and n for $c > c_{\text{crit}}$. The fusion of two respective k -states, which we already observed in Figs. 4.2(a) – 4.2(l), is also confirmed here. Furthermore, it shows that two states with the same k end up exactly in the same state.

Thus also the densities yield the same behaviour as for the square well potential. Also in the harmonic case k -states tend to the borders of the well and their density decreases to zero in the center while n -states have maxima in the center and a vanishing density at the borders for large dissipation c . So for $c \rightarrow \infty$ we are again left with three independent potential wells just like in the case of a square well potential. However, in contrast to this case, we can not have an analogous discussion of ω_{crit} as we had for the square well potential in subsection 3.2.3 since on the one hand we have no analytical function for the saturation values of ε_R^k and ε_R^n to calculate intersections and on the other hand there is no finite upper boundary for the waist for the harmonic potential and thus also no ω that yields the half of the well.

Anyhow instead of directly calculating $\lim_{c \rightarrow \infty} \varepsilon_R$ from (4.37) and (4.80) we can take advantage of our knowledge from the square well potential and the so far obtained similarities in the results of both systems. Therefore we assume that also in the case of a harmonic potential independent wells develop and that the imaginary potential has the same effect as a potential barrier. Considering that for $c \rightarrow \infty$ the density of the k -states vanishes for $|\chi| < \omega$ and yields the states of a harmonic potential well for $|\chi| \geq \omega$. Comparing this with the results of a system with a potential barrier should provide the same results:



$$V(\chi) = \begin{cases} \frac{1}{2} \hbar \Omega \chi^2 & , |\chi| \geq \omega \\ \infty & , |\chi| < \omega \end{cases} \quad (4.114)$$

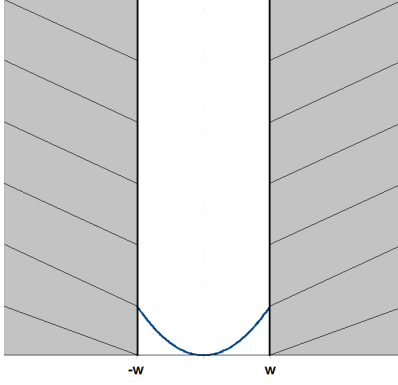
This is directly followed by the quantization condition

$${}_1F_1\left(\frac{1}{4}(1-\varepsilon); \frac{1}{2}; \omega^2\right) - 2\omega \frac{\Gamma\left(\frac{1}{4}(3-\varepsilon)\right)}{\Gamma(a_1)} {}_1F_1\left(a_1 + \frac{1}{2}; \frac{3}{2}; \omega^2\right) = 0 \quad (4.115)$$

for both symmetric and antisymmetric states. Taking $c \rightarrow \infty$ in (4.37) and (4.80) has no effect on the left hand since only a_2 and θ are direct functions of c . So the quantization condition is fulfilled in this limit if the right hand side does not diverge which is ensured if exactly (4.115) is true. Thus we can calculate numerically the saturation values for the real parts of the energies of the k -states which coincide perfectly with the results of the direct calculation from (4.37) and (4.80) and thus also with Figs. 4.2(a) – 4.2(1).

Let us do the same with the n -states. Since in this case the density vanishes at the borders for $|\chi| \geq \omega$, we thus take instead the potential

4 Complex harmonic potential



$$V(x) = \begin{cases} \infty & , |x| \geq w \\ \frac{1}{2}\hbar\Omega x^2 & , |x| < w \end{cases} \quad (4.116)$$

and obtain correspondingly the quantization condition

$${}_1F_1\left(\frac{1}{4}(1-\varepsilon); \frac{1}{2}; \omega^2\right) {}_1F_1\left(\frac{1}{4}(3-\varepsilon); \frac{3}{2}; \omega^2\right) = 0. \quad (4.117)$$

We can solve this numerically, too, but so far it was not possible to show that the results coincide with ε_R^n for large c . Furthermore we have to consider $\varepsilon_I^n \rightarrow -c \rightarrow -\infty$ so that the left hand sides as well as the right hand sides of (4.37) and (4.80) are complicated functions of c and it was not possible yet to extract some reasonable insights from this for the n -states so far.

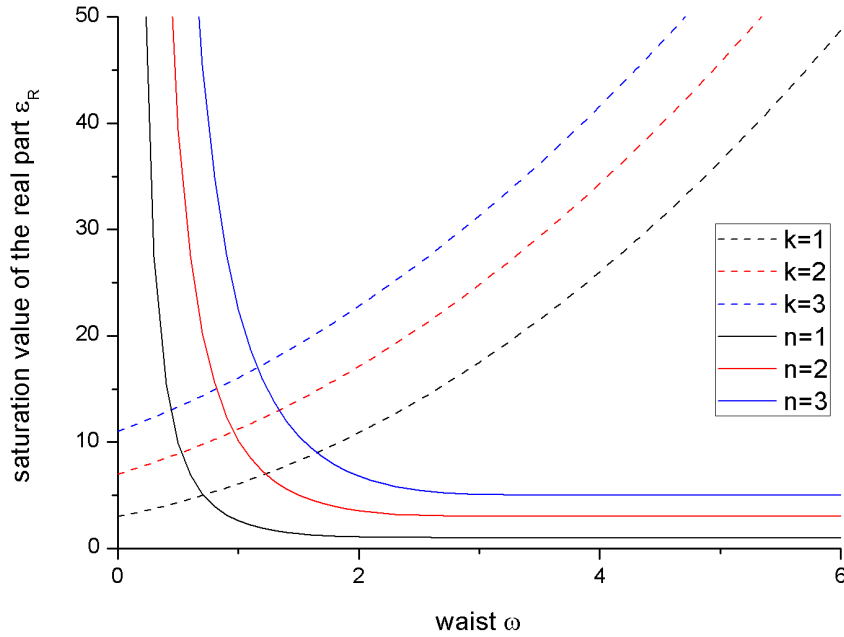


Figure 4.4: Solutions of (4.115), counted by k , and (4.117), counted by n . The solutions of (4.115) yield $\varepsilon_R = 3, 7, 11, \dots$ for $\omega = 0$, which are the energies of the antisymmetric states of a real harmonic potential well, and $\varepsilon \rightarrow \infty$ for $\omega \rightarrow \infty$. The situation is exactly vice versa for the solutions of (4.117) except that here it is $\varepsilon_R \rightarrow 1, 3, 5, \dots$ for $\omega \rightarrow \infty$ so the energies of both symmetric and antisymmetric states can be observed. This behaviour makes the assumption more reasonable that (4.115) and (4.117) represent the limits of ε_R for $\lim_{c \rightarrow \infty} \varepsilon_I = 0$ and $\lim_{c \rightarrow \infty} \varepsilon_I = 0$, respectively.

5 Outlook

There are several issues remaining for further studies. For example a better approximation of the Gaussian beam than the harmonic one or a model in more than only one dimension, but in fact the most interesting improvement would be the implementation of interaction.

Despite many satisfying insights our model provides for the square well potential as well as for the harmonic one, that is a hole in the condensate for large dissipation and evolution times, we still deal with very idealized results since no interaction has been implemented. In order to include also this we could consider a variational approach, which consists in making a suitable ansatz for the wave function ψ . It should yield approximately the same qualitative behaviour as the numerical calculated ones in Figs. 4.3(a) – 4.3(f) but have a quite simpler form as (4.35) and (4.78). Additionally ψ depends on some parameters $\lambda_1, \dots, \lambda_N$ to vary its particular shape in a similar way as the numerical calculated wave functions do for several c and ω . Subsequently we take the energy functional in order to calculate the energies of the interacting system:

$$\begin{aligned} \varepsilon(\lambda_1, \dots, \lambda_N, \omega, c, g) &= \int_{-\infty}^{\infty} \left(-\psi_{\lambda_1, \dots, \lambda_N}^*(x) \frac{\partial^2}{\partial x^2} \psi_{\lambda_1, \dots, \lambda_N}(x) + V(x) |\psi_{\lambda_1, \dots, \lambda_N}(x)|^2 + g |\psi_{\lambda_1, \dots, \lambda_N}(x)|^4 \right) dx \\ &= 2 \int_0^{\infty} \left(\left| \frac{\partial}{\partial x} \psi_{\lambda_1, \dots, \lambda_N}(x) \right|^2 + x^2 |\psi_{\lambda_1, \dots, \lambda_N}(x)|^2 + g |\psi_{\lambda_1, \dots, \lambda_N}(x)|^4 \right) dx \\ &\quad + 2ic \int_0^{\omega} \left(\frac{x^2}{\omega^2} - 1 \right) |\psi_{\lambda_1, \dots, \lambda_N}(x)|^2 dx. \end{aligned} \quad (5.1)$$

The next question is how to determine the optimal parameters $\lambda_1, \dots, \lambda_N$ for every value of c and ω . This can be done by a variation of $\varepsilon(\lambda_1, \dots, \lambda_N, \omega, c, g = 0)$, that is for vanishing interaction, with respect to the variational parameters $\lambda_1, \dots, \lambda_N$ in order to obtain an optimal form for the wave function ψ . If this wave function is in good accordance with the numerical results, we take it as an appropriate ansatz for the calculation of the energies even for an interacting system, that would be $g \neq 0$.

Unfortunately, due to the complexity of the system, this approach involves some difficulties that we were not able to eliminate so far. Of course the variational parameters have to be complex so if one aims at varying ε with respect to the complex $\lambda_1, \dots, \lambda_N$ in order to obtain optimal parameters, one has to ensure the complex differentiability of ε with respect to $\lambda_1, \dots, \lambda_N$. Unfortunately this is generally not the case since these parameters enter the energy functional via the absolute square of the supposed wave function $\psi_{\lambda_1, \dots, \lambda_N}$. Therefore we have to deal with functions like the complex conjugate as well as real or imaginary part of the parameters and it is well-known that these functions are not differentiable in the complex sense. Thus we have to try real valued functions of ε like either the real and the imaginary part or the absolute value, that we can take for the variation. Following this ansatz the next problem consists in the choice of the particular trial function.

5 Outlook

We tried on the one hand several expressions and possible real valued functions for ψ for this approach and on the other hand piecewise defined wave functions including a Gauss function in area 1 and 3 and a polynomial in area 2 but neither the variation of the real and the imaginary part nor of the absolute value yield satisfying results for the non-interacting density.

The fact that we are able to reproduce the densities with such an ansatz for $c = 0$, that is for the real case, implies that the complexness of the system is responsible for the non-applicability of this particular variational approach.

Bibliography

- [1] S. N. Bose, *Plancks Gesetz und Lichtquantenhypothese*, Z. Phys. **26**, 178 (1924)
- [2] A. Einstein, *Quantentheorie des einatomigen idealen Gases - Zweite Abhandlung*, Sitz. Ber. Preuss. Akad. Wiss. (Berlin) **22**, 261 (1924)
- [3] M. H. Anderson, J. R. Ensher, M. R. Matthews, C. E. Wieman, and E. A. Cornell, *Observation of a Bose-Einstein Condensation in a Dilute Atomic Vapor*, Science **269**, 198 (1995)
- [4] K. B. Davis, M. O. Mewes, M. R. Andrews, N. J. van Druten, D. S. Durfee, D. D. Kurn, and W. Ketterle, *Bose-Einstein Condensation in a Gas of Sodium Atoms*, Phys. Rev. Lett. **75**, 3969 (1995)
- [5] W. D. Phillips and H. J. Metcalf, *Cooling and Trapping Atoms*, Scientific American **256**, 36 (1987)
- [6] C. N. Cohen-Tannoudji and W.D. Phillips, *New Mechanism for Laser Cooling*, Physics Today, 33 (1990)
- [7] S. Chu, *Laser Trapping of Neutral Particles*, Scientific American **266**, 71 (1992)
- [8] W. Ketterle and N. J. van Druten, *Evaporative Cooling of trapped atoms*, Adv. Atom. Mol. Phys. **37**, 181 (1996)
- [9] M. R. Andrews, C. G. Townsend, H.-J. Miesner, D. S. Durfee, D. M. Kurn, and W. Ketterle, *Observation of interference between two Bose condensates*, Science **275**, 637 (1997)
- [10] M. Greiner, O. Mandel, T. Esslinger, T. W. Hänsch, and I. Bloch, *Quantum phase transition from a superfluid to a Mott insulator in a gas of ultracold atoms*, Nature **415**, 39 (2002)
- [11] I. Bloch, *Quantum coherence and entanglement with ultracold atoms in optical lattices*, Nature **453**, 1016 (2008)
- [12] J. E. Lye, L. Fallani, M. Modugno, D. S. Wiersma, C. Fort, and M. Inguscio, *Bose-Einstein Condensation in a Random Potential*, Phys. Rev. Lett. **95**, 070401, (2005).
- [13] J. Bardeen, L. N. Cooper, and J. R. Schrieffer, *Theory of Superconductivity*, Phys. Rev. **108**, 1175 (1957)
- [14] S. Giorgino, L. P. Pitaevskii, and S. Stringari, *Theory of ultracold atomic Fermi gases*, Rev. Mod. Phys. **80**, 1215-1274 (2008)
- [15] S. Schmid, A. Härter, and J. H. Denschlag, *Dynamics of a Cold Trapped Ion in a Bose-Einstein Condensate*, Phys. Rev. Lett. **105**, 133202 (2010)

Bibliography

- [16] P. Würtz, T. Langen, T. Gericke, A. Koglbauer, and H. Ott, *Experimental Demonstration of Single-Site Addressability in a Two-Dimensional Optical Lattice*, Phys. Rev. Lett. **103**, 080404 (2009)
- [17] T. Gericke, P. Würtz, D. Reitz, T. Langen, and H. Ott, *High-resolution scanning electron microscopy of an ultracold quantum gas*, Nature Phys. **4**, 949 (2008)
- [18] K. D. Nelson, X. Li, and D. S. Weiss, *Imaging single atoms in a three-dimensional array*, Nature Phys. **3**, 556 (2007)
- [19] N. Gemelke, X. Zhang, C.-L. Hung, and C. Chin, *In situ observation of incompressible Mott-insulating domains in ultracold atomic gases*, Nature **460**, 995 (2009)
- [20] M. Karski, L. Förster, J. M. Choi, W. Alt, A. Widera, and D. Meschede, *Nearest-neighbor detection of atoms in a 1D optical lattice by fluorescence imaging*, Phys. Rev. Lett. **102**, 053001 (2009)
- [21] W. S. Bakr, J. I. Gillen, A. Peng, S. Fölling, and M. Greiner, *A quantum gas microscope for detecting single atoms in a Hubbard regime optical lattice*, Nature **462**, 74 (2009)
- [22] C. Weitenberg, M. Endres, J. F. Sherson, M. Cheneau, P. Schauß, T. Fukuhara, I. Bloch, and S. Kuhr, *Single-spin addressing in an atomic Mott insulator*, Nature **471**, 319-324 (2011)
- [23] H. Ott, private communication
- [24] C. J. Pethick and H. Smith, *Bose-Einstein Condensation in Dilute Gases*, 2nd Edition, Cambridge University Press, 2008
- [25] S. Inouye, M. R. Andrews, J. Stenger, H.-J. Miesner, D. M. Stamper-Kurn, and W. Ketterle, *Observation of Feshbach resonances in a Bose-Einstein condensate*, Nature **392**, 151-154 (1998)
- [26] W. Nolting, *Grundkurs Theoretische Physik 5/1, Quantenmechanik - Grundlagen*, 6th Edition, Springer, 2001
- [27] W. Nolting, *Grundkurs Theoretische Physik 5/2, Quantenmechanik - Methoden und Anwendungen*, 6th Edition, Springer, 2007
- [28] F. Schwabl, *Quantenmechanik (QM I)*, 6th Edition, Springer, 2002
- [29] W. Greiner, *Theoretische Physik, Quantenmechanik - Einführung*, 6th Edition, Verlag Harri Deutsch, 2005